Functional and molecular characterization of pendrin, the anion exchanger involved in Pendred syndrome, non-syndromic deafness and respiratory distresses.

Dissertation

in fulfillment of the requirements for the degrees of:

Dr.rer.nat. at the Naturwissenschaftlicher Fakultät of the Paris Lodron Universität Salzburg

and

PhD in Molecular and Cellular Physiology at the Università degli Studi di Milano

Submitted by

Emanuele Bernardinelli, MA.rer.nat.

Evaluators:

Univ.Prof.Dr. Markus Paulmichl
Ao.Univ.Prof.Dr. Hubert Kerschbaum
Univ.Prof. Michele Mazzanti, PhD

Institut für Pharmakologie und Toxikologie
Paracelsus Medizinische Privatuniversität

Salzburg, March, 2015

A mio papá

Table of Contents

DISCLAIMER:

The data presented in this thesis are unpublished and confidential.

DISCLAIMER

This work was prepared during the research triennium according to requirements of the curriculum of the PhD in MOLECULAR PHYSIOLOGY (Dual Degree PhD program between the universities of Milan – UNIMI and Salzburg – PMU, PLUS) for acquiring the title of PhD and Dr.rer.nat. and according the regulations of the Paracelsus Medical University, UNIMI, PLUS.

Part of the experimental work presented in this thesis work is a collaborative project between the universities of Salzburg – PMU and the university of Campinas, Sao Paolo, Brazil done by Emanuele Bernardinelli together with Vanessa de Moraes, therefore, presentation of identical results in the PhD thesis of Emanuele Bernardinelli and the PhD thesis of Vanessa de Moraes are with permission of supervisors and in accordance with regulations of the Paracelsus Medical University, the Paris Lodron Universität Salzburg and the Universitá degli Studi di Milano.

Following, the abovementioned results published in the doctoral thesis of Vanessa de Moraes:

Pag. 146 Grafico 1
Pag. 147 Grafico 2
Pag. 149-157 Fig. 55-63
Pag. 158 Grafico 3
Pag. 159-163 Fig. 64-68
Pag. 164 Grafico 4
Pag. 169 Tab. 17
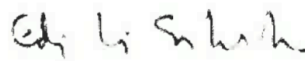
Vanessa de Moraes, PhD

Univ.Prof. Edi Sartorato

PD Silvia Dossena, PhD

Univ.Prof. Markus Paulmichl

Emanuele Bernardinelli

Univ.Prof. Michele Mazzanti

Abstract

Pendrin is an anion exchanger transporting several monovalent anions including iodide, chloride and bicarbonate. It is expressed in the inner ear, thyroid and kidney and more recently was also detected in the airways and in a number of other tissues. Pendrin was first identified as the protein whose mutations leading to a reduction or loss of transport function are responsible for the pathology referred to as Pendred syndrome, an autosomal recessive disorder characterized by bilateral sensorineural hearing loss associated to thyroid dysfunction with or without involvement of the vestibular system. Pendrin mutations also lead to the development of unilateral or bilateral hearing loss with enlargement of the vestibular aqueduct with no involvement of other organs (non-syndromic EVA). On the other hand, the overexpression and hyper-function of pendrin have been recently associated with a number of other pathologies, such as hypertension, bronchial asthma and chronic obstructive pulmonary disease (COPD).

The high phenotypic variability among individuals carrying pendrin mutations, the existence of phenocopies of Pendred syndrome and the high incidence of benign polymorphisms in the general population require both the sequencing of the pendrin coding region and assessment of the possible functional impairment of the identified protein variants in order to confirm or exclude the role of pendrin in determining deafness. In this work, we performed the functional characterization of 7 pendrin variants identified in a cohort of 58 deaf patients by our collaborators of the University of Campinas (Sao Paolo, Brazil). The analysis of pendrin activity was performed measuring the iodide influx in pendrin transfected cells by means of a fluorometric assay based on an enhanced yellow fluorescence protein (EYFP) variant sensitive to the intracellular iodide concentration. Furthermore, the molecular defect of such mutants was analyzed, defining their subcellular localization and expression levels by means of confocal microscopy and western blot.

Based on the results of the functional test, 4 pendrin variants (P142L, G149R, C282Y and Q413R) were classified as mutations with reduction of function, 2 (T193I and L445W) as mutations with loss of function and one (R776C) as a benign polymorphism. Assessing the degree of functional impairment of the analyzed pendrin variants contributed to the genetic diagnosis of the screened patients. Including our findings, the genetic diagnosis was conclusive for 6 patients (for 5 of them deafness was assessed as

linked to pendrin dysfunction and for one patient we were able to exclude pendrin as the genetic cause of deafness) while for 8 individuals, bearing monoallelic pendrin mutations, further investigations are needed, involving pendrin promoter and 3'-UTR, as well as further deafness related genes.

We could observe a clear correlation between measured functional impairment, sub-cellular localization and expression levels of these specific variants. In particular, mutants with loss of function (pendrin T193I and L445W) are retained in the ER, completely excluded from the plasma membrane and their expression levels are greatly reduced with respect to the wild type, while mutants with reduction of function (pendrin P142L, G149R, C282Y) show at least a partial trafficking to the PM and expression levels reduced with respect to the wild type but significantly higher with respect to the mutants with loss of function.

Based on the finding that expression levels of all pendrin mutants are reduced compared to the wild type, we hypothesized that they may be targeted for proteasomal degradation. Starting from this hypothesis we could show that pharmacological inhibition of proteasomal degradation with 10 μM MG132 was capable to recover (i) total and (ii) plasma membrane expression levels of pendrin variants and, most importantly, (iii) transport activity of specific mutants (pendrin P142L, T183I, Q413R, L445W) was improved upon treatment. These results allow for further development of possible approaches aimed to rescue pendrin transport activity as a potential treatment of pathologies related to pendrin malfunction.

The second part of the present study focuses on the search of a specific inhibitor of pendrin. No specific, non-toxic and potent inhibitors of pendrin could be identified so far and the screening of large compound libraries failed in identifying potential ligands. We therefore adopted a more targeted selection of candidate ligands to be submitted to the functional screening. We selected compounds among (i) established inhibitors of anion exchangers, (ii) inhibitors of the pendrin homologue DRA, (iii) commonly used diuretics and antihypertensive agents, and (iv) small molecules predicted *via* two bioinformatic tools, the meta-analysis and SHED alignments. Meta-analysis is an approach aimed to the mathematical definition of a protein topology based on its primary aminoacidic sequence, with no knowledge of its three-dimensional structure. SHED profile allows for the

9

mathematical definition of small compounds according to the intra-molecular distribution of specific atomic features. The effect of the candidate ligands on pendrin activity was evaluated by means of the same fluorometric assay mentioned earlier. In the present study we could (i) confirm the inhibitory effect of the previously assessed active compounds niflumic acid and 5-nitro-2-(3-phenylpropyl-amino) benzoic acid (NPPB) and (ii) show for the first time the inhibitory effect of the anti-inflammatory, anti-rheumatic drug tenidap. In a second phase screening of further compounds suggested by the alignment of niflumic acid and tenidap, according to the SHED profiling, we were able to identify two additional active compounds, N-(2-chlorophenyl)-2-(2,4-dibromophenoxy)acetamide and flufenamic acid. The identification of pendrin inhibitors may represent an important step in the treatment of pathological conditions associated to an increased pendrin function or expression.

1. Introduction

1.1   The anion transporter pendrin

Pendrin is an electroneutral anion exchanger [1] with affinity for a number of ions including iodide, chloride, formate, thyocianate, hydroxide and bicarbonate. It was initially described to be expressed in the inner ear [2], thyroid [3] and kidney [4], but more recently it has also been detected in the airways [5] and in a number of other tissues [6, 7], even though its role in most cases is still to be elucidated.

Pendrin was first cloned by Everett et al. in 1997 [8] and identified as the protein that, if mutated and non-functional or hypo-functional, is responsible for the pathology referred to as Pendred syndrome [8], an autosomal recessive disorder described for the first time in 1896 by the English physician Vaughan Pendred [9]. Pendred syndrome is characterized by bilateral sensorineural hearing loss associated with thyroid dysfunction and possibly goiter [10]. Pendrin-related deafness can be either syndromic or non-syndromic and it is usually characterized by an enlargement of the vestibular aqueduct (EVA). More recently, the deregulation of the transporter has been associated with other pathological issues and in particular its over-expression and/or hyper-function have been linked to hypertension [11] and airway distresses such as bronchial asthma and chronic obstructive pulmonary disease (COPD) [12].

In the inner ear (Figure 1a), pendrin is mainly expressed in the external sulcus and spiral prominence cells of the cochlea, in the mitochondria-rich cells of the endolymphatic sac and duct and in the transitional cells surrounding the sensory epithelia in the utricle, saccule and ampullae of the vestibular labyrinth [13]. In all the above mentioned compartments, pendrin is responsible for the exchange of chloride and bicarbonate [14], contributing to the regulation of the pH and ion composition of the endolymph, therefore maintaining the endocochlear potential, essential for the conversion of the acoustic signal in electric impulse. In case of an impaired pendrin activity, acidification of pH and alteration of the ion homeostasis of the endolymph are associated with EVA (Figure 1b) [15], degeneration of sensory cells, loss of endocochlear potential [16] and formation of calcium oxalate stones in the utricle and saccule [17]. Altogether these defects result in the development of severe to profound deafness, either syndromic or non-syndromic (*i.e.* accompanied or not with thyroid dysfunction, respectively), possibly associated in the worst cases with vestibular dysfunction. The role of pendrin appears to be crucial in the

correct maturation of the inner ear. Thanks to an inducible pendrin knock-out mouse, it has been shown that a loss of the transporter function between embryonic day 16.5 and postnatal day 2 leads to all the defects reported above and to an irreversible failure in developing a normal hearing phenotype [18].
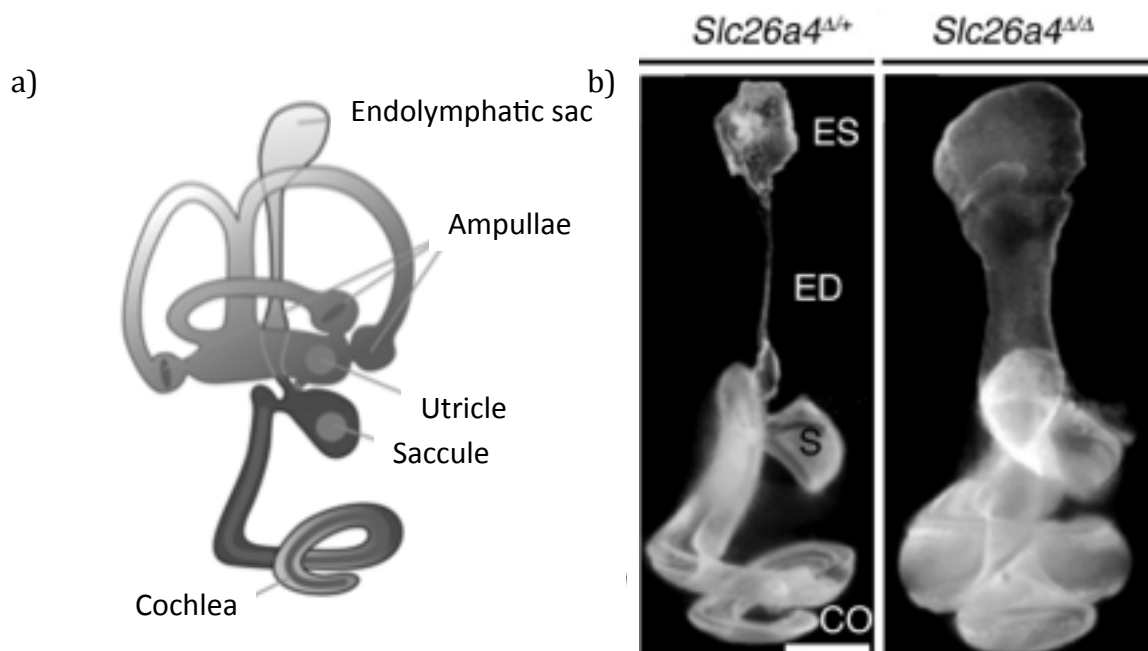
Figure 1: a) Schematic depiction of pendrin expression pattern in the inner ear; b) pendrin knock-out leads to loss of ion homeostasis of the endolymph, resulting in the enlargement of the whole vestibular aqueduct (EVA). ES: endolymphatic sac, ED: endolymphatic duct, S: saccule, CO: cochlea (Choi, B.Y., et al. The Journal of clinical investigation, 2011. **121**: 4516-25).

In the thyroid (Figure 2), pendrin is abundantly expressed on the apical membrane of the thyrocytes [19], where, together with the Na$^+$ iodide symporter (NIS) at the basolateral side, contributes to the trans-epithelial transport of iodide from the bloodstream to the follicular lumen of the gland [20]. Iodide is then organified on thyroglobulin as an essential step in thyroid hormones biosynthesis. Although the function of pendrin in the thyroid is controversial [21], it is widely accepted that it may act as a Cl$^-$/I$^-$ exchanger. A lack of pendrin activity would lead to a reduced iodide flux into the follicular lumen and, as a consequence, to the partial iodide organification defect seen in Pendred syndrome, eventually leading to hypothyroidism and/or goiter [22, 23]. The severity of the thyroidal phenotype appears to be extremely variable also within families [22] and can often be identified only by a positive perchlorate discharge test [24]. It is commonly hypothesized that further genetic or environmental factors may contribute to the incidence and the

severity of the thyroid phenotype. A specific example is represented by the dietary iodide intake, that has been shown to strongly influence the incidence of the development of pendrin-related hypothyroidism and goiter in different populations [25].
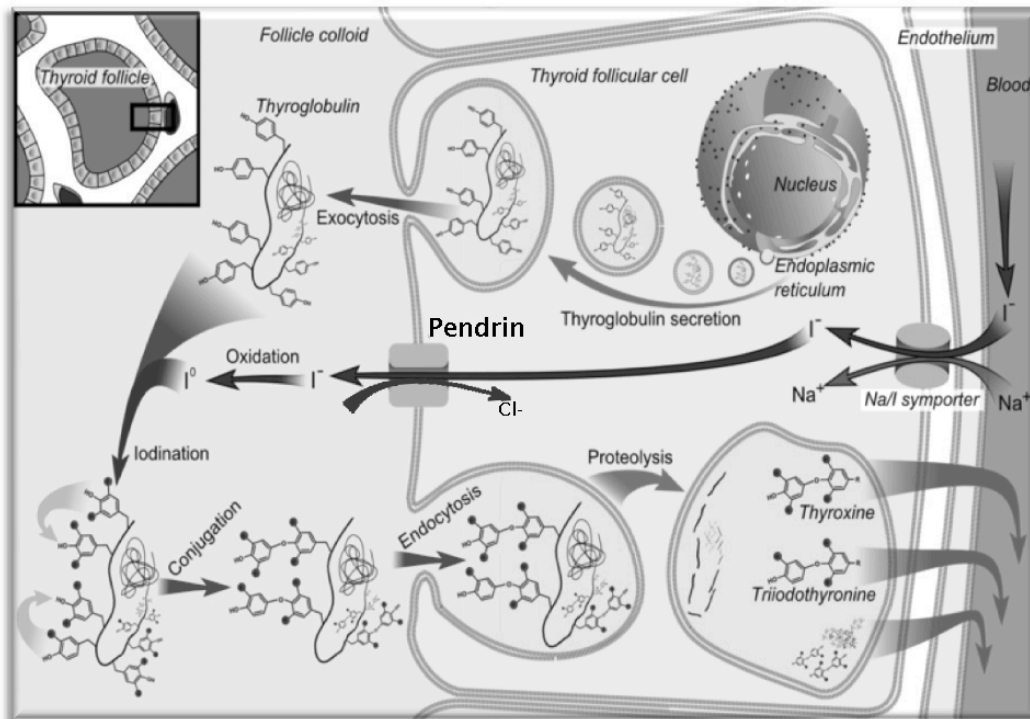
Figure 2: schematic representation of transepithelial iodide transport in the thyroid follicle. Pendrin is expressed at the apical side of thyrocytes and, together with the Na^+/I^- symporter NIS at the baso-lateral side, allows for the transport of iodide from the bloodstream into the lumen of the follicle, where it is organified in the thyroid hormones T3 (Triiodothyronine) and T4 (Thyroxine) (modified from: Boron, W.F. *Medical physiology: A Cellular and Molecular Approach*. 2003: W.B. Saunders).

In the kidney (Figure 3), pendrin has been identified on the apical membrane of β and non-α, non-β intercalated cells of the distal convoluted tubule, cortical collecting duct and connecting tubule [4, 26, 27]. Similarly to the inner ear, in the kidney pendrin is responsible for the exchange of Cl^-/OH^- or Cl^-/HCO_3^- [4], therefore conditioning the pH of the urine and contributing to the pH homeostasis of the whole organism. In addition to the HCO_3^- secretion, together with the epithelial Na^+ channel (ENaC) pendrin participates in the reabsorption of NaCl from the urine to the bloodstream [28], therefore contributing to the blood pressure regulation [29].

However, Pendred syndrome patients show no renal dysfunction, suggesting the presence of redundant mechanisms compensating for the lack of functional pendrin in the kidney under basal conditions. Interestingly, cases of metabolic alkalosis have been recently detected in Pendred patients, in association with pharmacological treatment with thiazides [30] or disturbed acid-base homeostasis due to inter-current illness [31]. The involvement of pendrin in pH homeostasis and salt reabsorption has also been confirmed in mouse models lacking pendrin expression. Recently, different groups showed an alteration of bicarbonate secretion in the kidney in pendrin knock-out mice, leading to metabolic alkalosis both in the basal state [32] and upon NaCl restriction [33]. Furthermore, Verlander et al. demonstrated that pendrin knock-out mice are resistant to aldosterone-analogs-induced hypertension, but develop metabolic alkalosis following aldosterone treatment [11].
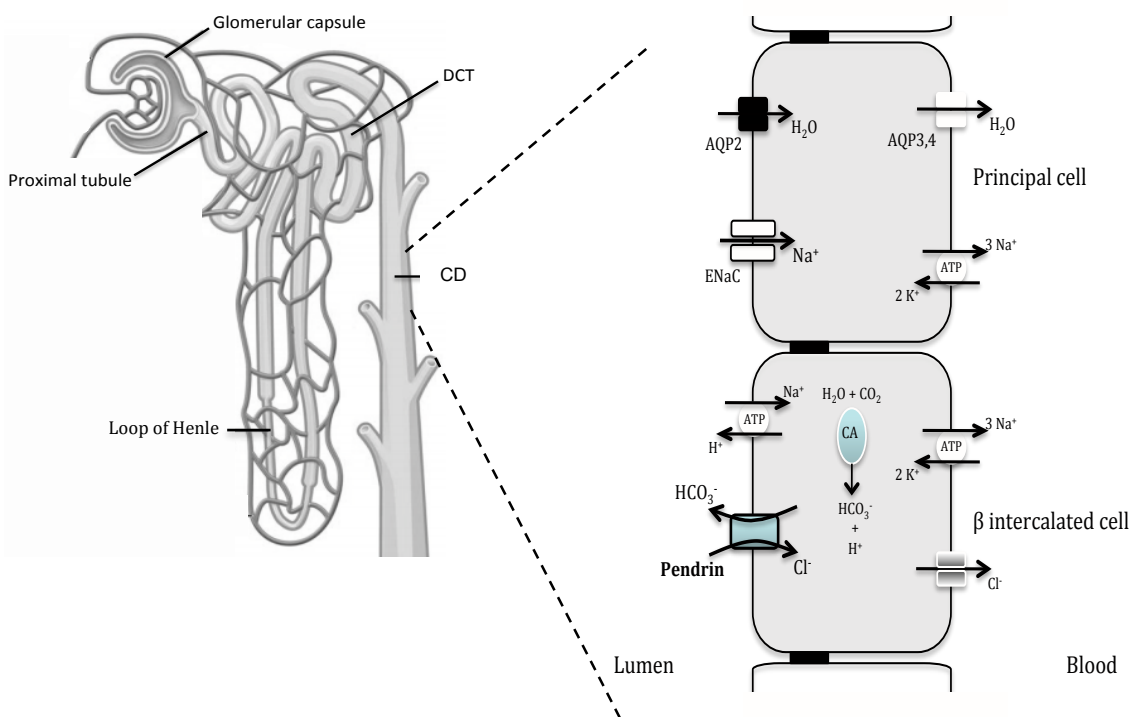
Figure 3: schematic representation of pendrin expression in the distal section of the nephron. Pendrin is expressed in β and non-α non-β intercalated cells of distal convoluted tubule, cortical collecting duct and connecting tubule. It exerts a Cl^-/HCO_3^- transport contributing on one side to the regulation of pH and on the other side, together with ENaC in the principal cells, to the transepithelial reabsorption of NaCl. DCT: distal convoluted tubule, CD: Collecting duct (modified from: OpenStax College, Anatomy & Physiology. OpenStax College. 25 April 2013. <http://cnx.org/content/col11496/latest/>).

As already mentioned, the expression of pendrin has been recently identified in tissues other than the inner ear, thyroid and kidney, such as airways [34], mammary gland [35], placenta [36], testis [37], endometrium [38] and liver [39]. In most of the cases, the pathophysiological role of pendrin is still to be elucidated. A notable exception is the expression of pendrin in the airways, where the transporter has been shown to play a crucial role in the exacerbation of symptoms typical of airway distresses such as asthma and COPD. Overexpression and hyperactivity of pendrin in the upper airways have been shown to be associated with inflammatory states characterized by stimulation via inflammatory cytokines, in particular interlukin-4, -13 and -17 [12, 34, 40].

The role of pendrin overexpression and hyperactivity in the airways will be discussed more in detail in later sections.

1.2   Putative structure of pendrin

Structural and topological definition of pendrin is still an elusive issue, as it is often the case of membrane proteins. Due to their high degree of flexibility and hydrophobicity, the experimental definition of three-dimensional structures for those proteins is still a real challenge, either by X-ray crystallography or nuclear magnetic resonance (NMR) [41]. Since its cloning in 1997 [8], a number of models have been suggested in an attempt of defining pendrin structure, according to different predictor approaches. At first, an 11 transmembrane segments model with the N-terminus located on the intracellular side and the C-terminus located on the extracellular side was predicted with the PHDhtm algorithm [8]. Royaux et al. adapted this early model with an additional transmembrane segment, therefore bringing the C-terminus on the intracellular side [3]. The intracellular localization of both N-terminus and C-terminus was experimentally supported by Gillam et al. in 2004, demonstrating that immunostaining of a hexahistidine tag fused either to the C-terminus or N-terminus of pendrin is only possible after membrane permeabilization [42]. Further supporting the intracellular localization of the C-terminus of pendrin, is the presence of a sulfate transporter antisigma factor antagonist (STAS) domain. The exact function of such domain is still to be elucidated, but it is supposed to be involved in the regulation of the transport activity *via* binding and hydrolysis of intracellular nucleotides [43]. In a comprehensive review, Dossena et al. [44] suggested a further model, predicted by the MEMSAT algorithm and adjusted according to the simple transmembrane alignment method (STAM) proposed by Shafrir and Guy [45]. Such model is characterized by 15

16

transmembrane segments with the N-terminus on the extracellular side and the C-terminus on the intracellular side (Figure 4). The 15 transmembrane segments include 2 amphipatic regions, whose localization may either be intracellular, extracellular or transmembrane, shifting therefore the number of transmembrane segments from 15 to 14 or 13.
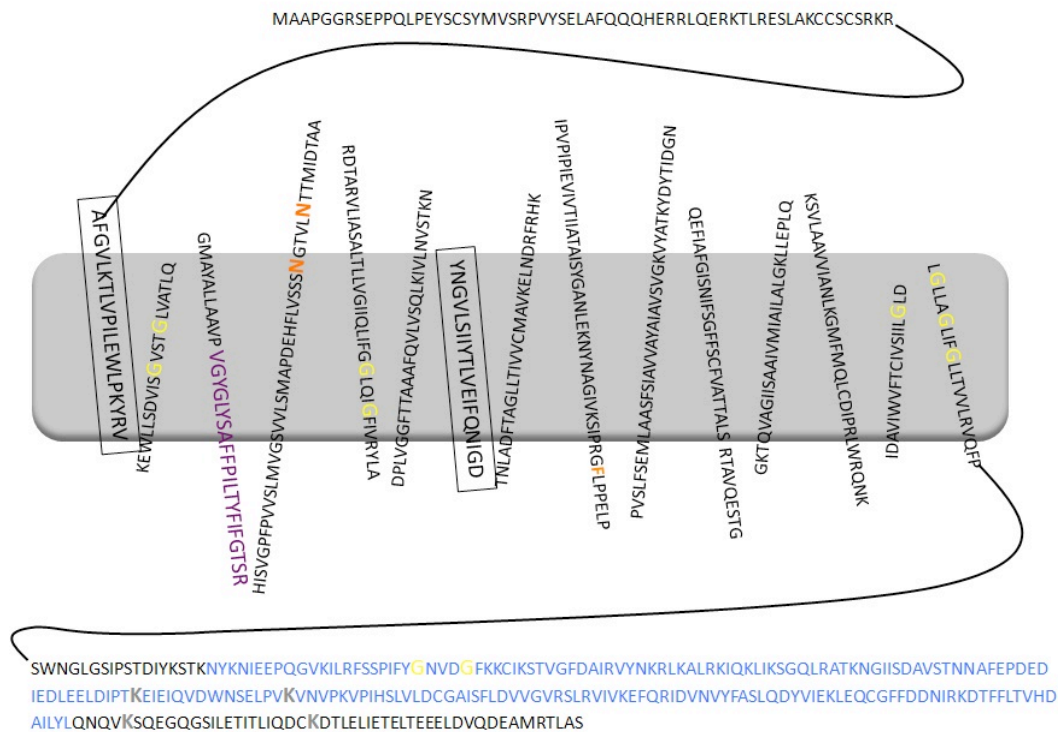
Figure 4: putative model of pendrin, as suggested by Dossena et al. in 2009, based on the algorithm MEMSAT and STAM. Highlighted features in the figure are the amphipatic segments (squared), the sulfate transport consensus sequence (purple) the glycophorin-A like motifs (yellow Gs), the STAS domain (light blue), the glycosylation sites (orange) and the polyubiquitilation sites (grey) (Modified from: Dossena, S. et al. Journal of molecular endocrinology, 2009. **43**:93-103).

It is anyhow important to point out that all of the abovementioned models are only speculative and lack of experimental validation. In the present study, I will refer to the last model described, suggested by Dossena et al. in 2009. In Figure 4, this model is graphically represented and some notable features are marked. At the C-terminus of pendrin (intracellular side), the sequence corresponding to the STAS domain is represented in light blue. In the 3rd transmembrane segment, the sulfate transport consensus sequence is marked. This sequence is present in all members of the SLC26 family of transporters, but, in the case of pendrin, it is slightly modified, consistently with the observation that pendrin, other than the other members of the family, is not reported to transport sulfate. The squared sequences correspond to the amphipatic segments, whose localization is ambiguous. The glycines marked in yellow have been recognized as

Glycophorin-A like motifs (GxxxG, where G is glicine and x any bulkier amino acid), whose presence is supposed to determine protein dimerization interfaces. In particular, the repetition in tandem of three of such motifs in the 15th transmembrane segment appears to be crucial for pendrin dimerization (Dossena and Paulmichl, manuscript in preparation). Other notable features represented on the model are 4 polyubiquitination sites at the C-terminus of the protein (highlighted in grey in Figure 4) (http://www.ubpred.org/), in accordance with the experimental observation that pendrin is targeted by poly-ubiquitination enzymes [46]. Furthermore, it was shown that pendrin is glycosylated and that such modification influences its dependence from intracellular pH. The two experimentally identified glycosylation sites, asparagine 167 and asparagine 172, are marked in orange in Figure 4 [47].

1.3   The correlation of genotype and phenotype

As previously mentioned, the main pathological issue linked to an impaired transport activity of pendrin is the development of deafness, either syndromic or non-syndromic, typically associated with an enlargement of the vestibular aqueduct detectable by computer tomography (CT) scan. Pendrin-related deafness is the most common form of syndromic hearing loss worldwide. Furthermore, pendrin is also involved in a large number of cases of non-syndromic deafness. It has been estimated that Pendred syndrome-related deafness may contribute to about 7.5 % of the reported cases of hereditary deafness [48] but the actual incidence of pendrin-related deafness has not been determined, mainly due to variable symptomatology penetrance [49]. An early diagnosis of deafness, at best within the first 6 months of life of the newborn, together with an efficient planning of the intervention, are crucial for language development and future integration of the individual in school and society, giving him/her the same chances of success of any normal hearing person [50, 51]. The intervention must include professional counseling of the family on how to deal with the diagnosed deaf baby, as well as early enrollment in specific assistance programs aimed to the development of proficient communication skills from the early age. Together with an early diagnosis, the definition of the specific genetic or environmental cause of the sensory defect is an essential step in the view of a possible counseling and intervention plan with the patient and the family, as well as for a possible therapeutical intervention, where available. For this reason, it is extremely important to develop an efficient and standardized hearing screening program for newborns [52] or, in

an ideal situation, a genetic screening, in order to determine as early as possible the chances of developing a hearing loss phenotype in correlation with the detected genotype. For what concerns pendrin-related deafness, more than 200 pendrin allelic variants have been detected so far in the deaf population worldwide (www.healthcare.uiowa.edu/labs/pendredandbor/slcMutations.htm). Some of the identified variants have been detected both in the deaf and normal hearing population, therefore candidating them to the status of benign polymorphisms. The identified mutations can be divided in aminoacidic substitutions (missense), insertions or deletions (some of which determine a frameshift and premature truncation of the protein), splice-site variants. Mutations are widespread throughout the whole pendrin coding region and promoter, and no hot-spots can be identified within the protein sequence. Despite the large number of pendrin mutations identified, in very few cases the actual role of the specific variant detected in the patient is clearly defined, as no functional test is routinely performed, preventing any clear correlation between the observed phenotype and the identified genotype. Furthermore, in those cases of functionally characterized variants, the degree of the experimentally determined functional impairment does not always reflects the severity of the observed symptoms. Symptoms related to pendrin dysfunction range from mild unilateral hearing loss to the full spectrum of defects typical of the syndrome. Furthermore, the same mutation can be found both in the deaf and in the healthy population or associated to different degrees of severity of hearing loss in different patients, therefore suggesting a more complex picture in the etiology of pendrin-related hearing defects, rather than a simple monogenic defect. The classical paradigm elaborated in the attempt of correlating genotype and phenotype stated that biallelic mutations leading to complete loss of function of the pendrin protein are necessary and sufficient for the development of Pendred syndrome, whereas those mutations leading to a reduction of function but not a complete abrogation of the transport activity were considered to be responsible for the development of non-syndromic deafness with unilateral or bilateral EVA [53]. Lately however, with the increasing number of mutations characterized on a functional level, it became clear that such a simple and linear correlation is to be excluded, and more complex genetic and environmental factors have to be taken into account [53] in order to clearly explain the phenotypic diversity of pendrin-related deafness.

For an exact identification of the cause of deafness, it is therefore necessary to consider the role played by the specific mutant together with other molecular entities (such

as transcription factors) and environmental factors (such as infections and traumas) often responsible for the aggravation of the hearing loss phenotype.

1.3.1 Functional characterization of pendrin mutations found in the Brazilian deaf population

The functional characterization of pendrin allelic variants identified in deaf patients in different populations is an essential step to define the role of pendrin in determining the hearing loss phenotype. Furthermore, the assessment of a correlation between genotype and phenotype would provide important insights in the definition of the global picture of pendrin-related deafness, as an index of the relevance of pendrin in determining the sensory defect worldwide. In this view, an efficient interplay between (i) clinical diagnosis of deafness, (ii) identification of the possible genetic determinants and (iii) validation of the role of the candidate molecular targets by means of functional and molecular tests is clearly necessary.

Thanks to the collaboration with the Center of Molecular Biology and Genetic Engineering at the State University of Campinas, Sao Paolo, Brazil (Prof. Edi Lucia Sartorato), we could access a cohort of Brazilian patients referring for deafness (with or without EVA) at the general hospital of Campinas. Our collaborators recently started a genetic screening with the aim of assessing the prevalence of the different genetic causes of deafness within the Brazilian population, or at least a portion of it. For some of the patients of this cohort, mutations in the pendrin coding sequence were found. We then performed the functional and molecular characterization of pendrin allelic variants detected in this cohort in order to assess the specific role of pendrin in determining deafness, *i.e.* to discriminate between pathological mutations and benign polymorphisms. In Brazil, about 18 million people, corresponding approximately to 9% of the population, are recognized with a degree of hearing impairment. Both genetic and environmental factors (mainly rubella infection, perinatal anoxia and meningitis) account for the development of deafness [54], with the environmental causes having a major role on the incidence of the sensory defect, especially in those vast areas of the country that lack an efficient health care system. The recent improvement of the health system throughout the country is rapidly increasing the impact of genetic factors with respect to the environmental ones, calling therefore for a greater attention in the investigation of the genetic causes of the disease.

However, the genetic factors determining the development of deafness are still poorly investigated in Brazil, and the interest in pendrin-related syndromic and non-syndromic deafness is almost a complete novelty. Before the present study, very little was known on the etiology of deafness in Brazil, especially regarding the role and incidence of pendrin mutations in the sensory defect [55]. For what concerns the specific role of pendrin in determining deafness in Brazil, only isolated cases of mutations [55, 56] in the pendrin coding gene (*SLC26A4)* have been reported in the literature so far (the truncations 96X, 430X and 453X, the missense mutations F667C, G497S and I490L and the single nucleotide deletion of a thymine at the position 1197 of pendrin mRNA, resulting in a premature truncation of the protein) [55-57], and for none of them a functional characterization of the corresponding protein variants was performed. This work is therefore the first aiming to the functional and molecular characterization of pendrin variants detected in Brazilian deaf patients, and may therefore contribute to spread light on the genetic determinants of deafness in this population.

Deafness is the most common sensory defect in developed countries, estimated to affect one in 500 newborns [58]. It can be either syndromic (*e.g.* associated with pathological defects outside the hearing organ) or, in most cases, non-syndromic. More than 50% of the reported cases of deafness worldwide are attributed to the so-called DFNB1 disorder, caused by mutations in the connexin-26 and connexin-30 coding genes, respectively the gap junction proteins B2 and B6 (*GJB2* and *GJB6*) [59]. Altogether, more than 80 different genetic loci and 30 genes are expected to contribute to the development of some degree of hearing loss, with different prevalence in different populations. The genetic screening carried out by our collaborators focused on the most common deafness-related genes, taking into account both syndromic and non-syndromic forms of deafness, as described in the following. The first target gene considered was the connexin-26 coding gene *GJB2*, known to be responsible for the majority of cases of non-syndromic deafness in the Brazilian and ethnically related (Spanish, Italian, Portuguese) populations [60]. As a first step, the *GJB2* coding region containing the most common deafness-causing mutation, *i.e.* a deletion of a guanine at position 35 of the transcript (35delG) [61], was sequenced and analyzed. The presence of this particular deletion causes a frame shift in the open reading frame and creates a premature STOP codon, leading to the production of a truncated form of the protein. The truncated protein resulting from the deletion is unable to homo- and/or hetero-dimerize and cannot form a functional gap-junction

between neighboring cells, resulting in an impaired intercellular potassium flux in the cochlea, essential for hearing function [62]. In those cases where no 35delG mutation could be identified, the whole *GJB2* coding sequence was sequenced and analyzed, looking for other possible mutations in different regions of the gene. Mutations other than 35delG are much less frequent but may still account for a number of cases of non-syndromic hearing loss [63]. If no mutations were found in the whole *GJB2* coding sequence, the further step consisted in the screening of the second most common deafness-causing gene, *GJB6*, coding for a functionally related gap-junction-forming protein, connexin-30. The analysis of the *GJB6* gene was specifically focused on the identification of two common genomic deletions, *i.e.* del(GJB6-D13S1830) and del(GJB6-D13S1854) [64], resulting in a lack of expression of connexin-30. If neither mutations in *GJB2* nor the two *GJB6* genomic deletions were detected, the further step was the sequencing of the mitochondrial encoded 12S RNA, *MTRNR1*, with the aim of verifying the presence of the nucleotidic substitution A1555G, a mutation found to be related to aminoglycoside-induced and/or non-syndromic deafness [65]. When the molecular cause of deafness could not be identified in a defect of the aforementioned genes, other known deafness-related genes have been sequenced and analyzed, with a particular attention to the pendrin coding gene, *SLC26A4*, as one of the most common genetic causes of syndromic deafness.

The sequencing of the 20 coding exons of *SLC26A4* involved a total of 58 deaf patients (30 females and 28 males aged between 4 and 55 years) divided in two groups according to the recorded diagnosis: a first group of 26 patients diagnosed deaf with an enlargement of the vestibular aqueduct (EVA) observed *via* CT scan, while a second group of 32 patients identified as deaf, but without any over-the-threshold enlargement of the vestibular aqueduct. Sequencing and analysis of the *SLC26A4* coding region of the patients in the abovementioned two groups lead to the identification of 14 different allelic variants [66], including 11 known (the missense mutations T193I, R409H, T410M, Q413R, L445W, V609G, R776C and V138F, the deletion del297T and the splice site mutations IVS15+5G>A and IVS8+1G>A) and 3 novel (P142L, G149R and C282Y) mutations (Table 1). Some of the known allelic variants had already been functionally and/or molecularly characterized and have been identified as disease-causing mutations, while 6 of the identified mutations had not yet been characterized, neither functionally nor molecularly, and were included in the present study. In addition, the aminoacidic substitution R776C

was included in the study because controversial results regarding its transport ability are present in the literature [67, 68] (further details on the genetic screening are given in the next section). In order to determine whether the uncharacterized *SLC26A4* allelic variants identified in this screening do have a role in the development of deafness in this cohort, a functional characterization has been performed in our laboratory by means of the fluorometric method developed by Dossena et al. in 2006. This method requires the co-transfection in human embryonic kidney (HEK) 293 Phoenix cells of the cDNA coding for the wild type or mutant form of pendrin and a fluorophore (a modified enhanced yellow fluorescent protein, EYFP) sensitive to the intracellular iodide concentration (see Methods for further details) [69].

1.3.2 Outcome of genetic screening of the pendrin coding region in a cohort of Brazilian deaf patients

As previously mentioned, the genetic screening was carried on by our collaborators at the State University of Campinas on a group of 58 deaf patients, 26 patients with and 32 patients without EVA. The sequencing and analysis of the coding region of pendrin in the selected individuals led to the identification of 14 patients bearing mutations in the pendrin coding sequence (Table 1). 9 of these patients belong to the group of deaf individuals with EVA and 5 patients belong to the group with no EVA. The identified pendrin allelic variants can be divided in 11 missense mutations leading to an aminoacidic substitution (P142L, G149R, T193I, R409H, T410M, Q413R, L445W, V609G, R776C, V138F and C282Y), 2 splice site mutations (IVS15+5G>A and IVS8+1G>A) and 1 single residue deletion (del297T), leading to a premature truncation of the protein after the first transmembrane segment (Table 1). Eight of the missense mutations identified (T193I, R409H, T410M, Q413R, V138F, L445W, V609G, R776C) have already been reported in the literature and in part characterized by us or others [67, 68, 70-73]; P142L and G149R were firstly identified in this screening and published in 2013 by de Moraes et al. [66] but in that particular study they were not characterized neither on a functional nor on a molecular level. One allelic variant, namely C282Y, is instead completely novel, neither communicated nor characterized previously. 6 of the identified variants (G149R, T193I, V609G, R776C, V138F, C282Y) were detected in heterozygosis with the wild type allele in 9 patients, while in 4 patients (21AA, 02AA, 06AA, 23AA) pendrin variants were detected in compound heterozygosis (*i.e.* both alleles are mutated and the two mutations are

different from each other). Interestingly, the aminoacidic substitution V609G has been detected in heterozygosis with the wild type allele both in deaf patients presenting EVA and in deaf patients with no EVA. In patient 22AA, the R409H mutation was found in homozygosis (*i.e.* both pendrin alleles show the same mutation). In patients C26 and L1AA, monoallelic pendrin mutations were detected in combination with a monoallelic mutation (35delG) in *GJB2*, the connexin-26 coding gene previously sequenced. The question marks reported in Table 1 identify the detected allelic variants of pendrin lacking a functional and/or molecular characterization in the present literature and therefore preventing a complete genetic diagnosis of the sensory defect in that specific patient. Importantly, total expression levels were never investigated for pendrin variants. In Figure 5 the distribution of the aminoacidic substitutions identified in the cohort are reported on the putative model of pendrin suggested by Dossena et al. in 2009.

Patient (n=58)	Nucleotide substitution	Aminoacid substitution	Patient Genotype (coding region)	Goiter	Function	Localiz.
Patients deaf *with EVA* (n=26)						
21AA	425C>T	P142L	P142L/del 297T	No	?	?
16AA	446G>A	G149R	G149R/WT	No	?	?
18AA	578C>T	T193I	T193I/WT	No	?	?
22AA	1226G>A	R409H	R409H/R409H	No	lost/red. [74]	partially PM
02AA	1229C>T	T410M	T410M/IVS15+5G>A	No	lost [73]	ER [73]
06AA	1238A>G	Q413R	Q413R/V138F	No	?	?
23AA	1334T>G	L445W	L445W/IVS8+1G>A	Yes	?	?
L1AA	1286T>G	V609G	V609G/WT *	No	reduced [71]	?
15AA	2326C>T	R776C	R776C/WT	No	?	?
Patients deaf *without EVA* (n=32)						
C15	412G>T	V138F	V138F/WT	No	lost [73]	ER [73]
C26	845G>A	C282Y	C282Y/WT *	No	?	?
C01	1286T>G	V609G	V609G/WT	No	reduced [71]	?
C04	1286T>G	V609G	V609G/WT	No	reduced [71]	?
C09	1286T>G	V609G	V609G/WT	No	reduced [71]	?

Table 1: Genetic analysis of pendrin coding region in 58 deaf patients performed at the hospital of Campinas, Sao Paolo, Brazil; *: a mono allelic mutation (35delG) in the connexin-26 gene, *GJB2,* was also found; ?: non-characterized feature.
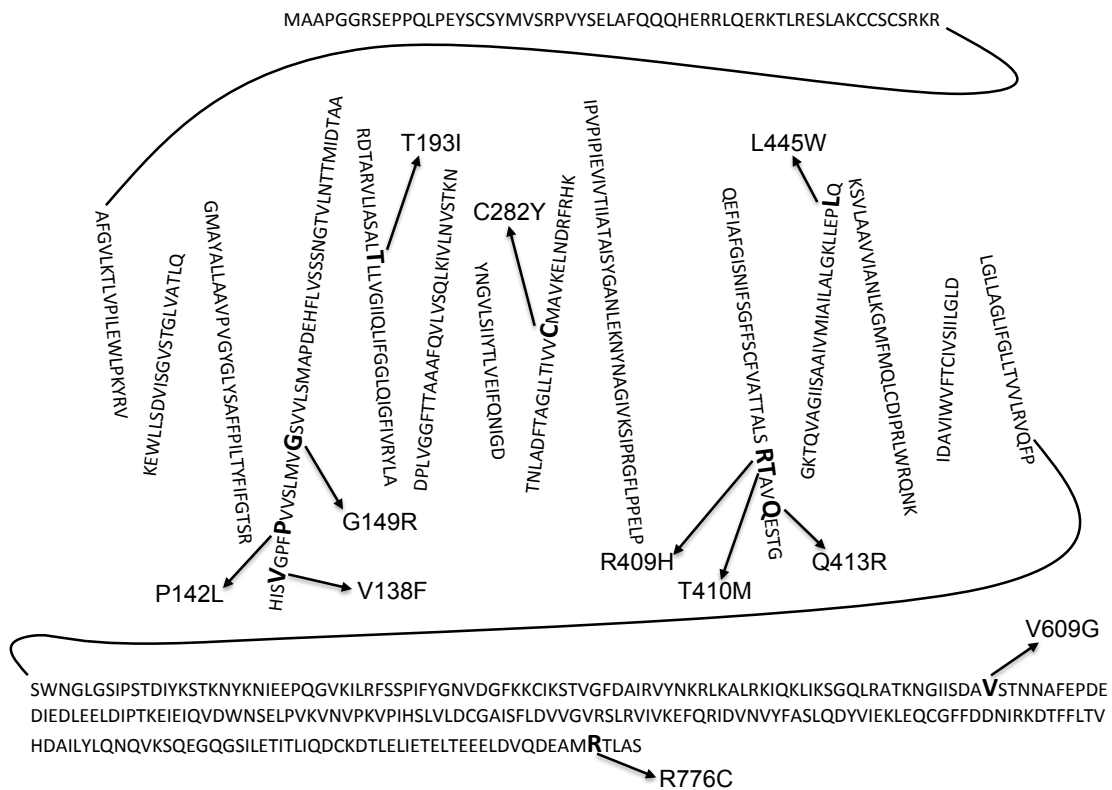
Figure 5: Putative structure of pendrin showing the distribution of the mutations identified in the cohort of Brazilian deaf patients (Modified from: Dossena, S. et al. Journal of molecular endocrinology, 2009. **43**:93-103).

1.3.3 Subcellular localization and expression levels of pendrin variants

The functional characterization of pendrin variants is the key for determining the actual degree of impairment in the transport activity of mutated forms of the protein. Such knowledge is necessary for discriminating between protein variants with loss or reduction of function (mutations, potentially disease-causing) and variants with no functional impairment (benign polymorphisms).

In order to define the actual molecular defect resulting in the experimentally determined degree of functional impairment, it is necessary to analyze further the specific mutant forms. The next step in the analysis and definition of the potentially pathogenic variants of pendrin is therefore the characterization of their specific molecular defect by determining their (i) subcellular localization and (ii) abundance in the cell.

A mutant isoform may undergo different destinies, according to the type of molecular defect. A specific mutation may:

(I)   determine a misfolding of the protein, preventing its correct trafficking to the plasma membrane (PM) and leading to its accumulation in an immature form in the endoplasmic reticulum (ER) and possibly to its degradation;

(II)   impair the transport activity *per se* without disrupting the correct folding and trafficking of the protein to the PM; this is the case of mutations affecting the ion binding sites.

(III)   interfere with the correct insertion of the polypeptide in the PM and/or its proper function, disrupting its interaction with other molecular entities, such as chaperones, cytoskeletal elements, regulatory proteins.

The definition of the subcellular localization and abundance of the different pendrin variants, in combination with the related functional data, can deliver precious information regarding the specific type of molecular defect conferred by a specific aminoacidic substitution. Such knowledge can then drive the effort in the difficult challenge of investigating a possible mechanism for rescuing the transport activity of hypo-functional or non-functional proteins. Those mutants that are retained in the ER, may still be capable of an efficient ion transport if degradation is circumvented and/or folding is assisted pharmacologically. On the other side, mutants that show a partial trafficking to the plasma membrane may instead be potentiated in order to recover part of their transport activity. In the next chapters the "rescuing issue" and its possible approaches will be discussed more in detail.

1.3.4 Rescuing of pendrin activity

Retention of the mutated forms of pendrin in the intracellular compartments is considered the main mechanism leading to the phenotype observed in many patients affected by syndromic and non-syndromic pendrin-related deafness [75]. Defective variants of pendrin cannot properly fold in the mature form of the transporter and are therefore retained in the ER, preventing their correct trafficking to the PM. The degradation of misfolded proteins mainly takes place in the complex called proteasome, where the defective polypeptide chain is chopped in small pieces by multiple enzymatic subunits

within the core of the complex [76]. An alternative pathway of degradation active in the cell involves the lysosomal enzymatic digestion [77]. This pathway is particularly active in degrading membrane proteins and phagocytized products but it also finds a role in the degradation of misfolded protein together with the proteasome complex. In this sense, for an effective modulation of the degradation/folding of mutant protein it is necessary to consider also this alternative pathway.

The processing of newly synthesized proteins in the ER is driven through a number of checkpoints where the correct folding of the polypeptide is verified. Failure to pass any of the checkpoints leads to the arrest of the further maturation of the protein and activation of folding assisting mechanisms [76]. Accumulation of misfolded proteins in the ER induces the activation of a series of stress response mechanisms altogether termed the unfolded protein response (UPR), eventually leading to the activation of the ER associated degradation (ERAD) pathway [78]. In order to prevent excessive stress in the ER, different pathways can be activated. An ER-stress counteracting mechanism involves the expression of molecular chaperones in order to assist the correct and functional folding of the retained proteins [79]. The folding of a protein is assisted by a number of molecular chaperones along its pathway of maturation, activated according to the detected level of impairment. A second opportunity to reduce the ER stress is the stimulation of phospholipids synthesis and enlargement of the ER, necessary for the enhancement of its folding capacity [76, 80]. If the correct folding of the proteins accumulated in the ER is no more achievable or is too energy consuming, the misfolded polypeptide undergoes the poly-ubiquitination process, ultimately leading to the degradation in the 26S proteasome complex [76, 81]. Poly-ubiquitination of proteins is a three step process carried out by three different enzymes transferring ubiquitin molecules on specific residues on the polypeptide to be targeted to the proteasomal degradation. The first step of the process involves the activation of the ubiquitin molecule by a ubiquitin-activating-enzyme (E1) in an ATP-dependent fashion [82]. The activated ubiquitin molecule is then bound by a ubiquitin-conjugating enzyme (E2) also called ubiquitin-carrier enzyme. E2 enzymes are responsible for transferring the ubiquitin molecule to the target protein, and finally, together with ubiquitin-ligase enzymes (E3), covalently bind the activated ubiquitin to a lysine of the polypeptide to be degraded. Many different E3 enzymes have been identified, with a high specificity for different target proteins, whereas much fewer different E2 enzymes and still fewer E1 enzymes have been identified in genome-wide analysis [83]. Ultimately, if the

accumulation of misfolded proteins and the correlated ER stress cannot be overcome and reduced by any of the mentioned mechanisms, the overproduction of reactive oxygen species (ROS) resulting from the ER forced hyperactivity leads to the activation of the final rescue mechanism, namely the apoptotic cell death, in order to prevent any further damage to the system [76, 84]. Defective and mutant proteins are often misfolded and retained in the ER lumen, triggering all of the above mentioned stress response mechanisms, and ultimately targeted for degradation. Ameliorating specific folding mechanisms and/or circumventing protein degradation may be the key for a targeted functional recovery of the activity of a protein of interest.

The possibility to rescue the activity of pendrin hypo-functional and non-functional mutants has been considered and explored so far only in a small number of studies [85, 86]. Ishihara et al. managed to rescue the trafficking to the PM and a partial ion transport activity of 4 pendrin mutants (P123S, M147V, S657Y and H723R) by treatment with 10 mM salicylate [85]. The ability of salicylate to influence protein folding and maturation had been previously shown with regard to a paralogue of pendrin, SLC26A5 or prestin [87]. The same treatment was shown to be ineffective on the surface expression and activity of other 4 pendrin mutants (A372V, N392Y, S666F and T721M). Yoon et al. have shown the efficient recovery of Cl^-/HCO_3^- exchange activity and protein abundance at the PM of pendrin H723R after incubation of transfected cells at low temperature and treatment with the histone deacetylase inhibitor Na^+-butyrate. In this study, the same approach was applied to another pendrin mutant variant, namely L236P, but neither functional nor molecular rescue could be observed [86]. Both studies clearly showed the heterogeneity in the processing of the different mutant forms of pendrin and their unique behavior. Such heterogeneity observed at the functional and molecular level reflects the high variability of phenotype severity observed in deaf patients displaying different mutant variants of pendrin. This heterogeneity may not allow for a unique approach toward a possible rescue of the transport activity of different pendrin mutants.

In that light, the functional and molecular characterization of defective pendrin allelic variants identified in the deaf population is a crucial piece of information in the view of a possible therapeutic approach against deafness caused by absent or reduced transport function of pendrin. In particular, the identification of mutant variants *per se* functional but mostly retained in the ER and eventually degraded results particularly interesting in driving

a possible therapeutical approach toward the inhibition of the degradation pathway and the assistance of proper folding.

1.3.5 Other genetic and molecular determinants of deafness

In 7 patients from the cohort subject of the study, deafness was reported in association to monoallelic pendrin mutations (Table 1). In these cases, monoallelic pendrin mutations may or may not be enough for determining deafness and other genetic defects or environmental factors may be involved in the development of deafness.

The hearing loss phenotype may be related to a possible double heterozygosity, a condition where monoallelic pendrin mutations are found in combination with monoallelic mutations in other genes known to be involved in the sensory defect, such as the pendrin transcription factor *FOXI1* or the potassium channel *KCNJ10* [88, 89]. In the cohort of deaf patients analyzed in the present study, both *FOXI1* and *KCNJ10* genes have been sequenced and have been found in the wild type form, therefore excluding their role in determining deafness in this particular cohort. It is as well possible that mutations within the pendrin promoter region, or the 3' untranslated region may influence the expression of the protein and therefore contribute to the development of the diagnosed phenotype.

It is common opinion that it is necessary a bi-allelic pendrin mutation in order to observe the full spectrum of hearing defects characteristic of Pendred syndrome. Nonetheless, many reported cases are characterized by a severe deafness phenotype associated with monoallelic pendrin mutations [53, 67]. In some cases the determining cause of the observed degree of deafness may be due to other genetic or environmental factors, as discussed in the previous section.

1.4   Functional screening of pendrin ligands

1.4.1 Role of pendrin overexpression and hyper-activity and the need for a specific inhibitor

As mentioned in the previous sections, deregulation of pendrin activity is associated with different pathological states, not only in the case of a loss or reduction of the transport function but also in those situation characterized by an over-expression and over-function of the transporter. In this regard, multiple studies in the last decade have shown that an increased expression and/or activity of pendrin may be associated with a number of pathologies, ranging from hypertension [29] to airway distresses such as asthma and COPD [40, 90].

Even though no correlation between pendrin mutations with gain of function and development of a hypertensive phenotype could be determined so far, the involvement of pendrin in the salt reabsorption in the distal section of the nephron has been shown in a number of studies [4, 13, 91].

In the kidney, the transporter is mainly expressed in the distal convoluted tubule (DCT), in the connecting tubule (CNT) and in the apical membrane of beta- and non-α-non-β-intercalated cells of the collecting duct (CD), where it has been shown to participate in the Cl^-/HCO_3^- exchange [4]. Pendrin exchange activity contributes therefore to the regulation of systemic pH on one side, and to the reabsorption of Cl^- on the other. Royaux et al. demonstrated pendrin being the major responsible for Cl^- reabsorption in the distal section of the nephron and in particular in the CD [92]. Cl^- reabsorption in the beta-intercalated cells of the CD is coupled to the reabsorption of Na^+ in the principal cells *via* ENaC, or *via* an alternative transporter [93], resulting in the movement of NaCl from the urine to the blood, followed by water, therefore regulating fluid volume and ultimately blood pressure [94]. The expression of pendrin in the kidney has been shown to be upregulated by aldosterone analogues [11] and angiotensin II [95]. Pendrin involvement in fluid volume homeostasis in the kidney is further supported by the observation that pendrin knock-out mice, even if not showing any abnormality at the basal state, submitted to NaCl restriction result in a severe Cl^- wasting phenotype and development of hypotension [33].

Furthermore, the same mice, treated with the aldosterone analogue deoxycocorticosterone pivalate (DOCP), developed metabolic alkalosis due to a complete lack of HCO_3^- secretion and resulted protected against aldosterone analogue-induced hypertension. In the same study it was shown that a moderate NaCl restriction is associated with an increase in pendrin expression at the apical side of beta-intercalated cells in the CD, probably as a compensatory mechanism. Increased chloride reabsorption associated with an increased pendrin expression in the distal section of the nephron could also be directly or indirectly coupled to an increased sodium reabsorption via other transporters or channels [11]. Supporting this hypothesis, Kim et al. have shown that lack of pendrin expression is associated with a decrease in the expression level of ENaC upon aldosterone stimulation, possibly due to the alkalosis resulting from the absence of pendrin-dependent HCO_3^- secretion [94], thus further supporting pendrin crucial role in NaCl reabsorption and blood pressure regulation.

In the airways, an increased expression of pendrin at the bronchial level possibly contributes to the development and exacerbation of symptoms of asthma and COPD [5]. An abnormal Cl^-/HCO_3^- transport activity is associated with an increase in chloride reabsorption followed by water. Pendrin hyperactivity leads therefore to a reduction in airway surface liquid (ASL) thickness and fluidity as the consequence of the increased water reabsorption [96]. A separate study shows that pendrin overexpression is associated with an increased mucus production [90] (Figure 6). The reduction of ASL thickness and the increase in mucus production may in turn exacerbate the symptoms of asthma as well as the diffusion of the inflammatory state and bacterial infections.

On the other side, pendrin has been shown to contribute to the transport of thiocyanate into the ASL [34]. In the presence of hydrogen peroxide (H_2O_2), generated by the dual NAPDH oxidase (DUOX), thiocyanate is then oxidize to hypothiocyanate, known to exert an antimicrobial action (Figure 6). The expression of pendrin in the airways is regulated by stimulation with pro-inflammatory cytokines, and in particular by the action of interleukins 4 and 13 *via* the STAT-6 transcription regulation pathway [12, 34, 40].
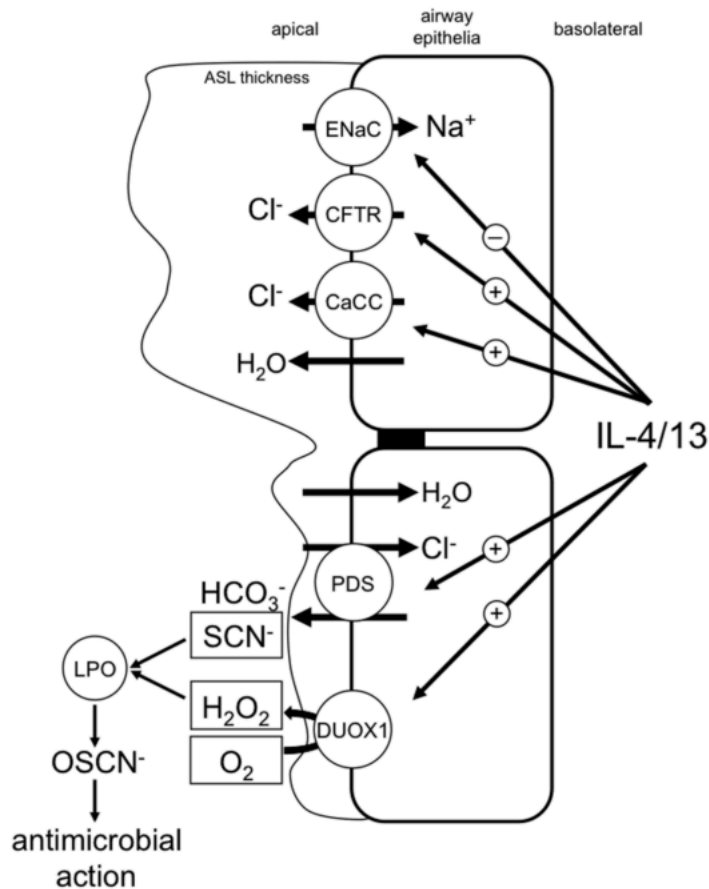
Figure 6: Pendrin in the airways. The expression of pendrin in the airways is stimulated by the pro-inflammatory cytokines IL-4 and IL-13. An increase in the transport activity of pendrin leads to the reduction of airway surface liquid thickness and increase mucus production. On the other side, pendrin is also responsible for the transport of thyocianate into the ASL. Thyocianate is then oxidized by H_2O_2 produced by DUOX, to produce the anti-microbic hypothiacyanate (Nofziger, C. et al. Cellular Physiology and Biochemistry, 2011. **28**:571-578).

In addition to an increased expression, also an increased intrinsic activity may lead to pendrin hyper-function. Indeed, gain of function mutations (*i.e.* showing and enhanced ion transport activity) of pendrin have been recently identified [71]. The existence of such hyper-functional forms of the transporter may be linked to the development of the pathological states just described.

The need for a specific inhibitor becomes therefore clear when facing such pathological issues linked to a hyper-function/overexpression of the transporter. Pendrin constitutes a potential key target for the treatment of common pathological conditions such as bronchial asthma and hypertension, and the identification of a specific inhibitor is becoming a pressing issue. Some compounds showing an inhibitory effect on pendrin activity have indeed been identified but none of them is specific [97, 98].

One of the goals of my research activity is the identification and characterization of new inhibitors of pendrin by functional screening of different compounds, selected among (i) substances with known inhibitory activity on transporters evolutionarily related to pendrin as well as (ii) diuretics and anti-hypertensive agents and (iii) small ligand molecules predicted via informatics tools (described more in detail in the following section). Possible side effects of a pendrin inhibitor on the inner ear, which would theoretically lead to hearing damages similar to those observed in Pendred patients, can be excluded since the role of the transporter seems to be limited to the completion of organogenesis of the hearing system [18], while an essential function later in the development has not been proven. Even though these results have been shown in mice pups, it is reasonable to imagine a similar situation in humans.

1.4.2 Selection of putative pendrin ligands for the functional screening

The role of pendrin in the maintenance of ionic homeostasis in different biological compartments and its involvement in a number of pathologies suggests that this protein may be regarded to as an interesting and novel pharmacological target for different diseases. So far, no specific pendrin inhibitor or modulator could be identified, and even a high throughput screening of a large library of compounds failed in identifying new ligands for the transporter [34]. As mentioned in the previous section, few active compounds have indeed been identified, but none of them is specific for pendrin, and for some of them the actual efficacy is matter of debate. In particular, 4,4'-Diisothiocyano-2.2'-stilbenedisulfonic acid (DIDS), furosemide and probenecid at the concentration of 1 mM have been shown to inhibit the activity of the transporter both when expressed in *Xenopus laevis* oocytes [99], and in HEK 293 cells [100]. Evidences of an inhibitory activity of 5-Nitro-2-(3-phenylamino)benzoic acid (NPPB) and niflumic acid have been shown in Human Embryonic Kidney (HEK) 293 Phoenix cells [97].

The search for pendrin ligands aims to the identification of chemical compounds (both inhibitors and activators/enhancers) capable of modulating the activity of the transporter. Inhibitors of pendrin activity may be an extremely useful therapeutic approach

for controlling hypertension and exacerbations of asthma and other respiratory distresses. On the other hand, an activator of pendrin activity may help developing a therapy circumventing or reducing hearing loss and/or thyroid dysfunction in patients with pendrin mutations.

The functional screening of putative pendrin ligands can be efficiently carried out with the fluorometric method developed by Dossena et al. in 2006 and adapted for the use with a 96 well plate reader [69, 71, 101] (see Methods section for further details). As already mentioned, high-throughput screenings of large libraries of chemicals failed in identifying new pendrin inhibitors [34]. Our approach is therefore a more focused one, and requires a preliminary careful selection of a relatively small number of candidate compounds to be tested for their effect on pendrin activity *in vitro*.

The selected compounds were classified, according to the rationale driving their choice for the screening, into three different groups:

- a first group includes known inhibitors of anion exchangers or channels, including substances with a known effect on homologues of pendrin, in particular inhibitors of *Slc26a3,* also known as downregulated in adenoma (DRA);

- a second group includes more or less commonly used antihypertensive and diuretic agents. This choice was driven by the evidence that pendrin plays a crucial role in the regulation of blood pressure in the kidney;

- a third group of compounds emerges from a different rationale; candidates in this group have been identified by means of a bioinformatics approach called meta-analysis (described more in detail in the following section). This bioinformatics approach has been set up and delivered to us by Prof. R. Konrat, from the institute of Biochemistry & Biophysics, Structural & Computational Biology, University of Vienna (Austria).

In the following sections the individual groups of compounds selected for the screening are discussed more in detail.

1.4.2.1   Inhibitors of anion exchangers and anion channels

The closest homologue of pendrin is a member of the same SLC26 transporter family, namely *Slc26a3,* also known as DRA. The two proteins show a 44% of identity and a 60% of similarity.

DRA is an anion exchanger responsible for the transport of Cl^- and bicarbonate, as well as sulfate and oxalate. It is mainly expressed in the apical side of enterocytes of the proximal section of the colon [102] and in the duodenum [103], where it contributes to fluid reabsorption by mediating Cl^-/Cl^- and Cl^-/HCO_3^- exchange [104]. A loss of transporter function leads to congenital chloride-losing-diarrhea (CLD), characterized by loss of a large amount of fluid in the stool and disruption of the intestinal mucosa adherence [105]. Chernova et al. characterized the pharmacological profile of DRA identifying the inhibitory effect, among others, of two anti-inflammatory drugs, namely niflumic acid and tenidap. Both drugs are known to lower the intracellular pH (lowering the intracellular pH may inhibit the bicarbonate secretion *per se*), but it could be shown, especially for what concerns tenidap, that the inhibitory effect is independent from the acidification of the cytosolic environment [106]. In a different study, Lamprecht et al. showed that the anti-diabetic drug glibenclamide was also effective in reducing the Cl^- transport activity of DRA in Caco-2 cells [107]. Even if the two transporters, DRA and pendrin, show a different ion selectivity, (DRA is capable of transporting both monovalent and divalent anions while pendrin only monovalent anions) their relatively high sequence similarity allows for the speculation of a possible common pharmacological profile.

Other unselective inhibitors of anion exchangers and anion channels have been included in the screening, such as the anion exchanger blocker DIDS, the cystic fibrosis transmembrane conductance regulator (CFTR) inhibitor 172 (CFTR inh-172) and the chloride channel blocker 5-nitro-2-(3-phenylpropylamino)benzoic acid (NPPB).

Some of the tested compounds have already been tested on pendrin at different concentration [35], but were nonetheless included in the present study.

1.4.2.2   Diuretic and antihypertensive agents

The role played by pendrin in salt reabsorption and blood pressure regulation in the kidney candidates the transporter as a possible novel target for diuretic and anti-hypertensive therapy. Also, the observed effect of some known diuretic agents may be due, at least partially, to an inhibitory effect on pendrin transport activity. For instance, a thiazide-sensitive NaCl reabsorption is still present in $\underline{Na}^+$-$\underline{Cl}^-$-$\underline{c}$otransporter (NCC) knock-out mice [93] and may be due to pendrin. It is therefore not to be excluded that common diuretic and antihypertensive agents may modulate pendrin in addition to the classical target. Including diuretics in the functional screening may deliver precious information regarding the contribution of pendrin in blood pressure regulation and add novel information on the mechanism of action of known diuretics. Common diuretic and antihypertensive agents act by blocking transepithelial ion transport in the nephron, reducing therefore the consequent water movement from the urine into the bloodstream. This results in a decrease in plasma volume and blood pressure and, on the other side, in an increase of urine volume (diuresis).

Typical diuretic agents used in the treatment of hypertension are:

i)   the thiazides, acting on ion transport in the DCT;

ii)   aldosterone and vasopressin antagonists, reducing NaCl reabsorption in the CD;

iii)   acetazolamide, reducing NaCl reabsorption in the proximal tubule;

iv)   the so called loop diuretics (furosemide, bumetanide), acting on the ion transport mainly in the thick ascending limb of the loop of Henle [108, 109].

The known molecular targets of the mentioned diuretic agents are, respectively:

i)   the Na^+-Cl^--cotransporter (NCC) in the DCT;

ii)   the epithelial Na^+ channel (ENaC) in the CD;

iii)   the enzyme carbonic anhydrase and, indirectly, the Na^+/H^+ exchanger;

iv)   the Na^+-K^+-$2Cl^-$ cotransporter 2 (NKCC2) in the thick ascending limb of the Henle loop [110].

1.4.2.3   Protein meta-structure similarity clustering

The identification of putative ligands for a target protein often makes use of bioinformatics approaches and in particular of alignment algorithms aimed to the definition of similarity clusters of proteins sharing significant sequence/structural patterns. Proteins showing a significant aminoacidic sequence or structural similarity are often also sharing affinity for common ligands and interaction partners [111].

Most classical alignment approaches are based on the primary aminoacidic sequence of a protein in order to identify homology with other polypeptides. The risk in primary sequence alignment is the loss of potentially interesting partners that do not share a similar aminoacidic sequence but whose three-dimensional organization may still have a significant homology. In this view, one of the most established trends in similarity analysis nowadays is focusing on protein similarities on a structural level. Based on the observation that structural motifs are more conserved than primary amino-acidic sequences, the alignment of three-dimensional structures promises to be extremely useful when looking for similarities between proteins, in particular concerning the issue of ligand discovery. It has been shown that proteins sharing a similar 3D structure or similar domains often also share affinity for the same ligands [111]. Such a structural approach requires the definition of the three-dimensional structure of the protein of interest in order to be aligned with a database of structurally characterized proteins. Unfortunately, in many cases an experimentally defined structure is not available, especially when working with membrane proteins as pendrin. Due to their intrinsic flexibility and instability in aqueous media, the most common methods for structural analysis, crystallography and nuclear magnetic resonance (NMR), are often inapplicable. Lacking a full-length three-dimensional structure of our protein of interest, it is impossible to perform a classical structural alignment in order to predict putative binding molecules on a structural basis. It is therefore necessary the elaboration of a suitable alternative approach, in order to circumvent the lack of a defined three-dimensional structure. A very promising alternative approach is the so-called meta-analysis.

Meta-analysis is a bioinformatic approach aimed to the definition of a protein topology based on its primary amino acid sequence, without any knowledge regarding the three-dimensional structure of the protein of interest [112]. In order to do so, the interaction

probability of any given pair of residues within the target protein is calculated according to the formula $\rho(\theta, A, B, l_{AB})$, where θ represent the shortest path length observed between the two residues, A and B define the characteristic of the two specific residues involved in the interaction and l_{AB} is their distance on the primary aminoacidic sequence of the protein of interest. The probability formula is based on the analysis and extrapolation of structural information collected from a number of characterized protein templates, in particular it is derived from the observation of actual inter-residues interactions within structurally defined proteins from the protein data base (PDB). The collection of all the probability values calculated for any residue pair within the target protein results in a network of more or less probable intramolecular interactions. Such a collection allows for the prediction of a putative 3D-structure of the protein of interest. The algorithm delivers information regarding the compactness of domains and regions within the target protein, and the local organization in secondary structure elements (alpha-helices and beta-sheets).

Defined compactness values vary from 0 upwards and deliver information regarding how exposed different portions of the polypeptide are expected to be in the global 3D arrangement of the protein, telling us whether they are expected to be buried within the core of the protein or more exposed to the surface and to the solvent. A high compactness value is typically associated with residues buried in the interior of the protein structure, whereas values close to 0 are typical of residues located in more exposed and flexible regions or even disordered regions of the protein (Figure 7b). A further information delivered by the calculated probability function is the local secondary structure organization of the protein. Considering only short distance interactions (l_{AB}<5), the algorithm gives information regarding the local organization in alpha-helices, beta-sheets or disordered regions. Positive values of this function are typically associated with more compact structures, such as alpha helices, whereas negative values are typical for residues located in more relaxed and extended regions, typically beta-sheets conformations (Figure 7a).

The meta-structure of a protein is defined as the combination of information regarding local secondary structure organization and residue compactness throughout the whole polypeptide.
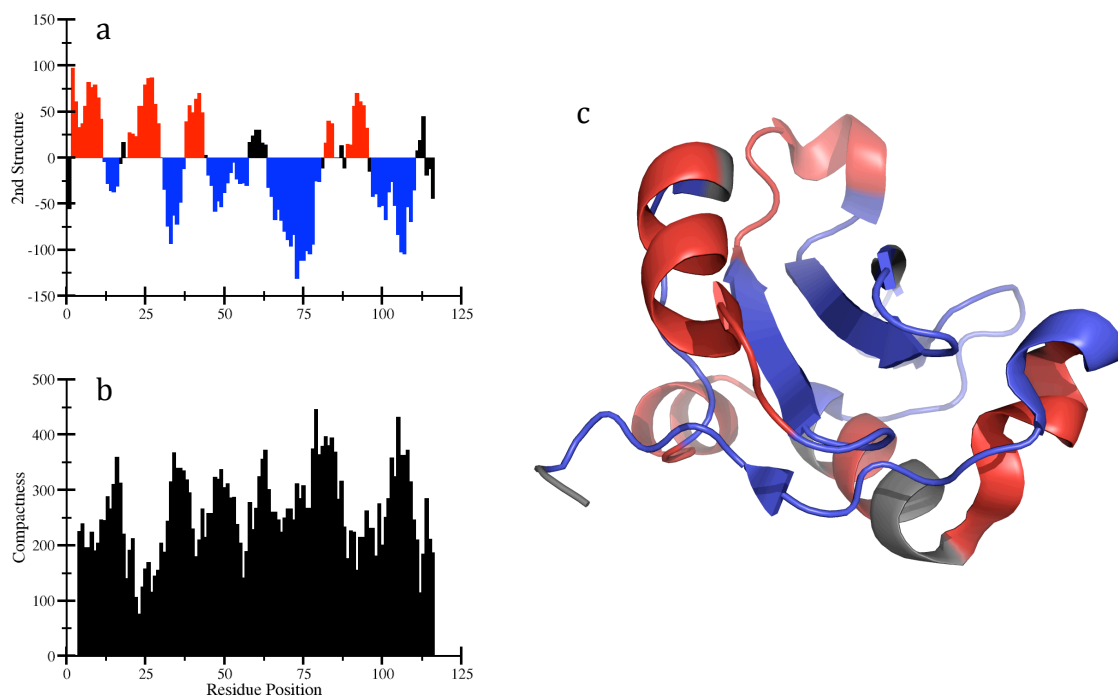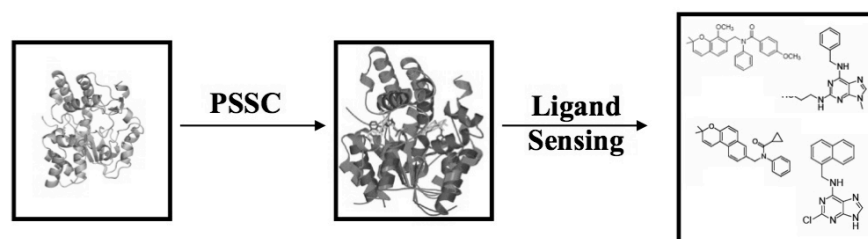
Figure 7: meta structure and model of the PI3-kinase p85 N-terminal SH2 domain. a) diagram representing the calculated local secondary structure organization along the analyzed domain of the protein. b) compactness value calculated for each residue in the region. c) predicted model; blue and red fragments correspond to the predicted secondary structure according to 7a (Konrat, R. Cellular and molecular life science, 2009. **66**:3625-39).

The meta-structure is to be considered as a topological abstraction of the primary sequence of a protein into the most probable three dimensional organization to be expected for the polypeptide. Being an abstraction, and not an actual model, it is capable of delivering more detailed information than an actual 3D model, revealing information also regarding disordered regions. Such regions of a protein are often escaping the classical structural characterization techniques, such as crystallography and NMR, but, due to their intrinsic flexibility, may be essential for the characterization of a protein function.

Similarly to what happens with primary sequence alignments or three-dimensional structure alignments, the calculated meta-structure of the protein of interest can then be aligned with meta-structures originating from characterized protein templates collected in a database. The alignment allows for the evaluation of the similarity between the target protein and subjects found in the database, thus creating protein clusters of similarity. As in the case of classical protein alignments, it is then possible to hypothesize that known ligands for the proteins within a similarity cluster may also display significant affinity for our query protein (Figure 8).

The creation of the so called protein meta-structure similarity clusters (PMSSC), according to the conservation of structural motifs among different proteins, does not only deliver precious information regarding the putative three-dimensional organization of the protein of interest, but it can also be exploited as a powerful tool in the systematic evaluation of protein-ligand interactions, when the target protein shares a ligand-binding motif with characterized templates, according to their calculated meta-structure.
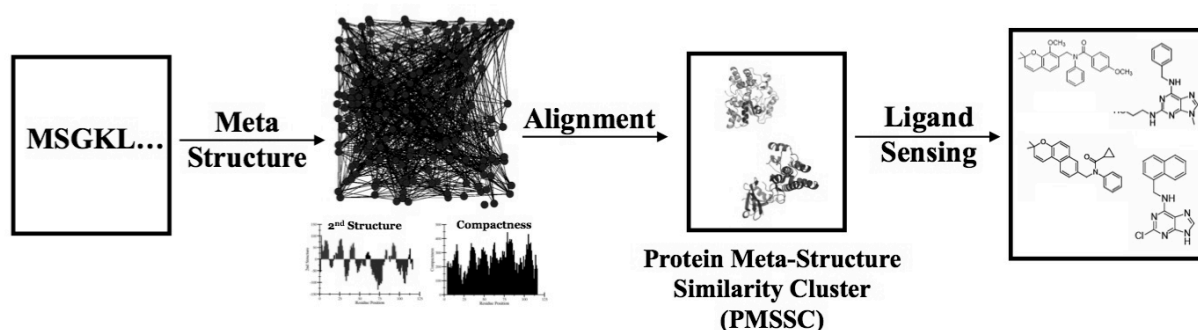

Figure 8: The definition of Protein Meta-Structure Similarity Clusters (PMSSC), similarly to what is commonly achieved with Protein Structure Similarity Clustering (PSSC), allows for the prediction of putative ligands of the target protein. The calculated meta structure takes the place of the 3D structure of a protein in case this is not available (Modified from: Konrat, R. Cellular and molecular life science, 2009. **66**:3625-39).

1.4.2.4 Shannon Entropy Descriptor ligand sensing

The identification of an active compound represents a starting point for obtaining other potential ligands/modulators of pendrin activity. In the classical drug discovery concept, a widely adopted approach is the chemical modification of an active compound in order to improve its properties, such as affinity for the target protein, potency or specificity. By means of combinatorial chemistry, it is then possible to produce a large number of new

compounds starting from the structure of the original ligand identified. In our approach we chose a conceptually different route, by exploiting a different bioinformatic tool in order to refine the search for the desired modulator of pendrin activity. The further step in the search for potential ligands and modulators of our protein of interest can be undertaken by aligning the structure of an experimentally identified ligand with a database of chemical compounds. To do this, it is necessary to univocally define and describe a small compound in a way that allows the meaningful comparison with other small molecules. This is made possible by a bioinformatic abstraction, as described in the following.

Based on the so called Shannon Entropy Descriptor (SHED), it is possible to define and categorize the nature of a small compound according to the functional relationship of atoms within the molecule. SHED is an information science-derived chemical descriptor whose aim is the classification of small molecules in similarity clusters according to the distribution of atom-centered feature pairs [113]. This means that every atom of the molecule is identified and classified according to defined chemical features (*e.g.:* hydrophobic, aromatic, proton acceptor or donor, etc.). The probability that each possible pair of atom-centered features is found at a certain distance within the small compound is calculated. The result of the calculation delivers an entropy value for the specific feature pair within the molecule. The same calculation is performed for any given features pair. The collection of all the entropy values of the molecule gives the so-called SHED score or SHED profile of the compound [113]. SHED profiles are univocal descriptors of the specific small compound and, as such, they can be compared and aligned to a database in order to define similarities with other small molecules. Such an approach, conceptually similar to the abstraction delivered by meta-analysis, has been proven extremely efficient concerning both chemical similarity and pharmacological profiling of compounds of interest. In other words, it has been shown that molecules displaying similar SHED profiles are not only chemically similar but, more importantly, they often show similarity also in what concerns their pharmacological behavior.

2. Aims of the study

2.1 Functional and molecular characterization of pendrin allelic variants

The definition of the genetic causes of deafness is the starting point for possible intervention processes for the affected patient and the family. Pendrin is a major player in the etiology of syndromic and non-syndromic hereditary deafness. The high phenotypical variability of pendrin-related deafness and the high incidence of benign polymorphisms does not allow for a straightforward correlation of genotype and phenotype. A definition of the actual role of pendrin in specific cases of hearing loss is only possible after functional characterization of the detected allelic variants.

Our first objective was the functional characterization of pendrin variants identified in a cohort of deaf patients at the General Hospital of Campinas, Sao Paolo, Brazil, in order to define the role of pendrin mutations in the diagnosed hearing loss phenotype. Furthermore, the present study will contribute to spread light on the incidence of pendrin-related deafness in this specific population, so far poorly investigated.

The phenotypical variability is also reflected in the difference in molecular processing of the mutant forms of pendrin. A further step in the characterization of the identified allelic variants consists in the definition of the type of molecular defect caused by the different mutations. For this purpose, we also analyzed the subcellular localization and the abundance of the different variants of pendrin, in order to discriminate between mutations affecting the folding and the trafficking and mutations directly affecting the transport activity.

The information collected from the functional and molecular characterization of the mutations is the starting point for a possible pharmacological approach aimed to the rescue of their transport activity. Such a rescue may be achieved by interfering with the degradation of misfolded proteins and facilitating their folding and trafficking process.

2.2 Functional screening of pendrin ligands

Pendrin hyperactivity and/or overexpression is linked to pathological states such as bronchial asthma, COPD and hypertension. Blocking or modulating the activity of the

transporter may define a novel paradigm in the treatment of the abovementioned pathologies. So far no potent, specific and non-toxic inhibitors for pendrin could be identified and the screening of large compound libraries failed in delivering any positive results.

Thanks to a fluorometric method developed by Dossena et al. in 2006, we were able to screen the effect of compounds on pendrin activity in a semi-high-throughput fashion. In the search of a possible ligand (inhibitor/modulator) of pendrin we used a focused approach, looking for possible candidate compounds among three groups of chemicals:

- known inhibitors of chloride channels and transporters and inhibitors of transporters homolog to pendrin, such as *Slc26a3* (DRA);
- antihypertensive and diuretic agents;
- small compounds predicted by a bioinformatic approach based on the abstraction of the primary aminoacidic sequence of pendrin, called meta-analysis.

3. Methods

3.1   Functional assay for the Cl⁻/I⁻ exchange activity of pendrin

The effect of selected compounds or mutations on the transport activity of pendrin has been investigated by means of a fluorometric method developed by Dossena et al. in 2006. This assay was first set up for measurements on a single cell level with a confocal microscope [17, 22, 44, 69] and later modified for a higher throughput approach on a multi-plate reader [6, 71, 101].

The functional test allows for the evaluation of pendrin activity by determining changes in the intracellular iodide concentration following exposure of cells to an extracellular milieu containing iodide. Being pendrin an iodide/chloride exchanger, in the presence of iodide in the extracellular solution it can lead to an iodide influx. Increases in the intracellular concentration of this anion are detected thanks to the specific sensitivity of a modified form of the enhanced yellow fluorescent protein EYFP (EYFP H148Q I152L). The two aminoacidic substitutions of this EYFP isoform confer an increased sensitivity to intracellular iodide with respect to chloride and other anions. Intracellular iodide quenches the fluorescence emitted by EYFP H148Q I152L [114], therefore giving an indication of pendrin activity.

Human Embryonic Kidney (HEK) 293 Phoenix cells were seeded on black 96-well plates (137101, Nunclon Delta Surface, Nunc, Denmark) and transiently double-transfected with a plasmid carrying the cDNA coding for EYFP H148Q I152L and a pTARGET plasmid carrying the cDNA coding for wild type or mutated pendrin or the pTARGET empty vector, as the control. The assay was performed 48-52 hours after transfection as described in the following. The cells were washed three times from the culture medium, bathed in 70 µl of a high chloride isotonic solution (see below for the composition) and the fluorescence emission of EYFP H148Q I152L was measured at a wavelength of 535 nm upon excitation at 485 nm (1 measurement/sec for 3 sec). Successively, 140 µl of a high iodide-containing isotonic solution (see below for the composition) were injected into the bath via an automatic liquid dispenser, increasing the extracellular concentration of iodide to 90 mM. Then, the fluorescence intensity was measured again (1 measurement/sec for 16 sec). In the presence of active pendrin, the extracellular iodide is exchanged with intracellular chloride, leading to an increased

intracellular iodide concentration and quenching of the fluorescence emitted by EYFP H148Q I152L. As previously mentioned, the level of activity of the transporter is proportional to the decrease in the intracellular fluorescence recorded after the injection of iodide into the extracellular solution.

Cell fluorescence was measured with the VICTOR™ X3 Multilabel Plate Reader (2030, Perkin Elmer, Finland) equipped with a liquid dispenser and the following filters: excitation: F485 (excitation center wavelength (CWL): 485 nm, bandwidth: 14 nm), emission: F535 (emission CWL: 535 nm, bandwidth: 25 nm). Experiments were performed at room temperature.

The solutions used for the assay were prepared as follows:

<u>Isotonic High Chloride Solution:</u>

135 mM NaCl, 2 mM KCl, 20 mM HEPES, 1 mM $CaCl_2$, 1 mM $MgCl_2$, 10 mM Glucose

pH=7.4

308 $mOsm/Kg_{H2O}$

<u>Isotonic High Iodide Solution:</u>

135 mM NaI, 2 mM KCl, 20 mM HEPES, 1 mM $CaCl_2$, 1 mM $MgCl_2$, 10 mM Glucose

pH=7.4

308 $mOsm/Kg_{H2O}$

3.2 Plasmids

pTARGET vector containing the cDNA encoding for wild type pendrin cloned from normal thyroid tissue (pTARGET PDS WT) was originally provided by Prof. P. Beck Peccoz, University of Milan, Italy, and encodes for human pendrin with an hexahistidine tag at the C-terminus. Pendrin mutants were obtained by site-directed mutagenesis on the pTARGET PDS WT vector as described below. These vectors were used for the functional

test. pEYFPN1 vector encoding for EYFP was from Clontech. H148Q an I152L mutations were obtained by site-directed mutagenesis [71].

For co-localization studies and evaluation of pendrin total and plasma membrane expression levels by confocal microscopy, the sequence coding for wild type pendrin was subcloned in frame with the EYFP coding sequence in the pEYFPN1 vector (Clontech). Following transfection of this construct in cells, pendrin is translated with EYFP fused to the C-terminus (PDS-EYFP). The pECFPN1 vector used in the evaluation of pendrin plasma membrane expression levels by confocal microscopy encodes for the enhanced cyano fluorescent protein ECFP (Clontech).

For western blot analysis, the hexahistidine tag fused at the C-terminus of pendrin had to be removed. The corresponding vector was obtained in house by site-directed deletion of the hexahistidine coding sequence of the original pTARGET PDS WT vector, and was named pTARGETΔHIS PDS WT. Pendrin mutants were obtained by site-directed mutagenesis on the pTARGETΔHIS PDS WT vector as described below.

All plasmids were sequenced by Microsynth AG, Switzerland, with the following primers, spanning the whole pendrin cDNA insert in the plasmid (Table 3):

RPDS 1R	5' – TTCCATTGCTGCTGGATACG – 3'
RPDS 2R	5' – GGAAAATGATGCAGCAGCCAGC – 3'
RPDS 2F	5' – TGGGATCTGTTGTTCTGAGC – 3'
RPDS 3R	5' – TTGCCATAGAAAATAGGACTGG – 3'
RPDS 4F	5' – GAAGCATCCCTAGCACAGATA – 3'
98198F	5' – TGTTAAATCCATCCCAAG – 3'

Table 3: sequencing primers for pendrin cDNA.

3.3   Cell Culture and Transfection

HEK 293 Phoenix [115] (originally provided by Prof. D. Di Francesco, University of Milan, Italy) and HeLa cells (CCL-2, Cervical Adenocarcinoma, ATCC) were grown in Minimum Essential Medium Eagle, supplemented with 10% fetal bovine serum, 2 mM L-glutamine, 10000 U/ml penicillin, 10 mg/ml streptomycin and 1 mM pyruvic acid, sodium

salt. The cells were maintained in an incubator (HERAcell 150, Thermo, Germany) at 37°C in a 5% CO_2, 95% air, 100% humidity atmosphere. The cells were kept sub-confluent and sub-cultured every second to third day.

For the functional assay, HEK 293 Phoenix cells were seeded in black 96 well plates and transfected 16 hours later. A cell confluence of ∼ 40% ensured optimal transfection yield. Transient transfection of cells was performed by calcium phosphate co-precipitation. In this method, the negatively charged phosphates of plasmid DNA form complexes with the positively charged calcium ions in the transfection mix and are internalized by the cells. The formation of complexes masks the negative charge on the DNA that would otherwise prevent it from traversing the plasma membrane.

The transfection mix for one row of 12 wells of a 96-well plate was prepared as follows:

Wild type (WT) or mutant (MUT) pendrin:

pTARGET-PDS WT/MUT	3 µl (0.5 µg/µl)
pEYFP H148Q I152L	3 µl (0.5 µg/µl)
20x $CaCl_2$	7.5 µl
H_2O	61.5 µl
2x HBS	75 µl

Control:

pTARGET-EMPTY	3 µl (0.5 µg/µl)
pEYFPN1 H148Q I152L	3 µl (0.5 µg/µl)
20x $CaCl_2$	7.5 µl
H_2O	61.5 µl
2x HBS	75 µl

The transfection mix was incubated for 10 minutes at room temperature in order to allow for the complexes to be formed. After the incubation, 10 µl of transfection mix (*i.e.* 0.1 µg of pTARGET-PDS WT/MUT plasmid and 0.1 µg pEYFP H148Q I152L plasmid) were carefully pipetted into each well.

For co-localization studies and evaluation of total pendrin expression levels by confocal microscopy, HeLa cells were seeded in 6 well plates and transfected for 72 h with 1.5 µg of plasmid DNA encoding for wild type or mutant PDS-EYFP and 3 µl of Metafectene PRO®, following the manufacturer instructions. Media was changed 7-8 hours after transfection.

For evaluation of plasma membrane pendrin expression levels by confocal microscopy, HeLa cells were seeded in 6 well plates and transfected for 72 h with 0.25 µg of plasmid DNA coding for ECFP (pECFPN1), 1.25 µg of plasmid DNA coding for wild type or mutant PDS-EYFP and 3 µl of Metafectene PRO®, following the manufacturer instructions. Media was changed 7-8 hours after transfection.

For western blot analysis, HEK 293 Phoenix cells were seeded in 6 well plates and transfected for 72 hours with the calcium phosphate co-precipitation method as described above. Each well was transfected with 150 µl transfection mix, containing 2 µg of plasmid DNA coding for wild type or mutant pendrin. Media was changed 7-8 hours after transfection.

Buffers and Solutions:

      20x CaCl$_2$Solution:

            2.5 M 2H$_2$O●CaCl$_2$

      2x HEPES-buffered solution (HBS):

            140 mM NaCl; 1.5 mM 2H$_2$O●Na$_2$HPO$_4$, 50 mM HEPES,
            pH=7.05

3.4   Site-directed mutagenesis

The point mutations in the coding sequence of pendrin were obtained by site-directed mutagenesis with the QuickChange® site-directed mutagenesis kit (200518, Stratagene, USA) according to the manufacturer's instructions with the primer pairs indicated in Table 4:

P142L	sense	5'- GTTGGACCTTTTCTAGTGGTGAGTTTAATGG -3'
	antisense	5'- CCATTAAACTCACCACTAGAAAAGGTCCAAC -3'
G149R	sense	5'- GAGTTTAATGGTGAGATCTGTTGTTCTGAGC -3'
	antisense	5'- GCTCAGAACAACAGATCTCACCATTAAACTC -3'
T193I	sense	5'- GCCAGTGCCCTGATTCTGCTGGTTGG -3'
	antisense	5'- CCAACCAGCAGAATCAGGGCACTGGC -3'
C282Y	sense	5'- CACCATTGTCGTCTATATGGCAGTTAAGG -3'
	antisense	5'- CCTTAACTGCCATATAGACGACAATGGTG-3'
Q413R	sense	5'- CCCGCACGGCCGTCCGGGAGAGCACTGGAGG -3'
	antisense	5'- CCTCCAGTGCTCTCCCGGACGGCCGTGCGGG -3'
L445W	sense	5'- GCTTCTGGAACCCTGGCAGAAGTCGGTCTTGGC -3'
	antisense	5'- GCCAAGACCGACTTCTGCCAGGGTTCCAGAAGC -3'
R776C	sense	5'- CCAGGATGAGGCTATGTGTACACTTGCATCC -3'
	antisense	5'- GGATGCAAGTGTACACATAGCCTCATCCTGG -3'
E29Q	sense	5'-GCCGGTCTACAGCCAGCTCGCTTTCCAG-3'
	antisense	5'-TGGAAAGCGAGCTGGCTGTAGACCGGC-3'
P140H	sense	5'-CAAGACATATCTCAGTTGGACATTTTCCAGTGGTGAGTTTAAT-3'
	antisense	5'-ATTAAACTCACCACTGGAAAATGTCCAACTGAGATATGTCTTG-3'
Q413P	sense	5'-GCACGGCCGTCCCGGAGAGCACTGG-3'
	antisense	5'-CCAGTGCTCTCCGGGACGGCCGTGC-3'
G424D	sense	5'-AAGACACAGGTTGCTGACATCATCTCTGCTGCG-3'
	antisense	5'-CGCAGCAGAGATGATGTCAGCAACCTGTGTCTTTC-3'
T485R	sense	5'-TTGATGCTGTTATCTGGGTGTTTAGGTGTATAGTGTCC-3'
	antisense	5'-GGACACTATACACCTAAACACCCAGATAACAGCATCAATC-3'
Q514K	sense	5'-GACTGTGGTCCTGAGAGTTAAGTTTCCTTCTTGGA-3'
	antisense	5'-TCCAAGAAGGAAACTTAACTCTCAGGACCACAGTC-3'
D724G	sense	5'-CATTCTTTTTGACGGTCCATGGTGCTATACTCTATCTACAGAA-3'
	antisense	5'-TTCTGTAGATAGAGTATAGCACCATGGACCGTCAAAAAGAATG-3'

Table 4: Mutagenesis primers for inserting the indicated aminoacidic substitution in pendrin sequence.

All oligonucleotide primers were purchased from Microsynth (Balgach, Switzerland).

3.5   Screening of pendrin ligands

The substances selected for the screening were purchased either from Sigma-Aldrich, USA, Fluka, Germany or SIA MolPort, Latvia. According to the indication of the vendor, each substance was resuspended in the suitable solvent (dimethyl sulfoxide (DMSO), absolute ethanol or polyethylene glycol 400, Table 5). For each substance, a

stock solution was prepared and stored at -20°C. The working dilution for the assay was 100 µM in high chloride and high iodide isotonic solution for all the substances, except when otherwise specified.

Substance	CAS number	Stock	Catalog number, Vendor
NB (5-nitro-2-(3-Phenypropylamino)benzoic acid)	107254-86-4	300 mM in DMSO	N4779, Sigma-Aldrich, USA
DIDS (4,4'-diisothiocyanatostilbene-2,2'-disulfonic acid)	207233-90-7	300 mM in DMSO	D3514, Sigma-Aldrich, USA
CFTR inhibitor – 172	307510-92-5	5 mM in DMSO	C2992, Sigma-Aldrich, USA
DNDS (4',4'-dinitrostilbene-2,2'-disulfonic acid)	128-42-7	300mM in isotonic sol.	S347523,Sigma-Aldrich,USA
Niflumic acid	4394-00-7	300 mM in DMSO	N0630, Sigma-Aldrich, USA
Tenidap	120210-48-2	300 mM in DMSO	PZ0196, Sigma-Aldrich, USA
Glybenclamide	10238-21-8	300 mM in DMSO	G0639, Sigma-Aldrich, USA
Probenecid	57-66-9	300 mM in chloroform	P8761, Sigma-Aldrich,USA
Eplerenone	107724-20-9	30 mM in DMSO	E6657, Sigma-Aldrich, USA
Acetazolamide	59-66-5	300 mM in DMSO	A6011, Sigma-Aldrich, USA
Bumetanide	28395-03-1	300 mM in DMSO	B3023, Sigma-Aldrich, USA
Furosemide	54-31-9	300 mM in DMSO	F4381, Sigma-Aldrich, USA
Hydrochlorothiazide	58-93-5	300 mM in DMSO	H4759, Sigma-Aldrich, USA
Cholesterol	57-88-5	300 mM in chloroform	C8667, Sigma-Aldrich, USA
Iloprost (Ilomedin® - Bayer)	--	--	Bayer Schering Pharma, Germany
Vasopressin	113-79-1	3 mM in isotonic sol.	V9879, Sigma-Aldrich, USA
Vitamin D (Dihydrotachysterol)	67-96-9	300 mM in DMSO	D9257, FLUKA, Germany
Vitamin E (α-Tocopherol)	10191-41-0	300 mM in DMSO	T3251, Sigma-Aldrich, USA
(-)Nicotine	54-11-5	300 mM in isotonic sol.	N3876, Sigma-Aldrich,USA
N-(2-chlorophenyl)-2-(2,4-dibromophenoxy)acetamide	not available	300 mM in DMSO	002-045-764, MolPort, Latvia
2-{[(2,3-dichlorophenyl)methyl]amino}-1-phenylethanol	not available	300 mM in DMSO	000-938-685, MolPort, Latvia
Naloxone	465-65-6	300 mM in DMSO	143005, FLUKA, Germany
Tolcapone	134308-13-7	300 mM in DMSO	SML0150, Sigma-Aldrich, USA
Topiramate	97240-79-4	300 mM in DMSO	T0575, Sigma-Aldrich, USA
Colchicine	64-86-8	300 mM in ethanol	C9754, Sigma-Aldrich, USA

Scopolamine	6533-68-2	300 mM in isotonic sol.	S0929, Sigma-Aldrich, USA
6-phenylamino nicotinic acid	13426-16-9	300 mM in DMSO	CSD009518, Sigma-Aldrich, USA
Levamisole	16595-80-5	300 mM in isotonic sol.	L0380000, FLUKA, Germany
Levallorphan	71-82-9	300 mM in isotonic sol.	L121, Sigma-Aldrich, USA
Ticlopidine	53885-35-1	300 mM in isotonic sol.	T6654, FLUKA, Germany
Flufenamic acid	530-78-9	300 mM in DMSO	F9005, FLUKA, Germany

Table 5: list of chemicals tested on pendrin activity with the fluorometric method. For each substance, the Chemical Abstracts Service (CAS) registry number, concentration and solvent of the stock solution, catalog number and vendor are specified.

3.6 Subcellular localization of pendrin variants

3.6.1 Co-localization with the plasma membrane

The staining of the plasma membrane was performed *in vivo* on HeLa cells with the CellMask™ Deep Red Plasma Membrane Stain (5 mg/ml stock solution in DMSO, C10045, Molecular Probes, USA). The Plasma Membrane Stain stock solution was diluted to 1.25 µg/ml in Hank's Balanced Salt Solution (HBSS).

HeLa cells were seeded in 6 wells plates, grown to 40% confluence and transfected with wild type or mutant PDS-EYFP as described above. 56 hours after transfection, cells were resuspended by trypsinization and transferred on 3 cm diameter microscope slides. 72 h after transfection, cells were washed three times with ice cold HBSS and incubated with 1.25 µg/ml CellMask Deep Red Plasma Membrane Staining Solution for 5 minutes on ice. The staining solution was then removed and cells were washed again three times with ice cold HBSS. Imaging was performed immediately after staining in cold HBSS using a Leica TCS SP5 II AOBS confocal microscope (Leica Microsystems, Germany), with a 63x PL APO Lambda blue water immersion objective (numerical aperture 1.2), a 514 nm Argon laser line for exciting EYFP (λex.: 514 nm, λem.: 525-600 nm) and a 633 nm HeNe laser line for exciting the Plasma Membrane Stain (λex.: 633 nm, λem.: 655-750 nm).

The quantitative analysis of the co-localization between PDS-EYFP and the plasma membrane was performed by determining the Pearson's coefficient of correlation of the

two signals according to the formula $R = \frac{\Sigma_i(S1_i - S1_{avg}) \times (S2_i - S2_{avg})}{\sqrt{\Sigma_i(S1_i - S1_{avg})^2 \times (S2_i - S2_{avg})^2}}$ where $S1_i$ and $S2_i$ represent the intensity of any *i* pixel respectively in the emission channel 1 and 2 while $S1_{avg}$ and $S2_{avg}$ represent the average intensity of all pixels respectively in the emission channel 1 and 2. A Pearson's coefficient of 0 indicates a random correlation, whereas values close to +1 and -1 indicate co-localization and mutual exclusion of the two signals, respectively. Sequential acquisition and analysis of images were performed with the LAS AF SP5 software (Leica Microsystems, Germany).

3.6.2 Co-localization with the endoplasmic reticulum

The staining of the endoplasmic reticulum was performed *in vivo* with ER-Tracker™ Red Glibenclamide BODIPY®-TR (E34251, Molecular Probes, USA). The dye was reconstituted in 110 µl DMSO to obtain a 1 mM stock solution and stored at -20°C. A 1 µM working dilution was obtained in Krebs-Henseleit Buffer (K3753, Sigma-Aldrich, USA).

HeLa cells were seeded in 6 wells plates, grown to 40% confluence and transfected with wild type or mutant PDS-EYFP as described above. 56 hours after transfection, cells were resuspended by trypsinization and transferred on 3 cm diameter microscope slides. 72 h after transfection, cells were washed three times with Krebs-Henseleit Buffer at room temperature and incubated with 1 µM ER-Tracker for 20 minutes at 37°C, 5% CO_2. The staining solution was then removed and cells were washed with HBSS. Imaging was performed in HBSS immediately after staining using a Leica TCS SP5 II AOBS confocal microscope, with a 63x PL APO Lambda blue water immersion objective (numerical aperture 1.2), a 514 nm Argon laser line for exciting EYFP (λex.: 514 nm, λem.: 525-555 nm) and a 561 nm DPSS laser line for exciting the ER-Tracker (λex.: 571 nm, λem.: 650 nm).

The quantitative analysis of the co-localization between the ER and PDS-EYFP signals was performed by determining the Pearson's coefficient of correlation as described above. Sequential acquisition and analysis of images were performed with the LAS AF SP5 software (Leica Microsystems, Germany).

3.7 Quantification of the expression levels of pendrin variants

Two complementary methodologies have been used in order to have a complete picture of the molecular fate of the different pendrin variants: imaging of EYFP-tagged proteins and western blot analysis of cellular protein extracts from transfected cells.

3.7.1 Fluorescence Imaging

Cells for imaging experiments were transfected with the different variants of pendrin fused to EYFP (PDS-EYFP). Either the total or the plasma membrane expression of pendrin variants was evaluated by detecting the signal emitted by PDS-EYFP.

3.7.1.1 Total pendrin expression

HeLa cells were seeded in 6 wells plates, grown to 40% confluence and transfected with WT or mutant PDS-EYFP as described above. 56 hours after transfection, cells were resuspended by trypsinization and transferred on 3 cm diameter microscope slides. 72 hours after transfection, cells were washed in HBSS and fixed for 15 minutes with 4% paraformaldehyde. After fixation, cells were incubated for 10 minutes with 0.1 µg/ml 4',6-diamidino-2-phenylindole (DAPI, D9542, Sigma-Aldrich, USA) in HBSS. The nuclear staining with DAPI can give an indication of the number of cells in the imaged field and was necessary in order to normalize the PDS-EYFP signal for the cell density. Cells were imaged immediately after preparation with a Leica TCS SP5 II confocal microscope, equipped with a 63x PL APO Lambda blue water immersion objective, numerical aperture 1.2, a 514 nm Argon laser line for exciting EYFP (λex.: 514 nm, λem.: 525-597 nm) and a 405 nm diode laser for exciting DAPI (λex.: 405 nm, λem.: 430-470 nm). The signal emitted by PDS-EYFP in the whole field of imaging was expressed as averaged levels of grey and normalized by the signal emitted by DAPI in the same field, also expressed as averaged levels of grey. Imaging parameters (laser power, photomultiplier gain, pixel size and zoom factor) were kept rigorously constant for all the acquisitions. Subtraction of

background fluorescence was performed for all acquisitions in both EYFP and DAPI emission channels.

3.7.1.2 Plasma membrane pendrin expression

For this set of experiments, a different normalization approach was set up, and considered the transfection efficiency of the single cell. HeLa cells were co-transfected as previously described with wild type or mutant PDS-EYFP and ECFP as an indicator of transfection efficiency of the single cell. The signal of PDS-EYFP in regions of interest of the plasma membrane (PM) of the selected cell, expressed as averaged levels of grey, was normalized for the emission of ECFP in the cytosol of the same cell, also expressed as averaged levels of grey. In order to clearly identify the PM, especially for those pendrin variants lacking a PM localization, cells were stained on ice with 1.25 µg/ml CellMask Deep Red Plasma Membrane Stain, as previously described. Imaging was performed *in vivo* immediately after staining with a Leica TCS SP5 II confocal microscope, equipped with a 63x PL APO Lambda blue water immersion objective, numerical aperture 1.2, a 514 nm Argon laser line for exciting EYFP (λex.: 514 nm, λem.: 525-580 nm), a 405 nm diode laser line for exciting ECFP (λex.: 405 nm, λex.: 450-490 nm) and a 633 nm HeNe laser line for CellMask (λex.: 633 nm, λex.: 643-750 nm). Imaging parameters, such as laser power, photomultiplier gain, pixel size and zoom factor, were kept constant for all the acquisitions. Subtraction of background fluorescence was performed for all acquisition in both PDS-EYFP and ECFP emission channels.

3.7.2 Western Blot

HEK 293 Phoenix cells for western blot were transfected with the pTARGET vector carrying the cDNA for wild type or mutant pendrin by the calcium phosphate co-precipitation method, as described above. As previously mentioned, the exahistidine tag originally fused to the C-terminus of pendrin was removed for this set of experiments.

3.7.2.1 Total protein extraction

72 hours after transfection, the cells and their culture medium were collected and centrifuged at 216 xg for 15 minutes at 4°C. The collected cell pellets were washed twice

with ice cold phosphate buffer saline (PBS) and lysed on ice in a denaturing lysis buffer (see below for the composition) supplemented with Halt Protease Inhibitor Single-use Cocktail.

Cell lysates were centrifuged for 30 minutes at 17000 xg, 4°C, in order to precipitate the non-lysated/non-soluble fraction. The supernatant was collected into a fresh tube and the total protein content of each sample was determined by the Bradford assay (500-0006, Biorad, Germany), following the manufacturer instructions. About 60 µg of each total protein extract were loaded on the gel.

Samples for Sodium Dodecyl Sulphate-Polyacrylamide Gel Electrophoresis (SDS-PAGE) were prepared by adding a denaturing loading dye containing dithiothreitol (DTT) as a reducing agent and boiled for 5 minutes before loading in a 7.5% polyacrylamide gel. As a standard, 10 µl of Page Ruler Prestained Protein Ladder (26616, Thermo Scientific, USA) were loaded in the gel. The gel was run at constant voltage (120 V) for 2 hours at room temperature. Subsequently, the separated proteins were transferred on polyvinylidene difluoride (PVDF) membranes (Immunoblot PVDF Membranes, BIO-RAD, Germany) by applying a constant voltage (75 V) for 2 hours at 4°C. The membranes were blocked for 1 hour at room temperature in 5% nonfat dry milk in tris buffered saline and Tween (TBST, 0.1% Tween) and then incubated overnight at 4°C with the primary antibodies in 3% nonfat dry milk in PBS. After 3 washing steps in TBST, the membranes were incubated for 1 hour at room temperature with the infrared dye-conjugated secondary antibodies diluted in 3% nonfat dry milk in PBS. Finally, the membranes were washed 3 times in TBST. Detection of the signal of immunocomplexes was performed with the ODYSSEY infrared imaging system (LI-COR, USA).

Blot images were densitometrically analyzed with the ImageJ 1.46r software (Wayne Rasband, NIH, USA). The signal intensity of the bands corresponding to pendrin, expressed as levels of grey, was normalized on the signal intensity of the bands corresponding to the housekeeping protein glyceraldehyde 3-phosphate dehydrogenase (GAPDH), similarly expressed as levels of grey.

3.7.2.2   Extraction of total cellular membranes proteins

The extraction of the total membranes fraction, including both plasma membrane and membranes from cellular organelles, was performed with the Plasma Membrane Extraction Kit (JM-K268-50, MBL, USA), according to the manufacturer instructions.

The cells were seeded and transfected as described above. 72 hours after transfection, the cells were collected by centrifugation. The pellet was washed twice in ice cold PBS and resuspended in Homogenizing Buffer from the above mentioned kit. Lysis was achieved using a syringe with a small gauge needle. Complete lysis was confirmed by the almost total absence of intact nuclei in the sample upon observation with a phase-contrast inverted microscope (AE31, Motic GmbH, Germany). The lysate was centrifuged for 10 minutes at 700 xg, 4°C, in order to remove the non-lysate/non-soluble fraction but conserving the membranes fraction in the supernatant. The supernatant was centrifuged a second time at 10000 xg for 30 minutes, 4°C. The pellet from the second centrifugation step represents the total cellular membranes fraction, while the supernatant contains the soluble proteins fraction. Samples for the gel were prepared resuspending the protein pellet in loading dye containing DTT. Before loading on the gel, the sample were boiled for 5 minutes. SDS-PAGE and western blotting were performed as described above. Detection of the signal of immunocomplexes was performed with the ODYSSEY infrared imaging system (LICOR, USA).

Blot images were densitometrically analyzed with the ImageJ 1.46r software (Wayne Rasband, NIH, USA). The signal intensity (expressed as levels of grey) of the bands corresponding to pendrin was normalized on the signal intensity (expressed as levels of grey) of the bands corresponding to the housekeeping protein calreticulin.

Buffers and Antibodies:

Denaturing Lysis Buffer (total proteins extraction)
50 mM Trizma base, 150 mM NaCl, 1% NP-40 alternative, 1% Halt Protease Inhibitor Single-use Cocktail.

Loading dye
240 mM Trizma HCl pH 6.8, 40% Glycerol, 0.04% Bromophenol blue, 5% β-mercaptoethanol or 100 mM DTT, 8% SDS.

Running Buffer

25 mM Trizma base, 144 mM Glycine, 1% SDS.

Transfer Buffer

27 mM Trizma base, 190 mM Glycine.

Wash Buffer

40 mM Trizma base, 270 mM NaCl, 0.1% Tween20.

pH=7.5

Primary antibodies:

Anti-PDS: rabbit anti-pendrin antibody against the C-terminal domain of human pendrin (kindly provided by Prof. Dominique Eladari, Paris, France).

Working dilution 1:10000.

Anti-GAPDH: goat anti-GAPDH antibody (A00191-100, GenScript).

Working dilution 1:1000.

Anti-Calreticulin: rabbit anti-Calreticulin antibody (ab4, abcam).

Working dilution 1:1000

Secondary antibodies:

Goat anti-Rabbit IRDye 800CW Conjugated (LI-COR).

Working dilution 1:20000

Donkey anti-Goat IRDye 800CW Conjugated (LI-COR).

Working dilution 1:20000

3.8   Rescuing of pendrin activity

The study of a possible functional rescue of pendrin upon treatment with a proteasome inhibitor was performed by means of the same functional test described above. For this aim, HEK 293 Phoenix cells were transfected as described earlier with the different pendrin variants. 48 hours after transfection, cells were incubated for 6 hours in complete media supplemented with the proteasome inhibitor MG132, 10 µM (C2211, Sigma-Aldrich, USA), or its vehicle (0.1% DMSO). Before measurements, cells were washed three times and bathed in high chloride solution. The functional test was performed as described earlier.

For the imaging experiments, HeLa cells were seeded in 6 wells plates, grown to 40% confluence and transfected with wild type or mutant PDS-EYFP as described above. 36 hours after transfection, cells were resuspended by trypsinization and transferred on 3 cm diameter microscope slides. 60 hours after transfection, the proteasome inhibitor MG132, 10 µM, or its vehicle (0.1% DMSO) were added to the media and cells were grown overnight in the incubator. 72 hours after transfection, cells were prepared for the imaging according to the respective protocols for total and plasma membrane pendrin evaluation, as described above.

3.9   Statistical analysis

Statistical analyses for all data sets presented in this thesis were performed with GraphPad Prism version 5.0b for MAC (GraphPad Software, San Diego, California, USA).

Data are expressed as mean values ± standard error of the mean (SEM). n corresponds to the number of independent measurements. Statistical differences between data sets were verified by the one-way analysis of variance (ANOVA) followed by Bonferroni's multiple comparison or Dunnett's post-tests or by the unpaired Student's t-test, as appropriated. Differences were considered statistically significant when the p value was ≤ 0.05.

3.10 Salts and Reagents:

All salts and reagents were of *pro-analysis* grade quality.

Minimum Essential Medium Eagle (M5650, Sigma, Austria)

Fetal Bovine Serum (DE14-801F, Lonza, USA)

L-glutamine (G7513, Sigma-Aldrich, USA)

Penicillin, Streptomycin (P0781, Sigma-Aldrich, USA)

Pyruvic acid, sodium salt (P2256, Sigma-Aldrich, USA)

Metafectene PRO$^®$ (T040, Biontex, Germany)

DMSO (D2650, Sigma-Aldrich, USA)

Ethanol absolute (1.07017.2511, Merk, Germany)

Polyethylene glycol 400 (202398, Sigma-Aldrich, USA)

HBSS (H1387, Sigma-Aldrich, USA)

NaCl (A4256, Applichem, Germany)

KCl (P5405, Sigma-Aldrich, USA)

HEPES (A3268, Applichem, Germany)

$CaCl_2$ (21114, Fluka, Germany)

$MgCl_2$ (A4998, Applichem, Germany)

Glucose (49139, Sigma-Aldrich, USA)

NaI (040196, AlfaAesar, Germany)

$2H_2O●CaCl_2$ (172570,Merck, Germany)

$2H_2O●Na_2HPO_4$ (71649, Fluka, Germany)

Trizma base (T1503, Sigma-Aldrich, USA)

NP-40 alternative (492016, Calbiochem, Germany)

Halt Protease Inhibitor Single-use Cocktail (1860932, Thermo Scientific, USA)

Trizma HCl pH 6.8 (T5941, Sigma-Aldrich, USA)

Glycerol (A16205, AlfaAesar, Germany)

Bromophenol blue (A18469, AlfaAesar, Germany)

β-mercaptoethanol (M6250, Sigma-Aldrich, USA)

DTT (443852A, VWR, England)

SDS (444464T, VWR, England)

Glycine (G8898, Sigma-Aldrich, USA)

Tween 20 (437082Q, VWR, England)

4. Results

4.1 Functional characterization of pendrin allelic variants identified in a cohort of Brazilian deaf patients

Disclaimer: the functional studies were performed in our laboratories at the Paracelsus Medical University, Salzburg, in collaboration with the University of Campinas, Brazil. I have participated in performing and analyzing all of the experiments described in this section.

Seven of the pendrin allelic variants identified in the genetic screening of a cohort of 58 deaf Brazilian patients, performed by our collaborators at the University of Campinas, Sao Paolo, Brazil (see Introduction, Table 1), were functionally characterized with the fluorometric method developed by Dossena et al. in 2006 and described in the Methods section. The 3 novel pendrin variants identified in this cohort (P142L, G149R [66] and C282Y) along with 3 known but functionally uncharacterized pendrin variants (L445W, Q413R and T193I) were included in the functional test. A further allelic variant (R776C) was also tested, even though it had already been characterized, because results were controversial [67, 68].
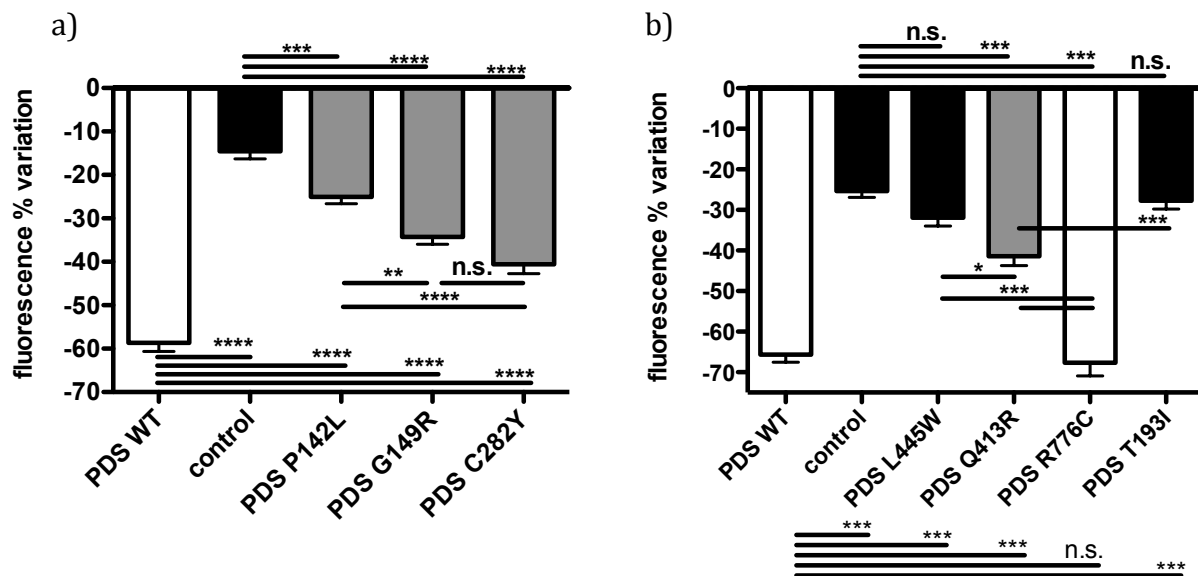
Figure 9: Functional test of pendrin allelic variants identified in Brazilian deaf patients with or without EVA. a) novel mutations; b) mutations already reported in the literature but not yet characterized on a functional level, or whose characterization was ambiguous. HEK 293 Phoenix cells were co-transfected with wild type or mutated pendrin and EYFP H148Q I152L, or with EYFP H148Q I152L alone (control). Black bars indicate complete loss of function, grey bars a reduction of function, white bars represent the wild type and unaffected function. n was 42 in a) and 70 in b). n.s. not significant, *p<0.05, **p<0.01, ***p<0.001, ****p<0.0001, one way ANOVA with Bonferroni's post-test.

In Figure 9, the % decrease in intracellular EYFP H148Q I152L fluorescence after addition of iodide to the extracellular solution is shown for all the different pendrin allelic variants analyzed. The decrease in intracellular fluorescence is the consequence of an iodide influx and is therefore indicative of the level of transport activity of wild type or mutated pendrin (see Methods for further details). The transport activity measured for the different pendrin allelic variants was statistically compared to the activity of the wild type and the control (cells expressing EYFP H148Q I152L only and no pendrin).

The functional tests were performed in two separated groups for technical convenience, as it is essential that pendrin variants are tested on the same 96 well plate as the wild type and the control. Therefore, the two groups are here presented and statistically analyzed separately. It is anyway possible to draw common conclusions. The functional screening of the mutants can be summarized as follows:

- 2 mutations (L445W and T193I) show a complete loss of function (the transport activity was not significantly different with respect to the control);

- 4 mutations (P142L, G149R, C282Y and Q413R) showed a transport activity significantly reduced with respect to the wild type, but not completely annihilated (the transport activity was significantly higher with respect to the control);

- the aminoacidic substitution R776C did not affect the transport of iodide with respect to wild type pendrin.

4.2   Subcellular localization of pendrin allelic variants

Disclaimer: the subcellular localization studies were performed in our laboratories at the Paracelsus Medical University, Salzburg, in collaboration with the University of Campinas, Brazil. I have participated in part of the co-localization experiments. However, for sake of completeness, the whole co-localization results are presented in this section.

The subcellular localization of the abovementioned pendrin allelic variants was determined in living HeLa cells by measuring the co-localization of the fluorescent signal emitted by the fusion protein pendrin-EYFP (PDS-EYFP) and two specific dyes, *i.e.* the

64

plasma membrane (CellMask Deep Red Plasma Membrane Stain) or the endoplasmic reticulum (ER-Tracker Red Glibenclamide BODIPY-TR) stains, respectively.

In Figures 10 and 11, examples of fluorescence imaging and co-localization scatter plots from the experimental series are shown. In the scatter plots, the position of each pixel represents its fluorescence intensity in the emission channel of EYFP and in the emission channel of the marker of plasma membrane (Figure 10) or endoplasmic reticulum (Figure 11). Pixels situated along the diagonal of the plot show similar emission intensity in both channels and therefore represent co-localization of the two signals. In contrast, pixels distributed along the axes of the graph show higher emission intensity in one of the two channels and lower emission intensity in the other channel, therefore indicating mutual exclusion of the two signals.

The co-localization was quantified by determining the Pearson's correlation coefficient. As mentioned in the Methods section, the value of the Pearson's coefficient can range between -1 and +1, where +1 represents complete co-localization, a value close to 0 is indicative of an absence of correlation and a value of -1 represents a complete mutual exclusion of the two signals within the region of interest.
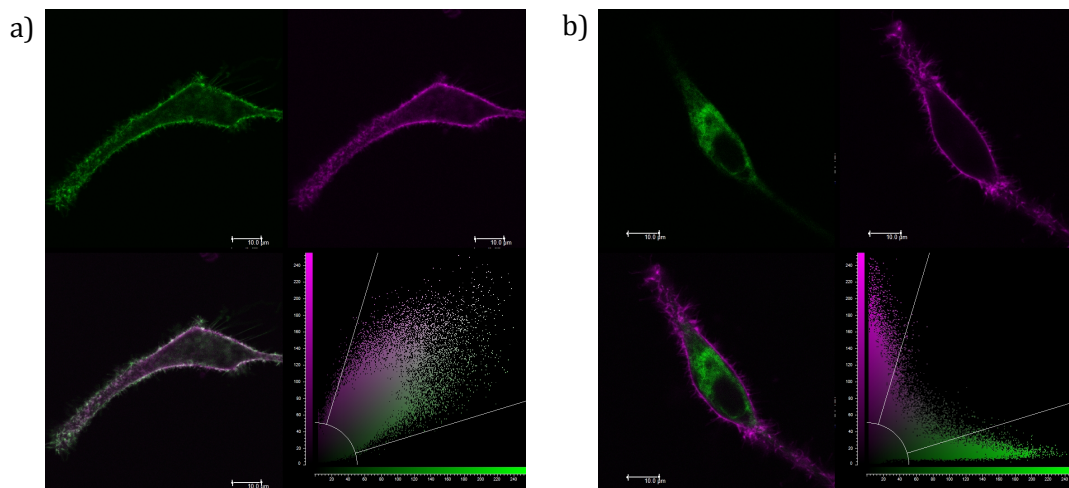
Figure 10: a) Representative images of wild type pendrin (PDS-EYFP, green, top left) and the plasma membrane marker (magenta, top right). At the bottom left, the merge of the two images and at the bottom right the co-localization scatter plot are shown. White pixels in the merged image and pixels located along the diagonal of the scatter plot indicate co-localization between wild type pendrin and the plasma membrane. b) Representative mutated pendrin (L445W-EYFP, green, top left), plasma membrane (magenta, top right) and merge (bottom left) images and corresponding co-localization scatter plot (bottom right). The absence of white pixels in the merged image and pixels located along the axes of the scatter plot indicate exclusion between the mutated pendrin and the plasma membrane. Scale bar: 10 µm.
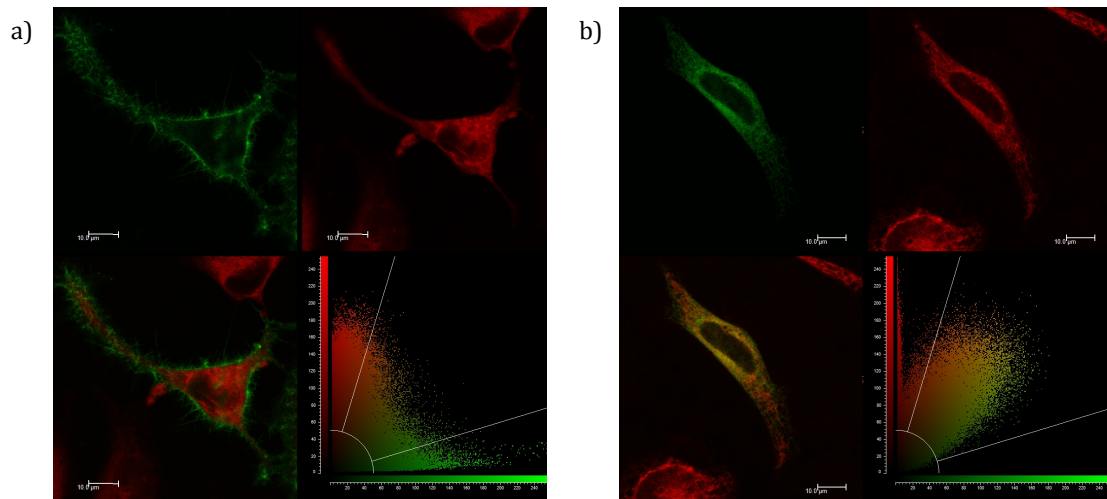
Figure 11: a) Representative images of wild type pendrin (PDS-EYFP, green, top left) and the endoplasmic reticulum marker (red, top right). At the bottom left, the merge of the two images and at the bottom right the co-localization scatter plot are shown. The absence of yellow pixels in the merged image and pixels located along the axes of the scatter plot indicate an absence of co-localization between wild type pendrin and the endoplasmic reticulum. b) Representative mutated pendrin (Q413R-EYFP, green, top left), endoplasmic reticulum marker (red, top right) and merge (bottom left) images and corresponding co-localization scatter plot (bottom right). Yellow pixels in the merged image and pixels located along the diagonal of the scatter plot indicate co-localization between the mutated pendrin and the endoplasmic reticulum. Scale bar: 10 µm.

The Pearson's correlation coefficient between PDS-EYFP and the plasma membrane or ER marker is calculated for every pendrin variant analyzed in the experimental series according to the formula reported in the methods. The calculated correlation values are compared to the wild type and a negative control (cells transfected with EYFP only). Being EYFP a water soluble protein, it is expected to show no significant co-localization with the plasma membrane. Accordingly, the respective Pearson's correlation coefficient (black bar in Figure 12a) results significantly reduced with respect to wild type PDS-EYFP. The results are represented in Figure 12 and show the Pearson's correlation coefficients of co-localization with the plasma membrane (Figure 12a) and the endoplasmic reticulum (Figure 12b). Data were interpreted as follows:

- pendrin variants with a Pearson's correlation coefficient with the PM not significantly reduced with respect to the wild type but significantly higher with respect to the negative control have been considered to have PM targeting and are represented in white in panel a;
- pendrin variants with a Pearson's correlation coefficient with the PM significantly reduced with respect to the wild type have been considered to be excluded from the PM and are represented in grey in panel a;

66

- pendrin variants with a Pearson's correlation coefficient with the ER not significantly higher with respect to the wild type have been considered not to be retained in the ER and are represented in white in panel b;
- pendrin variants with a Pearson's correlation coefficient with the ER significantly higher with respect to the wild type have been considered to be retained in the ER and are represented in grey in panel b.

To summarize, white bars in Figure 12 correspond to pendrin allelic variants with PM targeting and grey bars represents those variants that are instead significantly retained in the ER. The co-localization of the different pendrin variants with the plasma membrane is highly consistent with the co-localization with the endoplasmic reticulum, with those mutants showing a good co-localization with the PM being mostly excluded from the ER and *viceversa*. The only exception to this observation is the mutant G149R, showing a plasma membrane co-localization value comparable to the wild type in panel 12a but at the same time a significant co-localization with the endoplasmic reticulum as well, as shown in panel 12b.
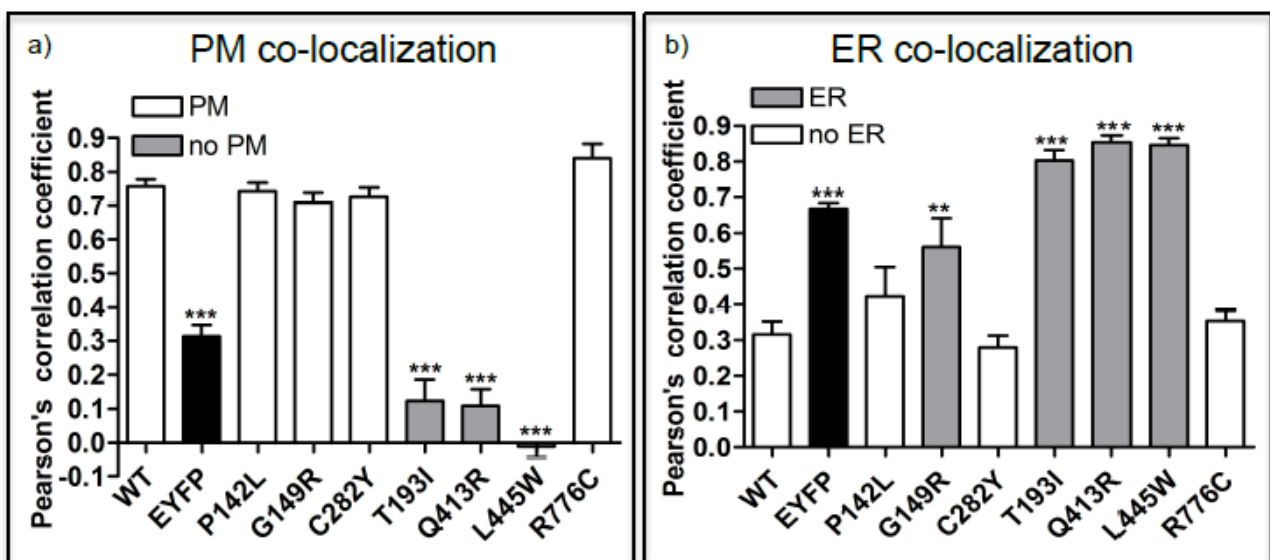
Figure 12: Pearson's correlation coefficients of wild type pendrin-EYFP and different pendrin variants with the plasma membrane (a) and the endoplasmic reticulum (b). For the control, cells were transfected with a vector bearing the EYFP sequence alone. EYFP is homogeneously distributed in the cytosol, therefore does not show preferential localization neither with the PM, nor with the ER. ***$p < 0.001$, **$p < 0.01$ *versus* wild type (PDS WT-EYFP), one way ANOVA with Bonferroni's post-test, $n \geq 6$.

4.3 Evaluation of expression levels of pendrin allelic variants

In association with different subcellular localization patterns, possible differences in the degree of expression of the different pendrin variants were also investigated and evaluated both at the whole cell, total membranes and plasma membrane level. The protein expression levels of wild type and mutant pendrin have been analyzed *via* two different experimental approaches: confocal imaging of pendrin-EYFP fusion proteins and western blotting on protein extracts from transfected cells.

4.3.1 Confocal imaging

Two sets of experiments have been set up in order to quantify the amount of protein in the whole cell and plasma membrane region, with two different normalization methods.

4.3.1.1   Total pendrin expression

To evaluate total pendrin expression, cells for imaging experiments were transfected with a plasmid bearing the cDNA coding for wild type or mutant pendrin with EYFP fused to the C-teminus (PDS-EYFP). Before imaging, the cells were fixed with 4% paraformaldehyde and stained with DAPI.

In the panels of figure 13, representative acquisition fields for the different pendrin variants analyzed are shown. For each mutant and the wild type, the acquisition in the emission channel of EYFP is shown beside the corresponding acquisition in the emission channel of DAPI. The intensity of the signal in both channels was expressed as averaged levels of grey. The mean signal intensity emitted by the fusion protein PDS-EYFP in the whole acquisition field was normalized for the cell density in the same field, represented by the signal emitted by the nuclear staining with DAPI (Figure 13). The results could be statistically analyzed in order to compare the expression levels of the different pendrin variants to the wild type (Figure 14).
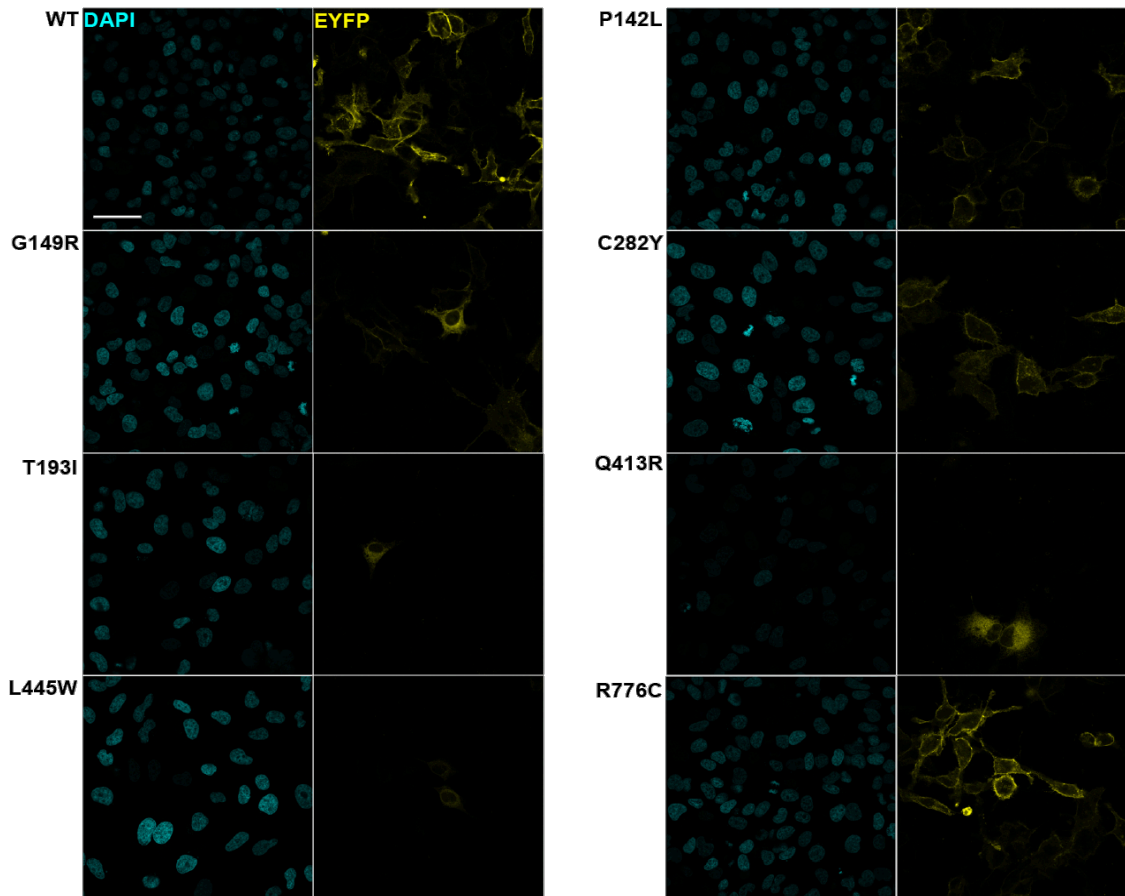
Figure 13: confocal imaging of fixed HeLa cells transfected with the fusion protein pendrin-EYFP (wild type or mutated, yellow, right panels). The normalization of the signal was performed according to the cell density in the field, given by the nuclear staining with DAPI (blue, left panels). Scale bar: 50 μM.
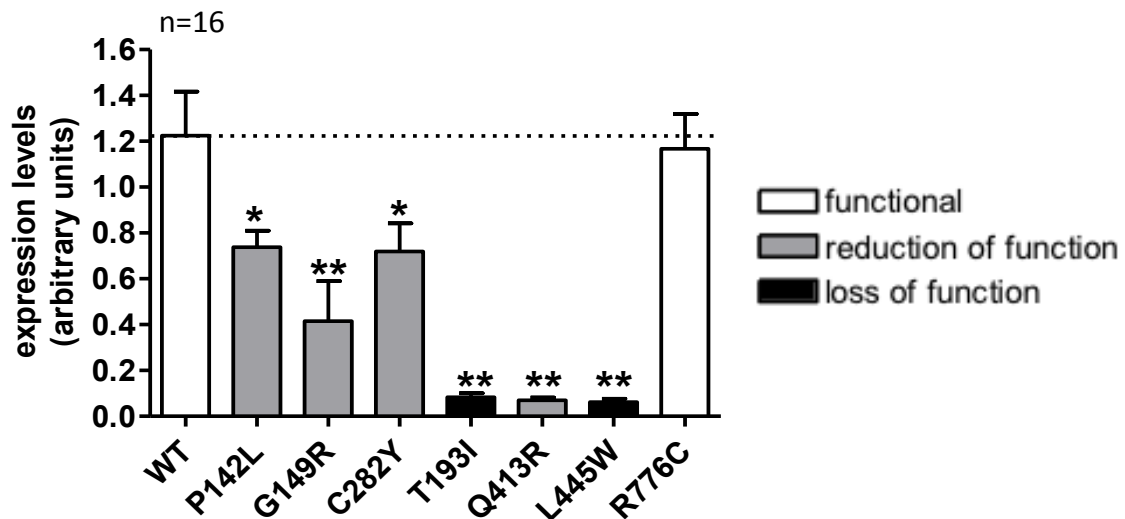

Figure 14: normalized total expression levels of pendrin-EYFP (wild type or mutated), expressed as ratio between pendrin-EYFP and DAPI emission intensities in the acquisition field. Pendrin variants that show a reduction of function according to the functional tests illustrated previously are marked in grey. The black bars identify those pendrin variants displaying a complete loss of function, while variants whose the function was not affected and the wild type are indicated by white bars. **$p < 0.01$, *$p < 0.05$ *versus* wild type, one way ANOVA with Bonferroni's post-test, n=16.

69

All the analyzed pendrin variants show a reduced overall expression, with the only exception of the variant R776C, whose expression levels are not statistically different from the wild type. The mutants with complete loss of function (T193I and L445W) show the lower expression levels. Surprisingly, also the mutant Q413R shows an extremely low expression level, comparable to the two loss of function mutations, even though it retains a residual transport activity.

4.3.1.2 Pendrin expression at the plasma membrane region

For the analysis of pendrin abundance at the plasma membrane level, cells have been co-transfected with a plasmid bearing the cDNA coding for wild type or mutated pendrin, with EYFP fused at the C-terminus (PDS-EYFP), and a plasmid carrying the cDNA for ECFP alone, as an indicator of the transfection efficacy of the single cell (Figure 15).

As for the previous set of experiments, the intensity of the signal emitted in EYFP and ECFP channels was expressed as averaged levels of grey.

In this case, the intensity of the signal emitted by PDS-EYFP in the plasma membrane region of a single cell has been normalized for the signal emitted by ECFP in the cytosol of the same cell (Figure 15). Furthermore, in order to efficiently identify the plasma membrane region, especially for those mutants previously shown to display a complete retention in the ER, cells have been treated with the same specific PM stain (CellMask Deep Red Plasma Membrane Stain) used in the co-localization experiments.

The results were statistically analyzed in order to compare the expression levels of the different pendrin variants to the wild type (Figure 16).
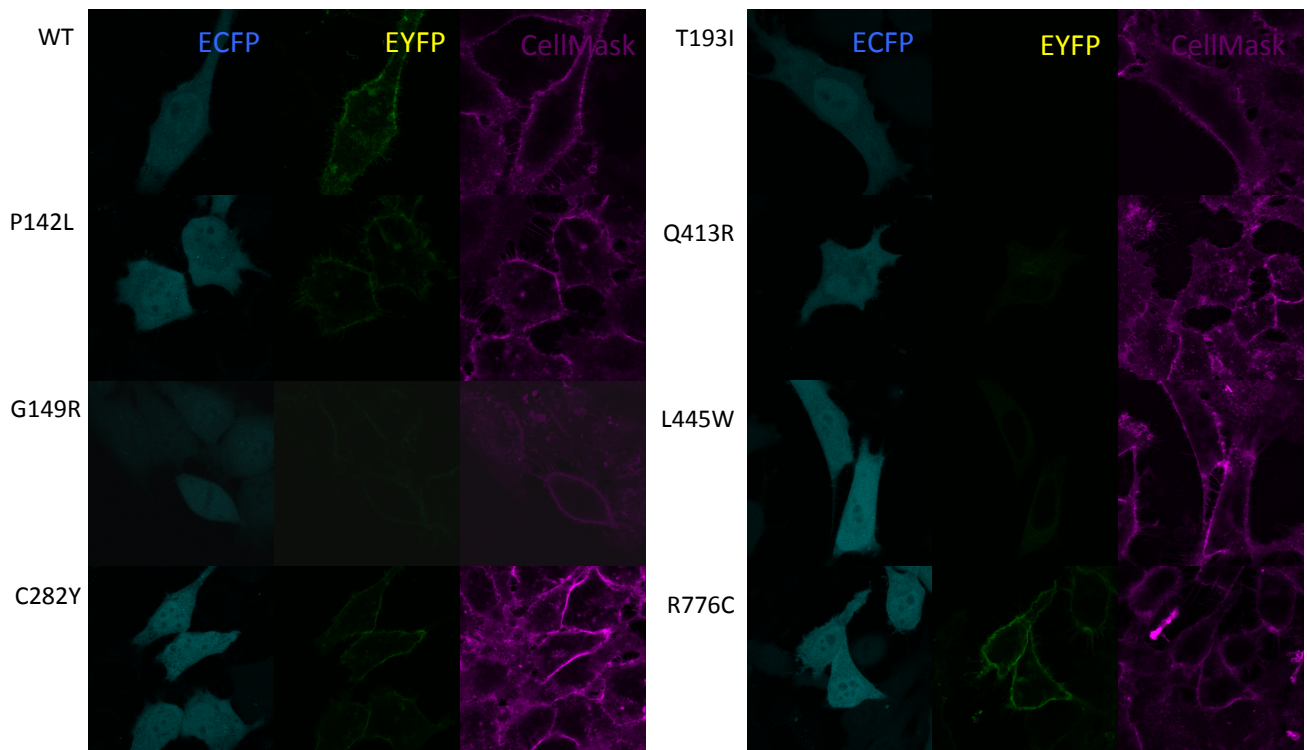
Figure 15: confocal imaging of living HeLa cells co-transfected with the fusion protein pendrin-EYFP (wild type or mutated, green, middle panels) and ECFP (blue, left panels) as a marker of the transfection efficiency of the single cell. The signal emitted by pendrin-EYFP in the plasma membrane region was normalized for the emission of ECFP in the cytosol of the same cell. In order to efficiently identify the plasma membrane of cells, a fluorescent dye specific for the plasma membrane was used (magenta, right panels) Scale bar: 20 µM.
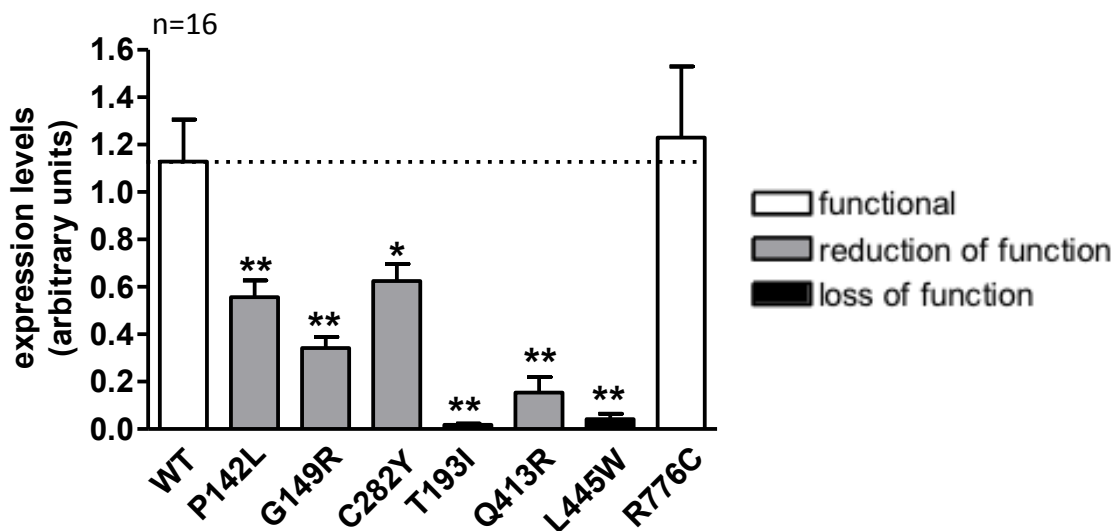
Figure 16: normalized plasma membrane expression levels of pendrin-EYFP (wild type or mutated) expressed as ratio between the signal emitted by pendrin-EYFP in the plasma membrane region and ECFP (expressed as averaged levels of grey) in individual cells. Pendrin variants that show a reduction of function according to the functional tests illustrated previously are marked in grey. Fully functional variants and the wild type are indicated by white bars. The black bars identify those pendrin variants displaying a complete loss of function. *p<0.05, **p<0.01 *versus* wild type, one way ANOVA with Bonferroni's post-test. n=16.

All the analyzed pendrin variants show a plasma membrane expression significantly reduced with respect to the wild type, with the only exception of R776C. A clear correlation between total and plasma membrane abundance can be observed for all the analyzed pendrin variants. Furthermore, expression levels of the different pendrin variants appear to be consistent with the level of transport activity determined previously *via* functional test (Figure 9). This important evidence will be better discussed in the next section.

4.3.2 Western Blot analysis

The results of imaging experiments on the expression levels of pendrin were obtained with a fusion protein (PDS-EYFP) and refer to the total (intracellular *plus* plasma membrane) and plasma membrane pendrin abundance. Theoretically, the presence of a relatively big tag (the EYFP protein) fused to the C-terminus of pendrin may alter its folding and trafficking. In order to verify this last hypothesis, expression levels were also determined by western blot analysis following transfection of untagged wild type and mutated pendrin.

Western blot analysis have been performed on protein extracts from HEK 293 Phoenix cells transfected with wild type or mutant pendrin. In two separate sets of experiments, the expression of pendrin in total proteins and total membranes proteins fractions were analyzed.

4.3.2.1   Expression levels of pendrin in total cellular proteins extracts

HEK 293 Phoenix cells were transfected with pTARGET vectors bearing the cDNA of wild type or mutant pendrin. In this case the pTARGET vectors were mutated in order not to express the hexahistidine tag at the C-terminus of pendrin, since it was observed in an independent set of experiments that its presence prevents the binding of the anti-pendrin antibody (data not shown). The negative control is a protein extract from mock transfected HEK 293 Phoenix cells.

In Figure 17, a representative blot is reported, showing multiple bands corresponding to pendrin between 90 and 120 kDa and a single band corresponding to the housekeeping protein GAPDH between 35 and 40 kDa. Multiple bands around 90-120 kDa are to be ascribed to the multiple glycosylation states of the protein, as suggested by the findings of Azroyan et al. in 2010 [116] and confirmed by Cirello et al. in 2012 [117]. The bands corresponding to pendrin are clearly visible in the wild type and P142L lanes, whereas they are relatively faint in all the other lanes. However, it was possible to analyze the blot densitometrically (Figure 18). The complete lack of signal relative to pendrin in the lane corresponding to the mutant R776C is likely to be attributed to a conformational disruption of the epitope recognized by the anti-pendrin antibody due to the presence of the mutation in position 776. Accordingly, this antibody is known to target the C-terminus of pendrin [118]. It is to be noticed the higher intensity of the signal corresponding to the mutant P142L if compared to the wild type. This may be due to an accumulation of this particular protein form, circumventing the degradation process.
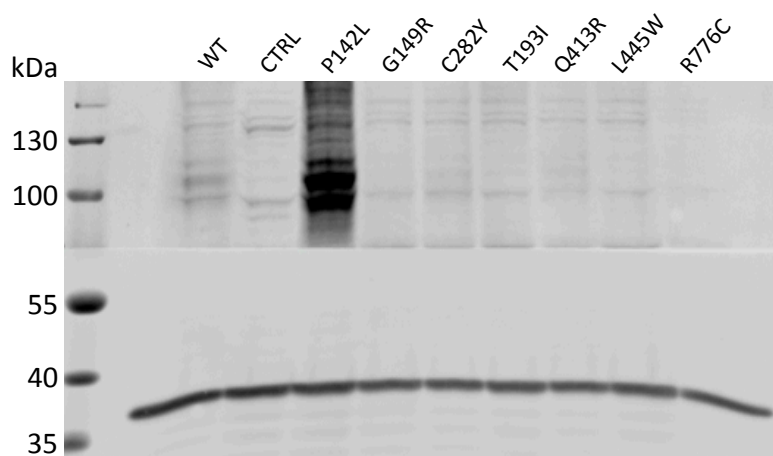

Figure 17: representative western blot from total protein extractions. The multiple bands between 90 and 120 kDa correspond to the different glycosylation forms of pendrin. The single band right above 35 kDa corresponds to GAPDH (expected molecular weight: 36 kDa). Curiously, the variant P142L appears to show a stronger signal than the wild type. The lack of signal in the R776C lane may be due to the disruption of the epitope recognized by the antibody.

The intensity of the bands corresponding to wild type and mutated pendrin was densitometrically determined and normalized to the intensity of the corresponding GAPDH band. Results show that the abundance of all pendrin variants in total protein extracts is strongly reduced compared to wild type, with the only exception of the mutant P142L that, unexpectedly, shows an expression level comparable to the wild type (Figure 18).
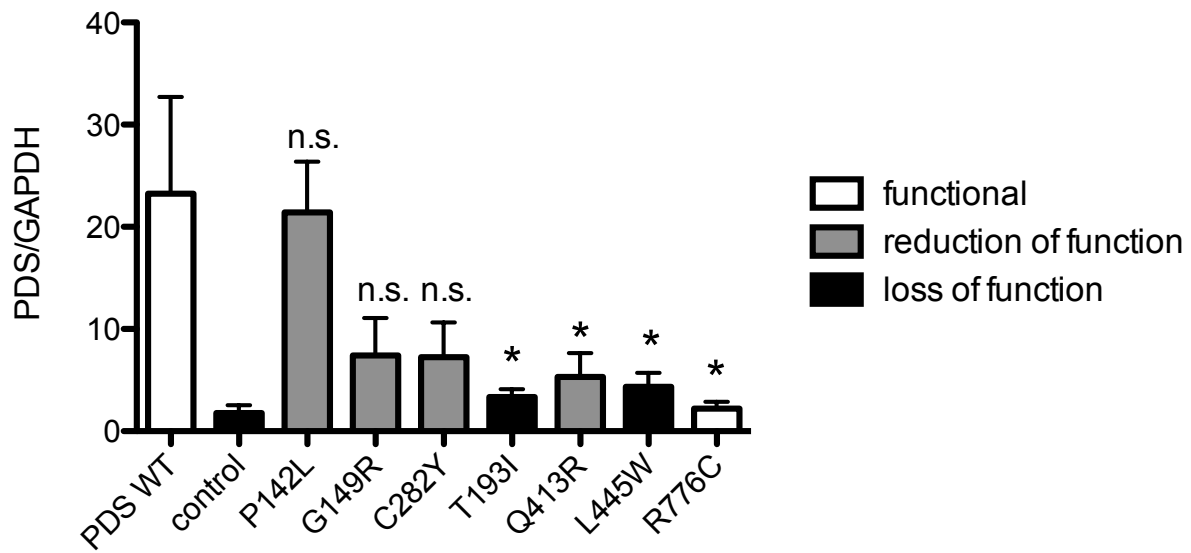
73

Figure 18: Densitometrical analysis of western blots on total protein extracts. Pendrin signal was normalized for the signal of the housekeeping protein GAPDH. The color of bars indicates the transport activity of the corresponding pendrin variant. n.s.: not statistically significant, *p<0.05, one way ANOVA with Dunnett's post-test *versus* PDS WT, n=4.

4.3.2.2 Expression levels of pendrin in total membranes extracts

For the analysis of pendrin expression in the total membranes fraction, a different protocol was followed. As for the previous set of experiments, HEK 293 Phoenix cells were transfected with pTARGET vectors coding for untagged wild type or mutant pendrin. The extraction of the total membranes fraction (including the plasma membrane as well as organelles membranes) was achieved with the Plasma Membrane extraction Kit. The whole pellet obtained was directly loaded on the gel after resuspension and denaturation in the Loading dye (see Methods).

In Figure 19, a representative blot is displayed, showing multiple bands corresponding to pendrin between 90 and 120 kDa and the band corresponding to the housekeeping protein calreticulin right above 55 kDa (expected molecular weight: 62 kDa). Bands corresponding to mutated pendrin are now significantly more distinguishable compared to the blot represented in Figure 17. As in the previous western blots on total proteins extracts, no signal could be detected in the lane corresponding to R776C. Interestingly, the bands corresponding to P142L are now slightly less intense than the wild type, in contrast to what seen in the total proteins blot (Figure 17).

The intensity of the bands corresponding to pendrin variants were densitometrically quantified and normalized according to the intensity of the corresponding calreticulin band (Figure 20).
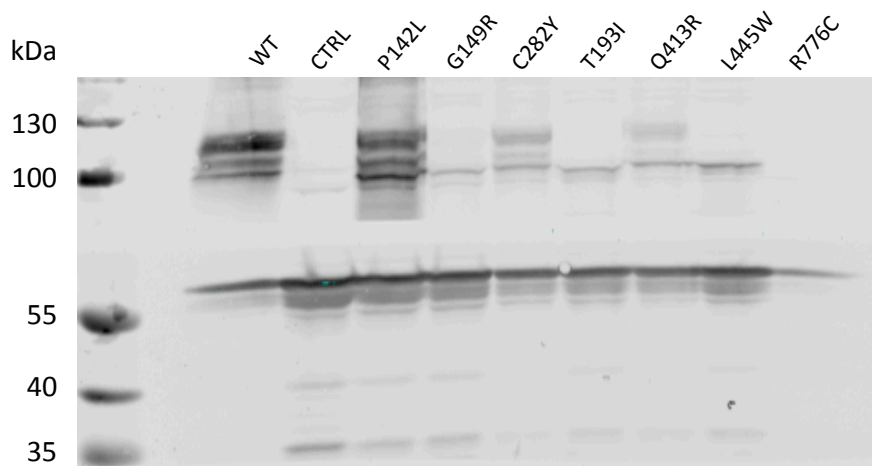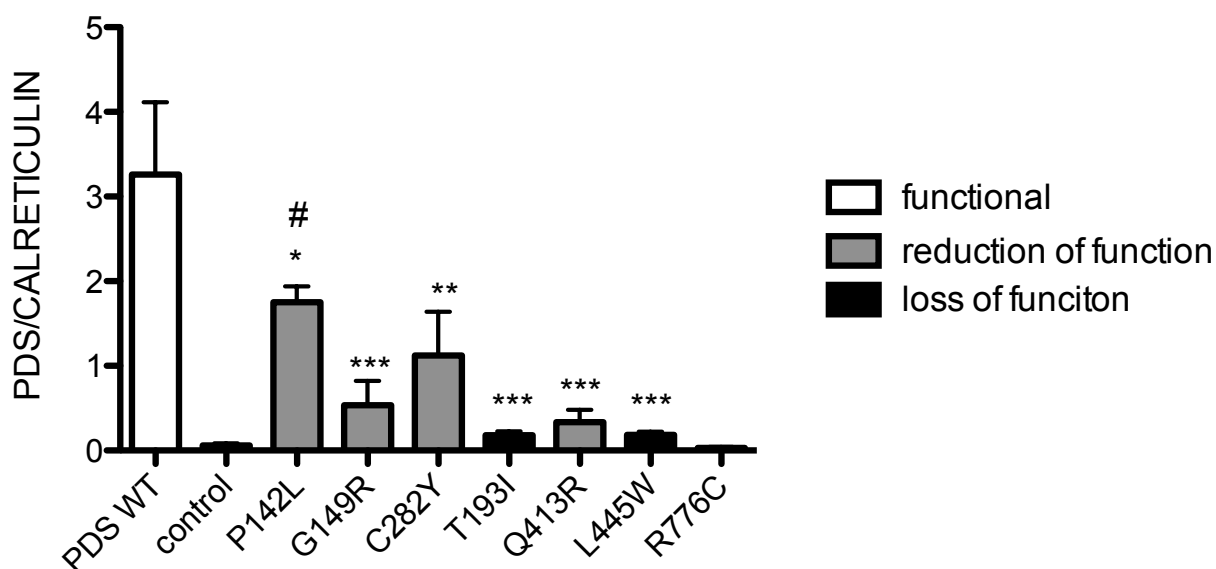

Figure 19: representative western blot on total membranes proteins extractions. The bands between 90 and 120 kDa correspond to the different glycosylation states of pendrin. The single band at ~60 kDa corresponds to calreticulin. The lack of signal in the R776C lane may be due to the disruption of the epitope recognized by the antibody.

Figure 20: Densitometrical analysis of western blots on total membranes proteins extracts. Pendrin signal was normalized for the signal of the housekeeping protein calreticulin. The color of bars indicates the transport activity of the corresponding pendrin variant. n.s.: not statistically significant, ***$p<0.005$, **$p<0.01$, *<0.05, one way ANOVA with Dunnett's post-test *versus* PDS WT; #$p<0.05$, one way ANOVA with Dunnett's post-test *versus* control, n=3.

Figure 20 includes the statistical analysis of western blot densitometry on total membranes proteins. All pendrin variants show membrane expression levels significantly reduced in relation to the wild type. Their expression level is statistically undistinguishable from the negative control, exception made for P142L.

These results correlate very well with those of the imaging experiments described in the previous sections (Figures 14 and 16), thus supporting the evidence that expression levels of pendrin variants with function reduced or annihilated are significantly lower compared to wild type.

4.4   Rescue of pendrin activity

All the functionally impaired pendrin variants analyzed in this work show reduced cellular expression levels with respect to the wild type and many of them are at least partially retained in the ER. Such evidence points to a role of the protein degradation machinery in the determination of the expression levels – and possibly, of the functional impairment – of pendrin mutants.

The most common protein degradation pathway active in the cell involves the proteasome complex machinery. Proteins destined to degradation are driven to the proteasome by polyubiquitination signals. Within the proteasome complex, a series of proteolysis steps degrade the proteins to single aminoacids. Under this light, a possible rescuing approach of pendrin transport activity may start from the inhibition or modulation of such a degradation process.

In order to test the effect of such a treatment, two sets of experiments were set up, in order to:

(i)   determine the effect of the inhibition of proteasomal degradation on the transport activity of pendrin mutants by means of the fluorometric functional test described in the previous sections;

(ii)   determine the effect of the inhibition of proteasomal degradation on pendrin protein abundance by confocal imaging. As described in the previous sections, both the total and the plasma membrane pendrin abundance were analyzed.

4.4.1 Function of pendrin variants following inhibition of the ubiquitin proteasome pathway

HEK 293 Phoenix cells for the functional tests were co-transfected with the different pendrin variants and the fluorescent intracellular iodide sensor EYFP H148Q I152L. The cells were incubated for 6 hours in complete culture medium supplemented with the proteasome inhibitor MG132 (10 µM), or its vehicle (0.1% DMSO).

The transport activity measured for the different pendrin variants in cells treated with MG132 was compared to the activity of the same variants in cells treated with the vehicle. This way it was possible to determine the efficacy of the proteasome inhibition on pendrin transport activity. In Figure 21, the results of the functional experiments are presented.
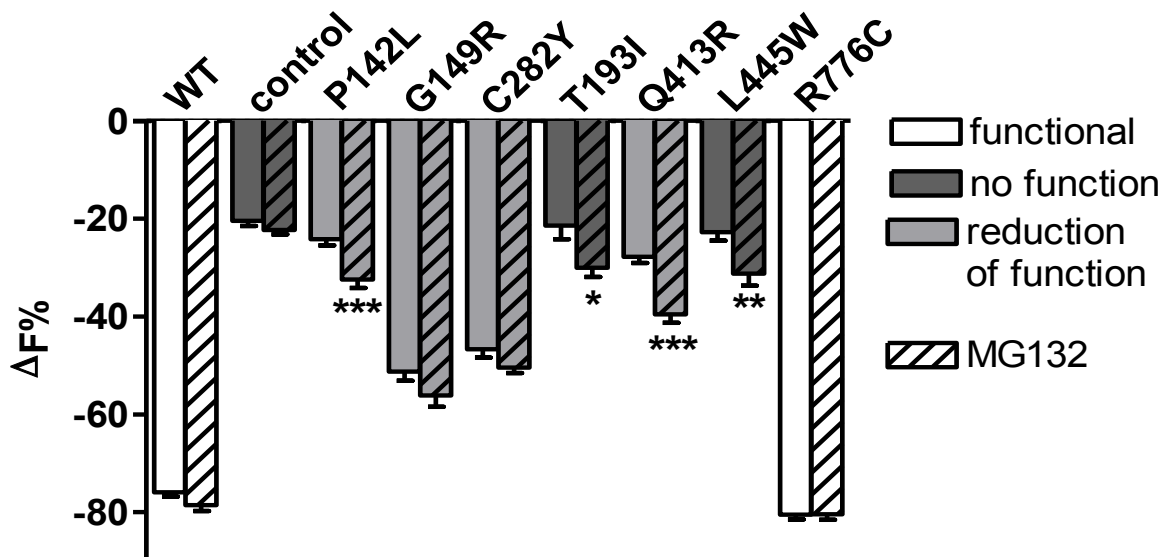

Figure 21: functional test on pendrin variants in cells treated with the proteasome inhibitor MG132 (10 µM, dashed bars) or its vehicle (DMSO, open bars). The statistical difference between MG132 and vehicle-treated cells was tested for each pendrin variant analyzed. *p<0.05, **p<0.01, ***p<0.005, two-tailed, unpaired Student's t-test *versus* vehicle-treated cells, n=12.

From the functional tests, a significant effect of the treatment in 4 cases out of 9 (4 out of 6 functionally impaired variants) emerges. Specifically, the transport activity of the functionally impaired pendrin variants P142L, T193I, Q413R and L445W significantly improved upon treatment of cells with MG132 with respect to the vehicle. MG132 treatment was ineffective on cells transfected with the functionally impaired pendrin variants G149R and C282Y. In addition, the activity of wild type pendrin and the functional variant R776C were not modified. Importantly, the endogenous transport activity of control cells was not affected.

4.4.2 Expression levels of pendrin variants following inhibition of the ubiquitin proteasome pathway

In order to verify if the increased function of the above mentioned pendrin variants following inhibition of proteasomal degradation is the consequence of an increase in their expression levels, the protein abundance of pendrin variants was measured by fluorescence imaging upon treatment with MG132 or its vehicle (DMSO).

Two sets of experiments were set up, as previously described. In the first set of experiments, the total pendrin abundance was evaluated, while in the second set of experiments, only pendrin abundance in the plasma membrane region was considered.

4.4.2.1   Total pendrin expression

HeLa cells were transfected with the different variants of pendrin fused to EYFP (PDS-EYFP). 72 hours after transfection, the cells were incubated overnight at 37°C with complete media supplemented with 10 μM MG132 or its vehicle (0.1% DMSO). Before imaging, the cells were fixed with 4% paraformaldehyde and stained with DAPI.
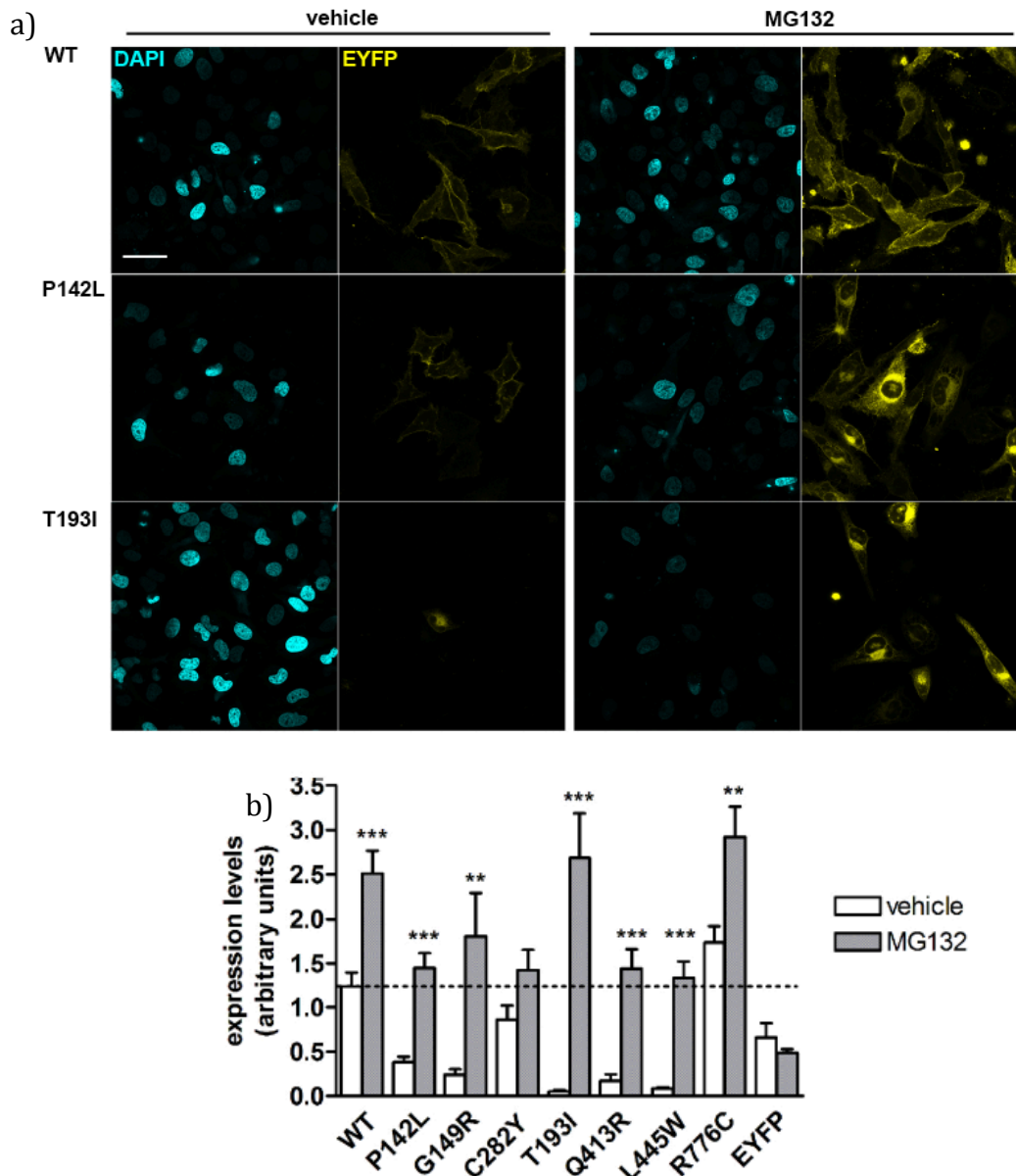
Figure 22: fluorescence imaging of fixed HeLa cells transfected with pendrin variants and treated with 10 μM MG132 or its vehicle. a) the effect of the proteasome inhibitor on the total expression levels of wild type and two representative pendrin variants (P142L, T193I) is shown in the picture. In the left ends panels, the acquisition in the emission channel of DAPI (blue) is shown. In the right ends panels, the emission of pendrin-EYFP (yellow) is shown. DAPI gives an indication of the cell density in the field, and was used to normalize the EYFP signal. Scale bar: 50 μm. b) Normalized expression levels determined for each pendrin variant and the control (EYFP). **p<0.01, ***p<0.005, two-tailed, unpaired Student's t-test *versus* vehicle-treated cells, n=12.

The signal emitted by pendrin-EYFP in the whole acquisition field, expressed as averaged levels of grey, was normalized for the cell density in the same field according to the signal emitted by DAPI, also expressed as averaged levels of grey. The treatment with MG132 (Figure 22) induced a significant increase in the total expression levels of all pendrin variants, except for C282Y (in this case, only a not statistically significant tendency was observed). A strong effect was also recorded for wild type pendrin and for the

functional variant R776C. In all cases, upon treatment with MG132, the protein expression of the different hypofunctional variants reached at least the level of expression of wild type pendrin in vehicle-treated cells (dashed line in Figure 22). MG132 was ineffective in increasing the expression levels of EYFP protein in control cells.

4.4.2.2 Pendrin expression at the plasma membrane region

The same approach was used to determine pendrin expression in the plasma membrane region. In this series of experiments, as described in the previous sections, the signal emitted by pendrin-EYFP in regions of interest of the plasma membrane was normalized on the emission of ECFP in the cytosol of the same cell, as an indication of transfection efficacy of the single cell.

As for the previous series of experiments, HeLa cells were transfected with the different mutant forms of pendrin fused to EYFP. 72 hours after transfection, the cells were incubated overnight at 37°C with 10 µM MG132 or its vehicle (DMSO). Right before imaging, living cells were stained with a specific PM dye (CellMask Deep Red Plasma Membrane Stain) as described in the methods. This staining was particularly necessary to identify the plasma membrane in cells transfected with those pendrin variants completely lacking a PM localization.

In Figure 23a, a representative example of evaluation of plasma membrane abundance of a pendrin variant following MG132 treatment is shown. On the left end panels the emission of ECFP is presented, while in the right end panels the emission of pendrin P142L-EYFP is displayed. Top panels refer to cells treated with the vehicle, lower panels refer to cells treated with MG132. The emission of P142L in cells treated with the vehicle (top right) is to be compared to the emission of the same pendrin variant in cells treated with MG132 (bottom right). The increased expression in the plasma membrane region upon treatment with the proteasome inhibitor is clearly visible. The graph in Figure 23b shows the expression levels of the different pendrin variants in the plasma membrane region normalized for the transfection efficacy of the single cell. For each variant, the plasma membrane expression levels with and without treatment with MG132 were compared.
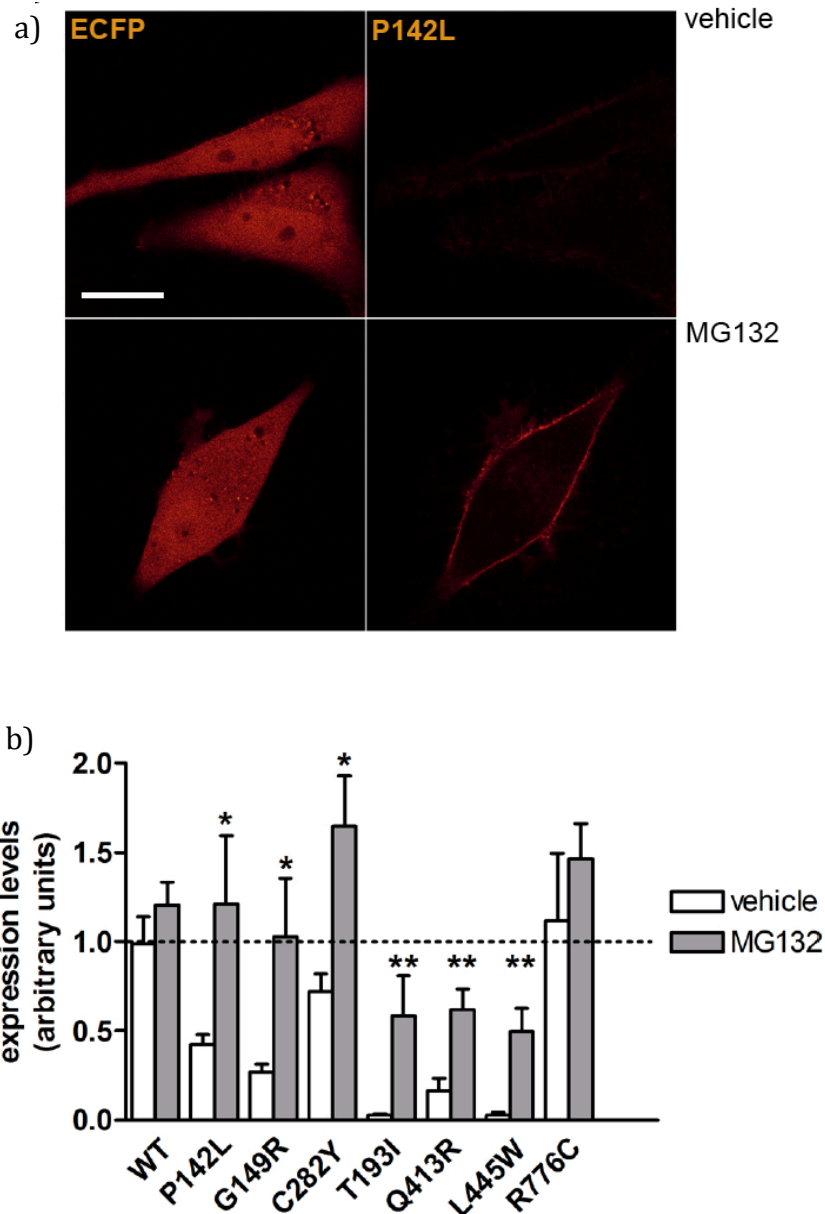
80

Figure 23: a) representative picture of living HeLa cells for the quantification of pendrin expression in the PM region. The variant P142L is here represented. On the top right, the emission of pendrin P142L in cells treated with the vehicle is shown, to be compared with the emission of the same variant in cells treated with the proteasome inhibitor MG132 (10 µM, overnight, bottom right). In the left end panels, the signal emitted by ECFP in vehicle and MG132-treated cells is shown and was used to normalize the pendrin P142L-EYFP signal for the transfection efficacy of the single cell. Scale bar: 10 µm. b) normalized expression levels of pendrin-EYFP variants. **$p<0.01$, *$p<0.05$, two-tailed, unpaired Student's t-test *versus* vehicle-treated cells, n=10.

A significant increase in plasma membrane expression upon treatment with MG132 was observed for each hypofunctional variant analyzed, including C282Y. This last variant appeared to be irresponsive to MG132 in the previous set of experiments, when total pendrin expression was evaluated. No increase in the plasma membrane expression levels could be determined for wild type pendrin and for the functional variant R776C following MG132 treatment.

4.5 Functional screening of pendrin ligands

In the following sections the results of the functional screening of putative pendrin ligands are reported. The tested compounds are presented according to the rationales described in the introduction:

- known inhibitors of chloride channels and transporters and inhibitors of transporters homolog to pendrin, such as *Slc26a3* (DRA);

- antihypertensive and diuretic agents;

- small compounds predicted by a bioinformatic approach based on the abstraction of the primary aminoacidic sequence of pendrin, called meta-analysis;

- small compounds predicted by SHED alignment with established pendrin inhibitors.
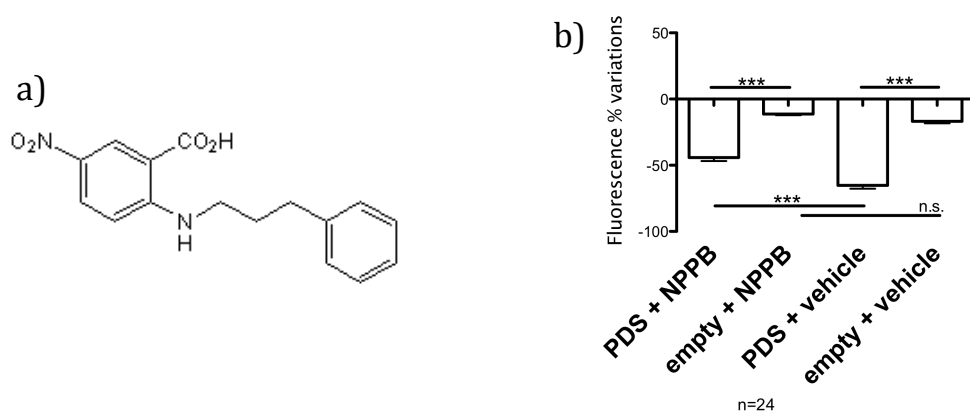
HEK 293 Phoenix cells were co-transfected with the pEYFP H148Q I152L and pTARGET PDS WT vectors or with the pEYFP H148Q I152L and pTARGET empty vectors as a negative control (empty). The substances or their vehicles were added to the extracellular high chloride and high iodide solutions. As described in detail in the methods section, an intracellular EYFP H148Q I152L-dependent fluorescence decrease indicates an influx of iodide in pendrin-transfected (PDS) or control (empty) cells. The decrease in intracellular fluorescence measured after iodide injection in the extracellular solution of cells over-expressing pendrin and treated with the test compound was compared to the decrease measured in vehicle-treated cells. At the same time, an eventual effect of the treatment on control cells was analyzed, in order to discriminate possible effects on endogenous transports, therefore not directly related to pendrin activity.

For every reported substance, concentration and solvent are indicated. A brief description of the substance and its eventual use in the praxis are mentioned, as well as the rational driving the choice of the specific compound. The graphs show the results of the functional tests and the possible effect on pendrin-dependent or endogenous transport activity. The statistical analysis for all the presented results was performed by means of one-way ANOVA with Bonferroni's post-test.

4.5.1 Chloride channels and transporters blockers

NPPB (5-nitro-2-(3-phenylpropylamino)benzoic acid)

NPPB (Figure 24a) was included in the screening as it is a well known inhibitor of anion channels and was shown in previous experiments to inhibit pendrin-driven chloride uptake in HEK 293 Phoenix cells [1]. The final concentration of NPPB was 100 µM, the vehicle was 0.1% DMSO.
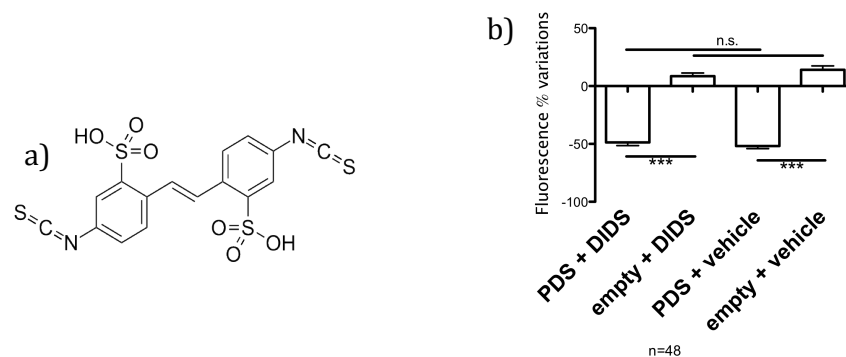

Figure 24. a) Structural formula of NPPB. b) Functional test on HEK 293 Phoenix cells transfected with pendrin or with an empty vector as a control. A fluorescence decrease (negative fluorescence % variation) indicates an influx of iodide in pendrin-transfected (PDS) or control cells (empty) following treatment with 100 µM NPPB or its vehicle (0.1% DMSO). n=24, one-way ANOVA with Bonferroni's post-test. ***$p < 0.005$, n.s.: not significant.

A 32% inhibition ($p < 0.005$) of iodide intake in pendrin-transfected cells (PDS) was determined upon treatment with NPPB with respect to the vehicle. No effect on control cells (empty) was measurable (Figure 24b).

DIDS (4,4'-diisothiocyanatostilbene-2,2'-disulfonic acid)

DIDS (Figure 25a) was included in the screening as it is widely recognized as an anion exchanger and anion channels inhibitor [119]. The final concentration of DIDS was 100 µM in 0.1% DMSO.
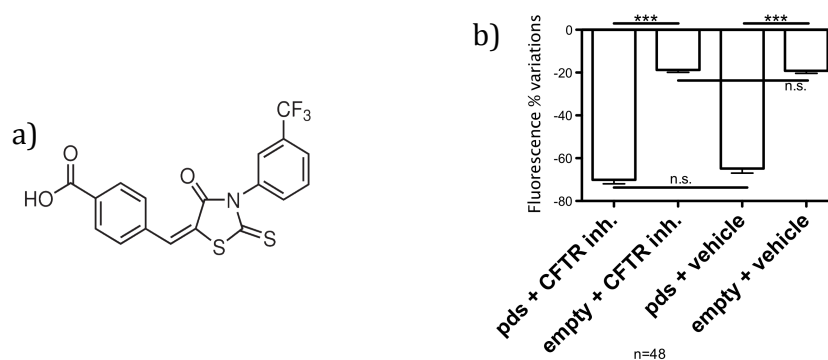
Figure 25. a) Structural formula of DIDS. b) Functional test on HEK 293 Phoenix cells transfected with pendrin or with an empty vector as a control. A fluorescence decrease (negative fluorescence % variation) indicates an influx of iodide in pendrin-transfected (PDS) or control cells (empty) following treatment with 100 µM DIDS or its vehicle (0.1% DMSO). n=48, one-way ANOVA with Bonferroni's post-test. ***p<0.005, n.s.: not significant.

No inhibition of iodide intake in pendrin transfected or control cells was determined upon treatment with DIDS with respect to the vehicle-treated cells (Figure 25b).

CFTR inhibitor-172

CFTR inhibitor-172 (Figure 26a) was included in the screening as it is a blocker of the cystic fibrosis transmembrane conductance regulator (CFTR) chloride channel [120]. The final concentration of CFTR inhibitor-172 was 1.6 µM [121] in 0.1% DMSO.
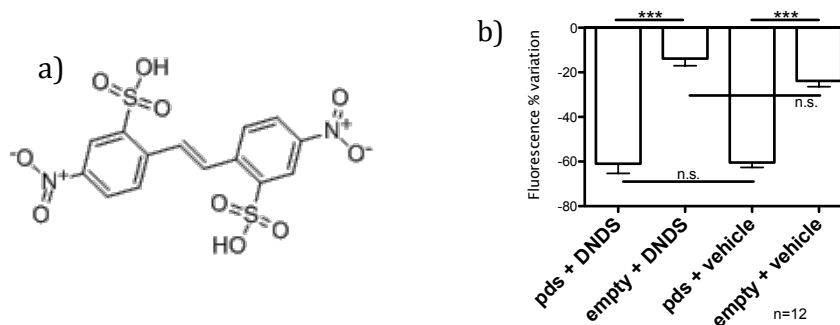

Figure 26. a) Structural formula of CFTR inhibitor-172. b) Functional test on HEK 293 Phoenix cells transfected with pendrin or with an empty vector as a control. A fluorescence decrease (negative fluorescence % variation) indicates an influx of iodide in pendrin-transfected (PDS) or control cells (empty) following treatment with 1.6 µM CFTR inhibitor-172 or its vehicle (0.1% DMSO). n=24, one-way ANOVA with Bonferroni's post-test. ***p<0.005, n.s.: not significant.

84

No inhibition of iodide intake in pendrin transfected or control cells was determined upon treatment with CFTR inhibitor-172 with respect to the vehicle-treated cells (Figure 26b).

DNDS (4',4'-dinitrostilbene-2,2'-disulfonic acid)

DNDS (Figure 27a) was included in the screening as a widely recognized anion channels and transporters inhibitor [122]. The final concentration of DNDS was 100 µM in isotonic solution.
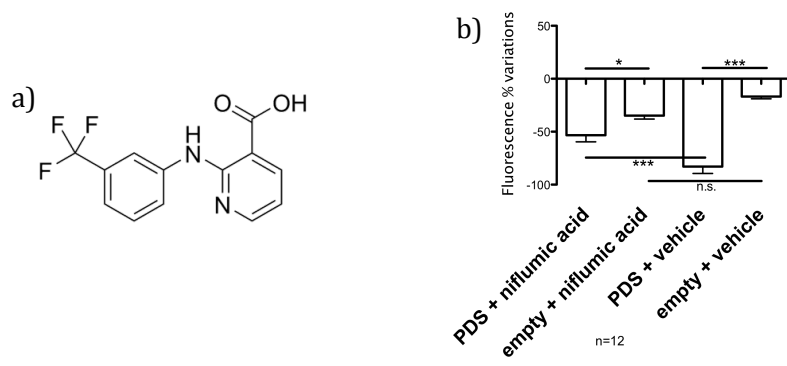

Figure 27. a) Structural formula of DNDS. b) Functional test on HEK 293 Phoenix cells transfected with pendrin or with an empty vector as a control. A fluorescence decrease (negative fluorescence % variation) indicates an influx of iodide in pendrin-transfected (PDS) or control cells (empty) following treatment with 100 µM DNDS or its vehicle (isotonic solution). n=12, one-way ANOVA with Bonferroni's post-test. ***p<0.005, n.s.: not significant.

No inhibition of iodide intake in pendrin transfected or control cells was determined upon treatment with DNDS with respect to the vehicle-treated cells (Figure 27b).

4.5.2 Inhibitors of DRA and previously assessed inhibitors of pendrin

Niflumic acid

The anti-inflammatory drug niflumic acid (Figure 28a) was included in the screening as it was recognized to inhibit the pendrin analog DRA [123]. The final concentration of niflumic acid was 100 µM in 0.1% DMSO.
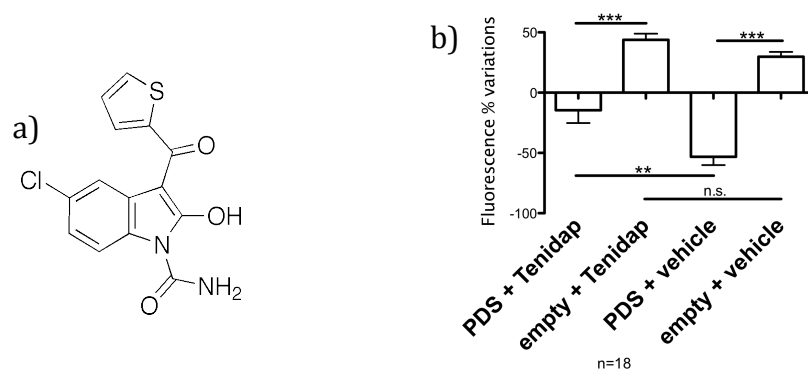
Figure 28. a) Structural formula of niflumic acid. b) Functional test on HEK 293 Phoenix cells transfected with pendrin or with an empty vector as a control. A fluorescence decrease (negative fluorescence % variation) indicates an influx of iodide in pendrin-transfected (PDS) or control cells (empty) following treatment with 100 µM niflumic acid or its vehicle (0.1% DMSO). n=12, one-way ANOVA with Bonferroni's post-test. ***p<0.005, *p<0.05, n.s.: not significant.

A 28% inhibition (p<0.005) of iodide intake in pendrin transfected cells was determined upon treatment with niflumic acid with respect to the vehicle-treated cells. No effect on control cells was measurable (Figure 28b). In some experiments though, an intracellular acidification was observed (see discussion).

Tenidap

The anti inflammatory drug tenidap (Figure 29a) was included in the screening as inhibitor of Cl^-/HCO_3^- exchange [124] and inhibitor of pendrin analog DRA [107]. The final concentration of tenidap was 100 µM in 0.1% DMSO.
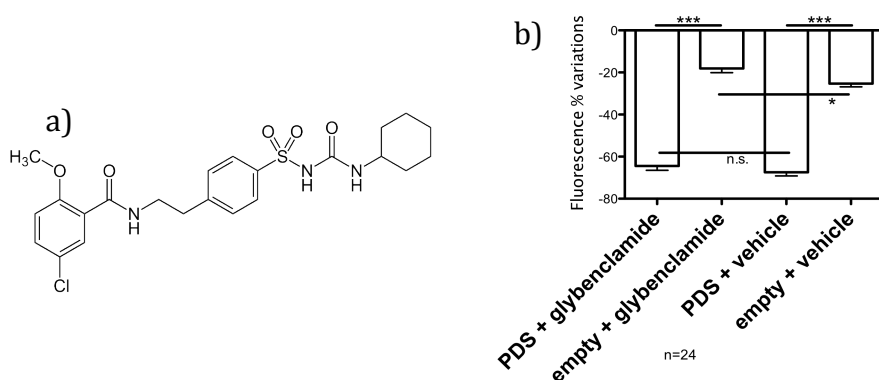

Figure 29. a) Structural formula of tenidap. b) Functional test on HEK 293 Phoenix cells transfected with pendrin or with an empty vector as a control. A fluorescence decrease (negative fluorescence % variation) indicates an influx of iodide in pendrin-transfected (PDS) or control cells (empty) following treatment with 100 µM tenidap or its vehicle (0.1% DMSO). n=18, one-way ANOVA with Bonferroni's post-test. ***p<0.005, **p<0.01, n.s.: not significant.

An 85% inhibition ($p < 0.01$) of iodide intake in pendrin transfected cells was determined upon treatment with tenidap with respect to the vehicle-treated cells. No effect on control cells was measurable (Figure 29b).

Glybenclamide

Glybenclamide (Figure 30a) was included in the screening as inhibitor of the pendrin analog, DRA [107]. The final concentration of glybenclamide was 100 µM in 0.1% DMSO.
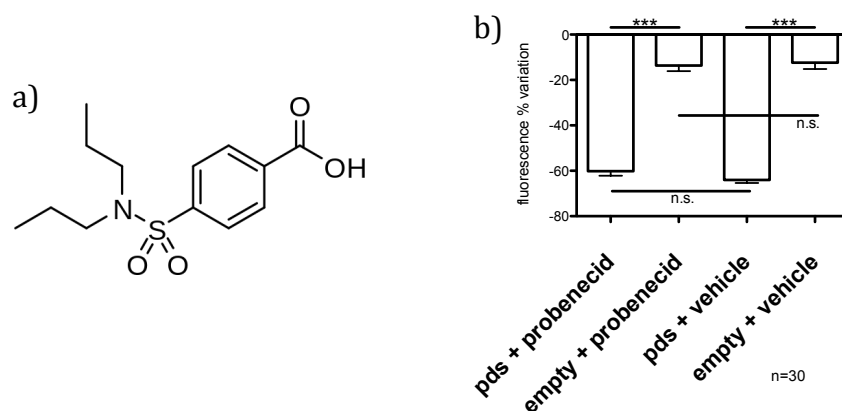

Figure 30. a) Structural formula of glybenclamide. b) Functional test on HEK 293 Phoenix cells transfected with pendrin or with an empty vector as a control. A fluorescence decrease (negative fluorescence % variation) indicates an influx of iodide in pendrin-transfected (PDS) or control cells (empty) following treatment with 100 µM glybenclamide or its vehicle (0.1% DMSO). n=24, one-way ANOVA with Bonferroni's post-test. ***$p < 0.005$, *$p < 0.05$, n.s.: not significant.

No inhibition of iodide intake in pendrin transfected cells was determined upon treatment with glybenclamide with respect to the vehicle-treated cells (Figure 30b). A slight effect on control cells was observed, possibly due to an effect of glybenclamide on endogenous transports.

Probenecid

Probenecid (Figure 31a) is an uricosuric drug used for treatment of gout and hyperuricemia. An inhibitory effect on pendrin has been shown by Scott et al. in 1999 [99]. The final concentration of probenecid was 100 µM in 0.1% chloroform.
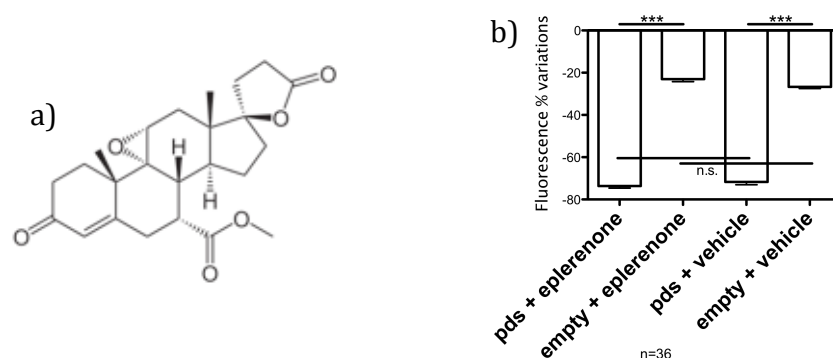
Figure 31. a) Structural formula of probenecid. b) Functional test on HEK 293 Phoenix cells transfected with pendrin or with an empty vector as a control. A fluorescence decrease (negative fluorescence % variation) indicates an influx of iodide in pendrin-transfected (PDS) or control cells (empty) following treatment with 100 µM probenecid or its vehicle (0.1% chloroform). n=30, one-way ANOVA with Bonferroni's post-test. ***$p < 0.005$, n.s.: not significant.

No inhibition of iodide intake in pendrin transfected or control cells was determined upon treatment with probenecid with respect to the vehicle-treated cells (Figure 31b).

4.5.3 Diuretics and antihypertensive agents

Eplerenone

Eplerenone (Figure 32a) is an aldosterone antagonist exerting a diuretic effect. The final concentration of eplerenone was 10 µM in 0.1% DMSO, due to its poor solubility.

Figure 32. a) Structural formula of eplerenone. b) Functional test on HEK 293 Phoenix cells transfected with pendrin or with an empty vector as a control. A fluorescence decrease (negative fluorescence % variation) indicates an influx of iodide in pendrin-transfected (PDS) or control cells (empty) following treatment with 10 µM eplerenone or its vehicle (0.1% DMSO). n=36, one-way ANOVA with Bonferroni's post-test. ***$p < 0.005$, n.s.: not significant.

88

No inhibition of iodide intake in pendrin transfected or control cells was determined upon treatment with eplerenone with respect to the vehicle-treated cells (Figure 32b).

Acetazolamide

Acetazolamide (Figure 33a) is a carbonic anhydrase inhibitor with a diuretic effect. The final concentration of acetazolamide was 100 µM in 0.1% DMSO.
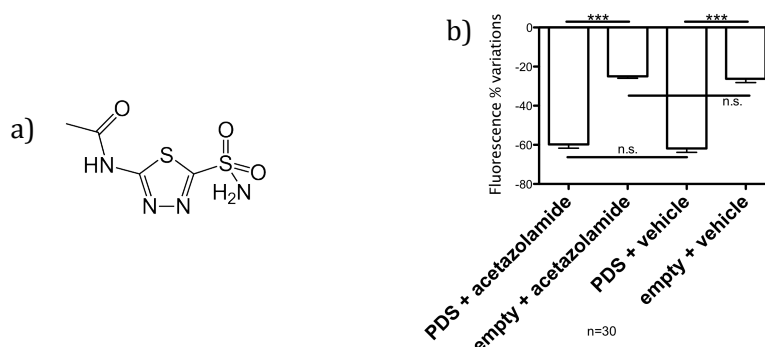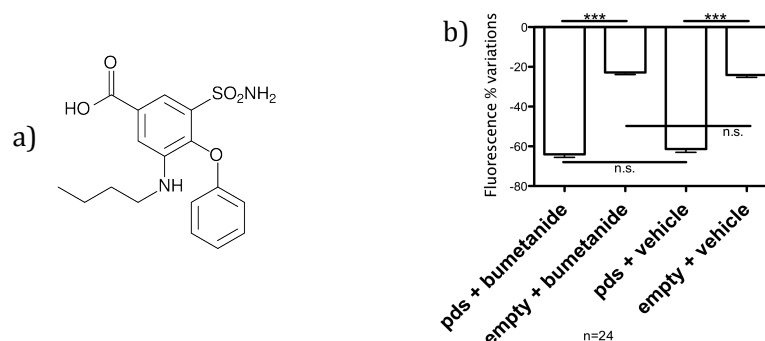

Figure 33. a) Structural formula of acetazolamide. b) Functional test on HEK 293 Phoenix cells transfected with pendrin or with an empty vector as a control. A fluorescence decrease (negative fluorescence % variation) indicates an influx of iodide in pendrin-transfected (PDS) or control cells (empty) following treatment with 100 µM acetazolamide or its vehicle (0.1% DMSO). n=30, one-way ANOVA with Bonferroni's post-test. ***$p < 0.005$, n.s.: not significant.

No inhibition of iodide intake in pendrin transfected or control cells was determined upon treatment with acetazolamide with respect to the vehicle-treated cells (Figure 33b).

Bumetanide

Bumetanide (Figure 34a) is a blocker of chloride reabsorption in the ascending loop of Henle [125]. The final concentration of bumetanide was 100 µM in 0.1% DMSO.

Figure 34. a) Structural formula of bumetanide. b) Functional test on HEK 293 Phoenix cells transfected with pendrin or with an empty vector as a control. A fluorescence decrease (negative fluorescence % variation) indicates an influx of iodide in pendrin-transfected (PDS) or control cells (empty) following treatment with 100 µM bumetanide or its vehicle (0.1% DMSO). n=24, one-way ANOVA with Bonferroni's post-test. ***$p < 0.005$, n.s.: not significant.

No inhibition of iodide intake in pendrin transfected or control cells was determined upon treatment with bumetanide with respect to the vehicle-treated cells (Figure 34b).

Furosemide

Furosemide (Figure 35a) is a blocker of the Na^+-K^+-$2Cl^-$ cotransporter in the ascending loop of Henle. Its final concentration was 100 µM in 0.1% DMSO.
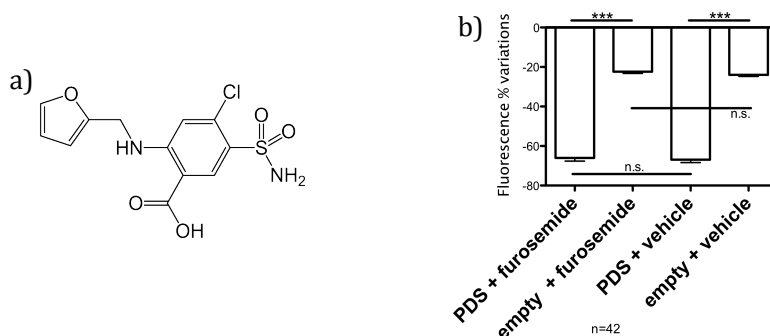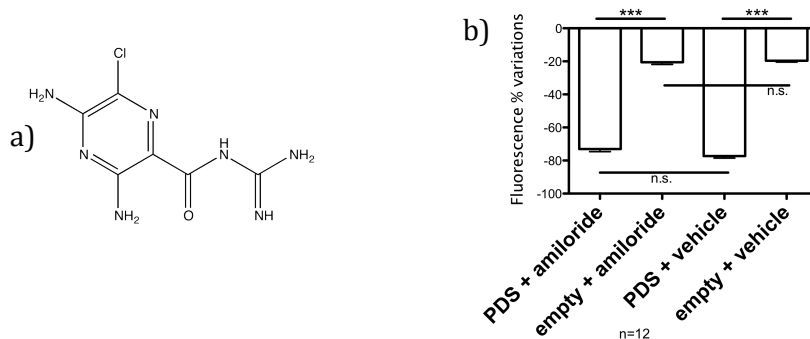

Figure 35. a) Structural formula of furosemide. b) Functional test on HEK 293 Phoenix cells transfected with pendrin or with an empty vector as a control. A fluorescence decrease (negative fluorescence % variation) indicates an influx of iodide in pendrin-transfected (PDS) or control cells (empty) following treatment with 100 µM furosemide or its vehicle (0.1% DMSO). n=24, one-way ANOVA with Bonferroni's post-test. ***p<0.005, n.s.: not significant.

No inhibition of iodide intake in pendrin transfected or control cells was determined upon treatment with furosemide with respect to the vehicle-treated cells (Figure 35b).

Amiloride

Amiloride (Figure 36a) is a blocker of the epithelial Na^+ channel (ENaC) in the distal nephron. The final concentration of amiloride was 100 µM in 0.1% DMSO.

Figure 36. a) Structural formula of amiloride. b) Functional test on HEK 293 Phoenix cells transfected with pendrin or with an empty vector as control. A fluorescence decrease (negative fluorescence % variation) indicates an influx of iodide in pendrin-transfected (PDS) or control cells (empty) following treatment with 100 µM amiloride or its vehicle (0.1% DMSO). n=12, one-way ANOVA with Bonferroni's post-test. ***p<0.005, n.s.: not significant.

No inhibition of iodide intake in pendrin transfected or control cells was determined upon treatment with amiloride with respect to the vehicle-treated cells (Figure 36b).

Hydrochlorothiazide

Hydrochlorothiazide (HCTZ, Figure 37a) is a blocker of the $\underline{Na}^+$-$\underline{Cl}^-$ cotransporter (NCC). The final concentration of hydrochlorothiazide was 100 µM in 0.1% DMSO.
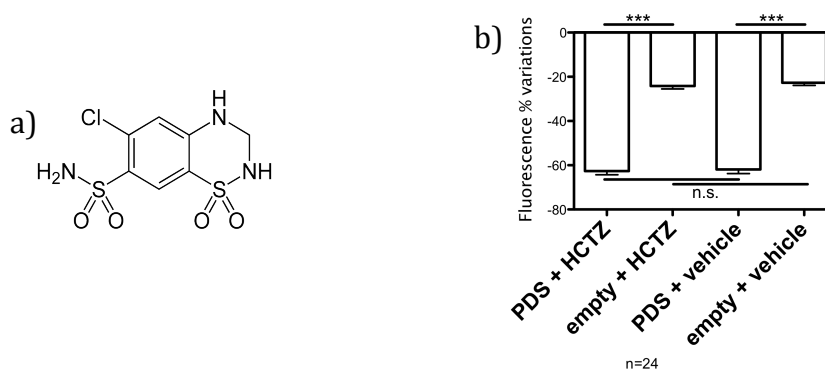

Figure 37. a) Structural formula of hydrochlorothiazide. b) Functional test on HEK 293 Phoenix cells transfected with pendrin or with an empty vector as a control. A fluorescence decrease (negative fluorescence % variation) indicates an influx of iodide in pendrin-transfected (PDS) or control cells (empty) following treatment with 100 µM hydrochlorothiazide or its vehicle (0.1% DMSO). n=12, one-way ANOVA with Bonferroni's post-test. ***p<0.005, n.s.: not significant.

No inhibition of iodide intake in pendrin transfected or control cells was determined upon treatment with hydrochlorothiazide with respect to the vehicle-treated cells (Figure 37b).

The following common diuretic and anti-hypertensive agents have also been tested for their potential effect on pendrin activity: 100 µM Methazolamide, 100 µM Triamterene, 100 µM Torsemide, 100 µM Hydroflumethiazide, 100 µM Indapamide, 100 µM Chlorothiazide, 100 µM Spironolactone. No inhibition of iodide intake in pendrin transfected or control cells was determined upon treatment with any of the mentioned substances.

4.5.4 Meta-analysis

Meta analysis prediction and further SHED alignments were performed by Prof. R. Konrat at the institute of Biochemistry & Biophysics, Structural & Computational Biology, University of Vienna (Austria) and the results were delivered to us in form of a list of reference numbers corresponding to entries in the drugbank reference database (www.drugbank.ca).

A selection of the compounds was then subjected to the functional test and results are presented in the following.

Cholesterol

Cholesterol (Figure 38a) was used to a final concentration of 100 µM in 0.1% chloroform.
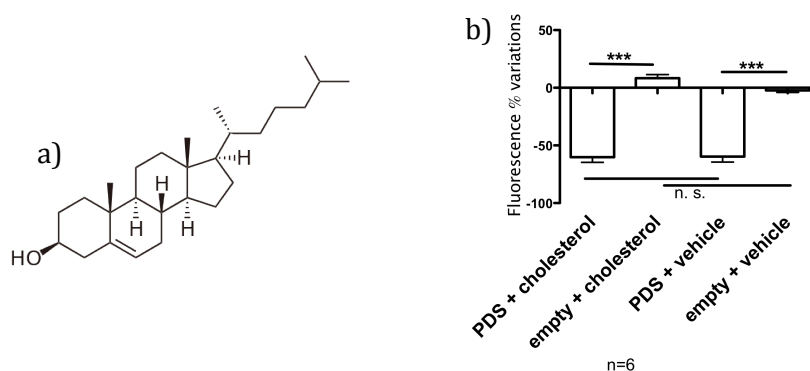
Figure 38. a) Structural formula of cholesterol. b) Functional test on HEK 293 Phoenix cells transfected with pendrin or with an empty vector as a control. A fluorescence decrease (negative fluorescence % variation) indicates an influx of iodide in pendrin-transfected (PDS) or control cells (empty) following treatment with 100 µM cholesterol or its vehicle (0.1% chloroform). n=6, one-way ANOVA with Bonferroni's post-test. ***$p < 0.005$, n.s.: not significant.

No inhibition of iodide intake in pendrin transfected or control cells was determined upon treatment with cholesterol with respect to the vehicle (Figure 38b).

Iloprost (Ilomedin[®] - Bayer)

Iloprost (Figure 39a) is the active ingredient of Ilomedin[®], a drug used to treat pulmonary arterial hypertension. Two different concentrations of Iloprost were tested: the therapeutic concentration (130 nM) and the 66 µM concentrated formulation.

Figure 39. a) Structural formula of Iloprost. Functional test on HEK 293 Phoenix cells transfected with pendrin or with an empty vector as a control. A fluorescence decrease (negative fluorescence % variation) indicates an influx of iodide in pendrin-transfected (PDS) or control cells (empty) following treatment with 13 nM (b) or 66 µM (c) Iloprost or its vehicle (isotonic solution). n=12, one-way ANOVA with Bonferroni's post-test. ***$p<0.005$, n.s.: not significant.

No inhibition of iodide intake in pendrin transfected cells was determined upon treatment with Iloprost with respect to the vehicle-treated cells (Figure 39b-c). An effect on control cells may hint to disturbance of endogenous transports.

Vasopressin

The concentration of Vasopressin (Figure 40a) used was 1 µM in isotonic solution. The concentration was chosen to mimic the physiological circulating hormone levels.
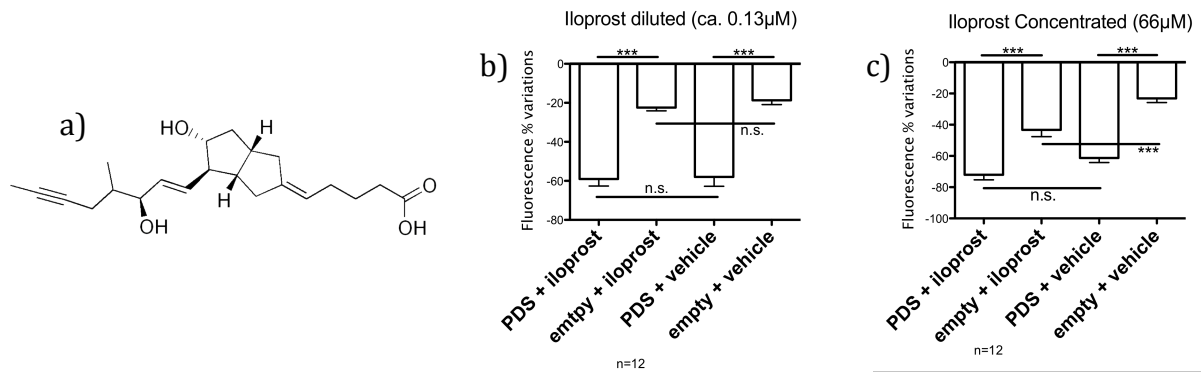

Figure 40. a) Structural formula of vasopressin. b) Functional test on HEK 293 Phoenix cells transfected with pendrin or with an empty vector as a control. A fluorescence decrease (negative fluorescence % variation) indicates an influx of iodide in pendrin-transfected (PDS) or control cells (empty) following treatment with 100 µM vasopressin or its vehicle (high chloride solution). n=6, one-way ANOVA with Bonferroni's post-test. ***$p<0.005$, n.s.: not significant.

93

No inhibition of iodide intake in pendrin transfected or control cells was determined upon treatment with vasopressin with respect to the vehicle-treated cells (Figure 40b).

Vitamin D4 (Dihydrotachysterol)

The concentration of vitamin D4 (Figure 41a) tested was 100 µM in 0.1% DMSO.
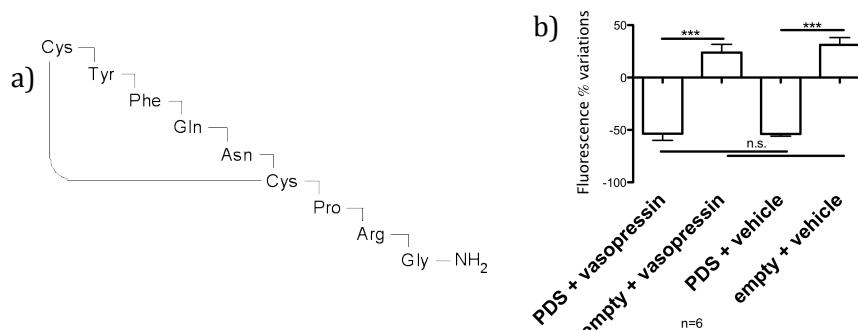

Figure 41. a) Structural formula of vitamin D4. b) Functional test on HEK 293 Phoenix cells transfected with pendrin or with an empty vector as a control. A fluorescence decrease (negative fluorescence % variation) indicates an influx of iodide in pendrin-transfected (PDS) or control cells (empty) following treatment with 100 µM Vitamin D4 or its vehicle (0.1% DMSO). n=24, one-way ANOVA with Bonferroni's post-test. ***$p < 0.005$, n.s.: not significant.

No inhibition of iodide intake in pendrin transfected or control cells was determined upon treatment with vitamin D4 with respect to the vehicle-treated cells (Figure 41b).

Vitamin E (α-Tocopherol)

The concentration of vitamin E (Figure 42a) used was 100 µM in 0.1% chloroform.

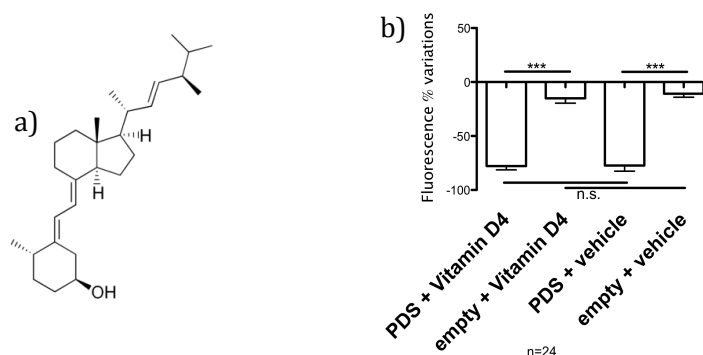**Figure 42.** a) Structural formula of vitamin E. b) Functional test on HEK 293 Phoenix cells transfected with pendrin or with an empty vector as a control. A fluorescence decrease (negative fluorescence % variation) indicates an influx of iodide in pendrin-transfected (PDS) or control cells (empty) following treatment with 100 µM Vitamin E or its vehicle (0.1% DMSO). n=24, one-way ANOVA with Bonferroni's post-test. ***$p < 0.005$, n.s.: not significant.

No inhibition of iodide intake in pendrin transfected or control cells was determined upon treatment with vitamin E with respect to the vehicle-treated cells (figure 42b).

(-)Nicotine

Nicotine (Figure 43a) was used to a final concentration of 100 µM in isotonic high chloride solution.
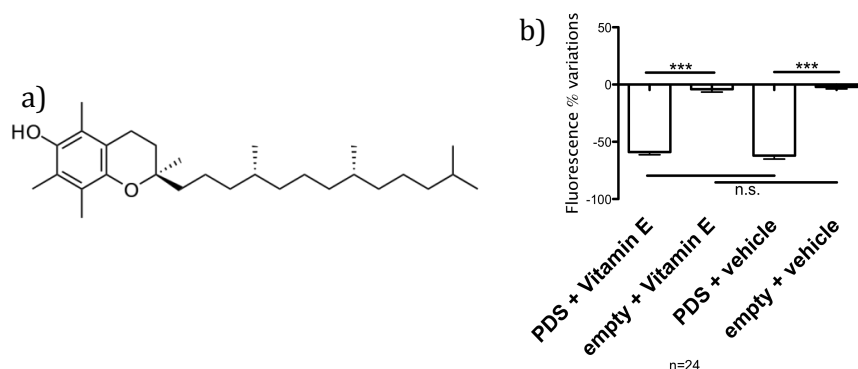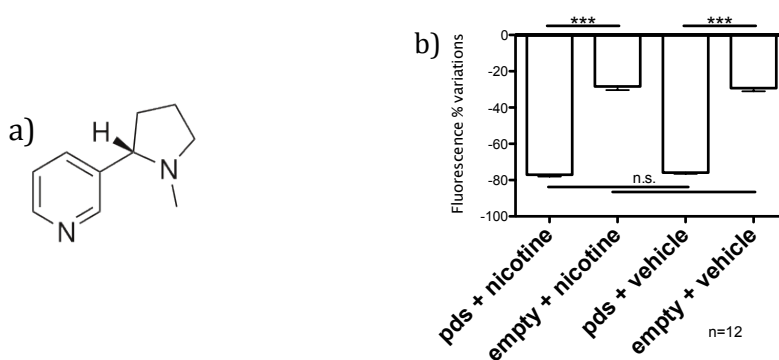

Figure 43. a) Structural formula of (-)Nicotine. b) Functional test on HEK 293 Phoenix cells transfected with pendrin or with an empty vector as a control. A fluorescence decrease (negative fluorescence % variation) indicates an influx of iodide in pendrin-transfected (PDS) or control cells (empty) following treatment with 100 µM (-)Nicotine or its vehicle (high chloride solution). n=6, one-way ANOVA with Bonferroni's post-test. ***$p < 0.005$, n.s.: not significant.

No inhibition of iodide intake in pendrin transfected or control cells was determined upon treatment with (-)Nicotine with respect to the vehicle-treated cells (Figure 43b)

4.5.5 SHED alignment

The identification of active compounds from the preliminary screenings allows for further refinement of the search of candidate ligands for pendrin. An alignment according to the SHED profile has been therefore performed for the two most promising compounds identified so far: the anti-inflammatory drugs tenidap and niflumic acid.

In the following section the compounds resulting from such alignment are presented, first those derived from tenidap alignment and then those predicted from niflumic acid alignment.

N-(2-chlorophenyl)-2-(2,4-dibromophenoxy)acetamide

A possible effect of N-(2-chlorophenyl)-2-(2,4-dibromophenoxy)acetamide (Figure 44a) was predicted by the SHED alignment of tenidap. N-(2-chlorophenyl)-2-(2,4-dibromophenoxy)acetamide was used to a final concentration of 100 μM in 0.1% DMSO solution.
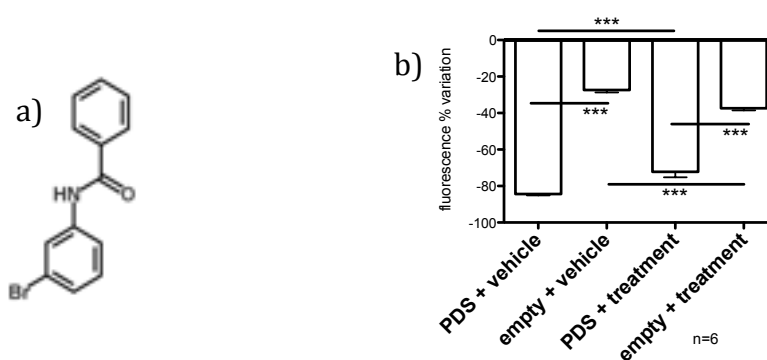
Figure 44. a) Structural formula of N-(2-chlorophenyl)-2-(2,4-dibromophenoxy)acetamide. b) Functional test on HEK 293 Phoenix cells transfected with pendrin or with an empty vector as a control. A fluorescence decrease (negative fluorescence % variation) indicates an influx of iodide in pendrin-transfected (PDS) or control cells (empty) following treatment with 100 μM N-(2-chlorophenyl)-2-(2,4-dibromophenoxy)acetamide (treatment) or its vehicle (0.1% DMSO). n=6, one-way ANOVA with Bonferroni's post-test. ***$p<0.005$, n.s.: not significant.

A slight, but significant (14%, $p<0.005$), effect on iodide intake in pendrin transfected cells upon treatment with N-(2-chlorophenyl)-2-(2,4-dibromophenoxy)acetamide was measured with respect to the vehicle-treated cells. An effect of the treatment can also be observed on control cells (Figure 44b).

2-{[(2,3-dichlorophenyl)methyl]amino}-1-phenylethanol

A possible effect of 2-{[(2,3-dichlorophenyl)methyl]amino}-1-phenylethanol (Figure 45a) was predicted by the SHED alignment of tenidap. The compound was used to a final concentration of 100 µM in 0.1% DMSO solution.
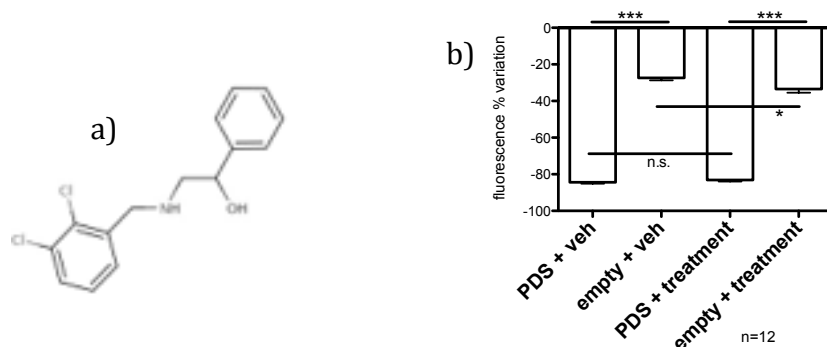
Figure 45. a) Structural formula of 2-{[(2,3-dichlorophenyl)methyl]amino}-1-phenylethanol. b) Functional test on HEK 293 Phoenix cells transfected with pendrin or with an empty vector as a control. A fluorescence decrease (negative fluorescence % variation) indicates an influx of iodide in pendrin-transfected (PDS) or control cells (empty) following treatment with 100 µM 2-{[(2,3-dichlorophenyl)methyl]amino}-1-phenylethanol (treatment) or its vehicle (0.1% DMSO). n=12, one-way ANOVA with Bonferroni's post-test. ***$p<0.005$, n.s.: not significant.

No inhibition of iodide intake in pendrin transfected or control cells was determined upon treatment with 2-{[(2,3-dichlorophenyl)methyl]amino}-1-phenylethanol with respect to the vehicle-treated cells (Figure 45b).

Naloxone

A possible effect of the opioid antagonist naloxone (Figure 46a) was predicted by the SHED alignment of tenidap. Naloxone was used to a final concentration of 100 µM in 0.1% DMSO solution.

Figure 46. a) Structural formula of naloxone. b) Functional test on HEK 293 Phoenix cells transfected with pendrin or with an empty vector as a control. A fluorescence decrease (negative fluorescence % variation) indicates an influx of iodide in pendrin-transfected (PDS) or control cells (empty) following treatment with 100 µM naloxone or its vehicle (0.1% DMSO). n=12, one-way ANOVA with Bonferroni's post-test. ***$p<0.005$, n.s.: not significant.

97

No inhibition of iodide intake in pendrin transfected or control cells was determined upon treatment with naloxone with respect to the vehicle-treated cells (Figure 46b).

Tolcapone

A possible effect of tolcapone (Figure 47a) was predicted by the SHED alignment of tenidap. Tolcapone was used to a final concentration of 100 µM in 0.1% DMSO solution.

Figure 47. a) Structural formula of tolcapone. b) Functional test on HEK 293 Phoenix cells transfected with pendrin or with an empty vector as a control. A fluorescence decrease (negative fluorescence % variation) indicates an influx of iodide in pendrin-transfected (PDS) or control cells (empty) following treatment with 100 µM tolcapone or its vehicle (0.1%DMSO). n=24, one-way ANOVA with Bonferroni's post-test. ***$p < 0.005$, n.s.: not significant.

No inhibition of iodide intake in pendrin transfected or control cells was determined upon treatment with tolcapone with respect to the vehicle (Figure 47b).

Topiramate

A possible effect of the anticonvulsant and antiepileptic drug topiramate (Figure 48a) was predicted by the SHED alignment of tenidap. Topiramate was used to a final concentration of 100 µM in 0.1% DMSO solution.

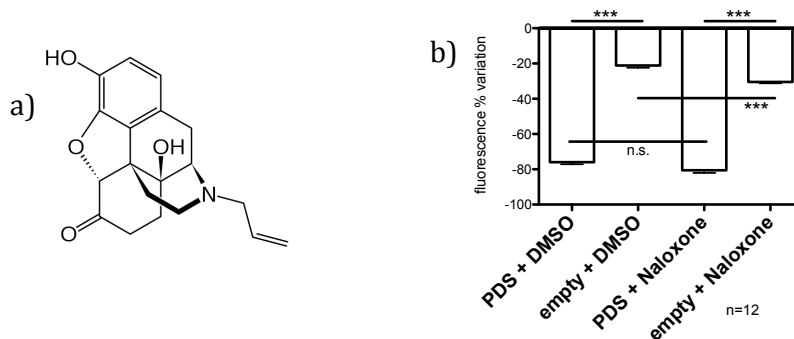**Figure 48.** a) Structural formula of topiramate. b) Functional test on HEK 293 Phoenix cells transfected with pendrin or with an empty vector as a control. A fluorescence decrease (negative fluorescence % variation) indicates an influx of iodide in pendrin-transfected (PDS) or control cells (empty) following treatment with 100 µM topiramate or its vehicle (0.1% DMSO). n=12, one-way ANOVA with Bonferroni's post-test. ***$p < 0.005$, n.s.: not significant.

No inhibition of iodide intake in pendrin transfected or control cells was determined upon treatment with topiramate with respect to the vehicle (Figure 48b).

Colchicine

A possible effect of colchicine (Figure 49a) was predicted by the SHED alignment of tenidap. Colchicine was used to a final concentration of 100 μM in 0.1% ethanol solution.
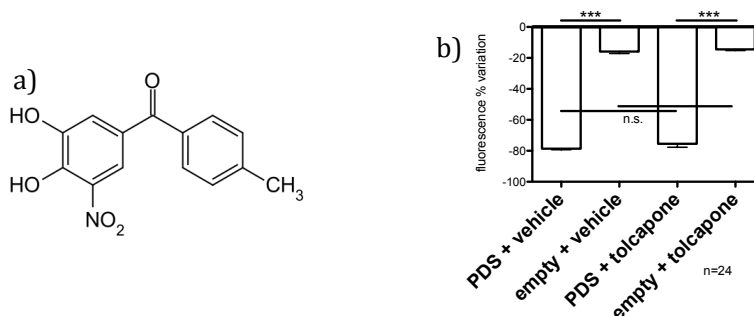

Figure 49. a) Structural formula of colchicine. b) Functional test on HEK 293 Phoenix cells transfected with pendrin or with an empty vector as a control. A fluorescence decrease (negative fluorescence % variation) indicates an influx of iodide in pendrin-transfected (PDS) or control cells (empty) following treatment with 100 μM colchicine or its vehicle (0.1% ethanol). n=18, one-way ANOVA with Bonferroni's post-test. ***$p<0.005$, n.s.: not significant.

No inhibition of iodide intake in pendrin transfected or control cells was determined upon treatment with colchicine with respect to the vehicle (Figure 49b).

Scopolamine

A possible effect of scopolamine (Figure 50a) was predicted by SHED alignment of tenidap. Scopolamine was used to a final concentration of 100 μM in isotonic high chloride solution.
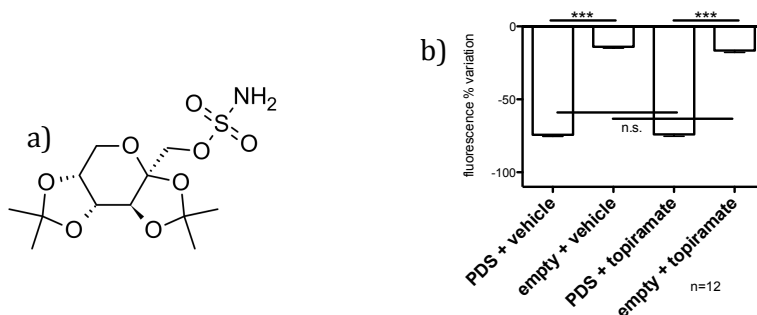

Figure 50. a) Structural formula of scopolamine. b) Functional test on HEK 293 Phoenix cells transfected with pendrin or with an empty vector as a control. A fluorescence decrease (negative fluorescence % variation) indicates an influx of iodide in pendrin-transfected (PDS) or control cells (empty) following treatment with 100 μM scopolamine or its vehicle (high chloride solution). n=12, one-way ANOVA with Bonferroni's post-test. ***$p<0.005$, n.s.: not significant.

No inhibition of iodide intake in pendrin transfected or control cells was determined upon treatment with scopolamine with respect to the vehicle (Figure 50b).

<u>**Levamisol**</u> ((S)-(−)-6-Phenyl-2,3,5,6-tetrahydroimidazo[2,1-b]thiazole hydrochloride)

A possible effect of the anthelmintic and immunomodulator drug levamisol (Figure 51a) was predicted by the SHED alignment of niflumic acid. Levamisol was used to a final concentration of 100 µM in isotonic high chloride solution.
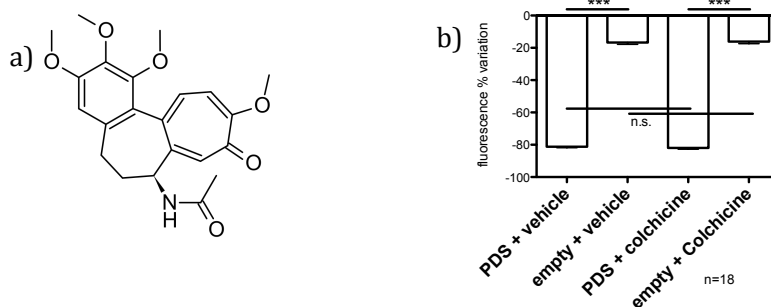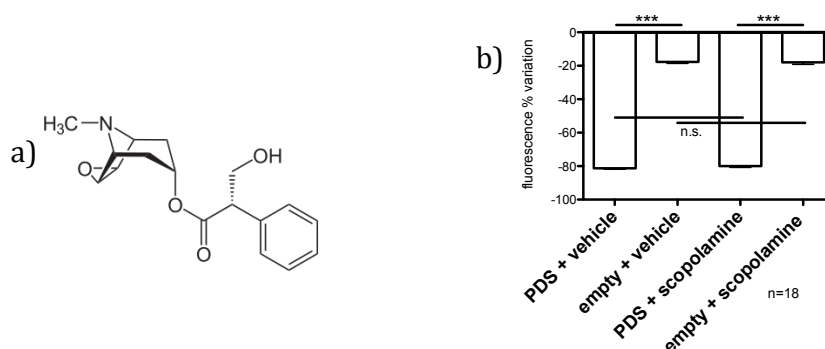

Figure 51. a) Structural formula of levamisol. b) Functional test on HEK 293 Phoenix cells transfected with pendrin or with an empty vector as a control. A fluorescence decrease (negative fluorescence % variation) indicates an influx of iodide in pendrin-transfected (PDS) or control cells (empty) following treatment with 100 µM levamisol or its vehicle (high chloride solution). n=12, one-way ANOVA with Bonferroni's post-test. ***$p < 0.005$, n.s.: not significant.

No inhibition of iodide intake in pendrin transfected or control cells was determined upon treatment with levamisol with respect to the vehicle (Figure 51b).

<u>**6-phenylamino nicotinic acid**</u>

A possible effect of 6-phenylamino nicotinic acid (Figure 52a) was predicted by the SHED alignment of niflumic acid. 6-phenylamino nicotinic acid was used to a final concentration of 100 µM in 0.1% DMSO solution.

Figure 52. a) Structural formula of 6-phenylamino nicotinic acid. b) Functional test on HEK 293 Phoenix cells transfected with pendrin or with an empty vector as a control. A fluorescence decrease (negative fluorescence % variation) indicates an influx of iodide in pendrin-transfected (PDS) or control cells (empty) following treatment with 100 µM 6-phenylamino nicotinic acid or its vehicle (0.1% DMSO). n=18, one-way ANOVA with Bonferroni's post-test. ***$p < 0.005$, n.s.: not significant.

No inhibition of iodide intake in pendrin transfected or control cells was determined upon treatment with 6-phenylamino nicotinic acid with respect to the vehicle (Figure 52b).

Levallorphan

A possible effect of levallorphan (Figure 53a) was predicted by the SHED alignment of niflumic acid. Levallorphan was used to a final concentration of 100 µM in isotonic high chloride solution.
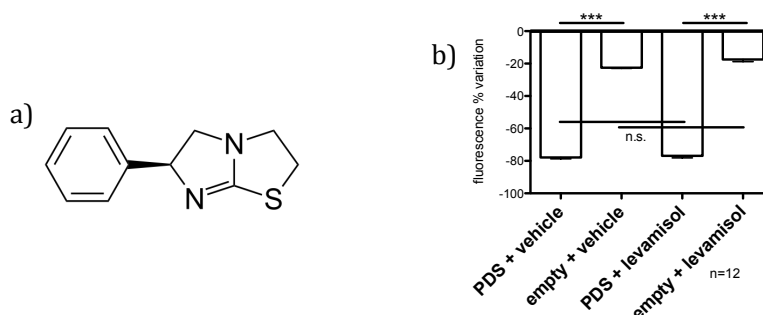

Figure 53. a) Structural formula of levallorphan. b) Functional test on HEK 293 Phoenix cells transfected with pendrin or with an empty vector as a control. A fluorescence decrease (negative fluorescence % variation) indicates an influx of iodide in pendrin-transfected (PDS) or control cells (empty) following treatment with 100 µM levallorphan or its vehicle (high chloride solution). n=12, one-way ANOVA with Bonferroni's post-test. ***$p < 0.005$, n.s.: not significant.

No inhibition of iodide intake in pendrin transfected or control cells was determined upon treatment with levallorphan with respect to the vehicle (Figure 53b).

Ticlopidine

A possible effect of the antiplatelet drug ticlopidine (Figure 54a) was predicted by the SHED alignment of niflumic acid. Ticlopidine was used to a final concentration of 100 µM in isotonic high chloride solution.
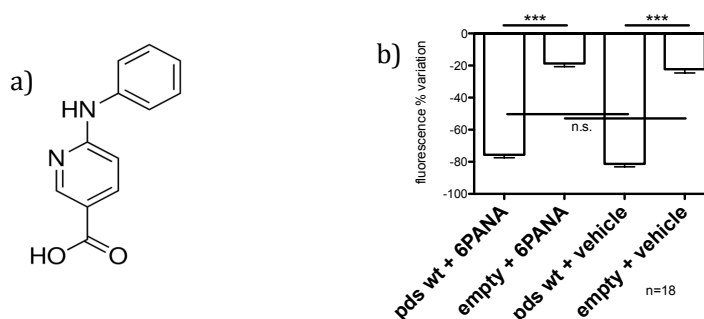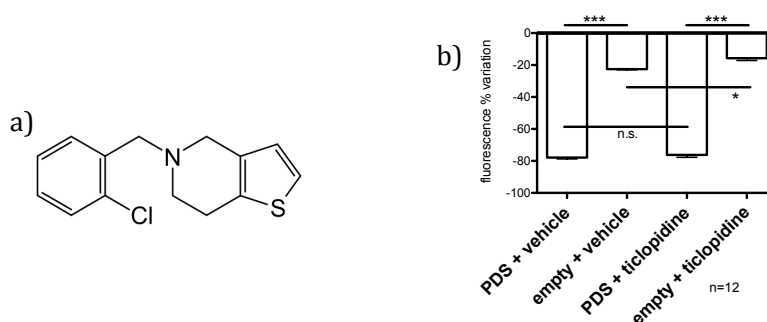

Figure 54. a) Structural formula of ticlopidine. b) Functional test on HEK 293 Phoenix cells transfected with pendrin or with an empty vector as a control. A fluorescence decrease (negative fluorescence % variation) indicates an influx of iodide in pendrin-transfected (PDS) or control cells (empty) following treatment with 100 µM ticlopidine or its vehicle (high chloride solution). n=12, one-way ANOVA with Bonferroni's post-test. ***$p < 0.005$, n.s.: not significant.

No inhibition of iodide intake in pendrin transfected or control cells was determined upon treatment with ticlopidine with respect to the vehicle (Figure 54b).

Flufenamic acid

A possible effect of flufenamic acid (Figure 55a) was predicted by the SHED alignment of niflumic acid. Flufenamic acid was used to a final concentration of 100 µM in a 0.1% DMSO solution.
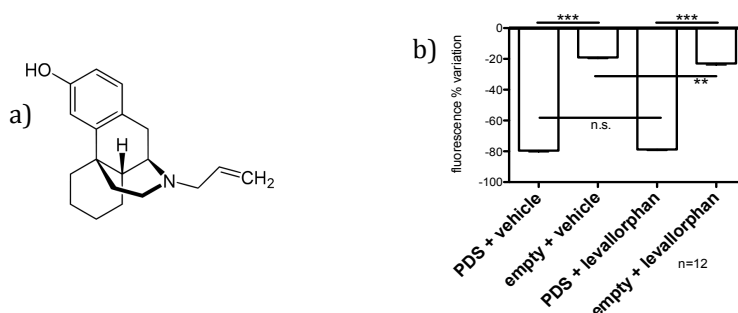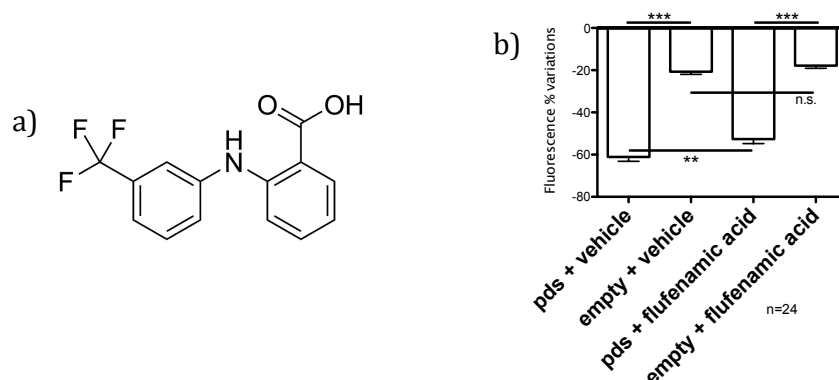

Figure 55. a) Structural formula of flufenamic acid. b) Functional test on HEK 293 Phoenix cells transfected with pendrin or with an empty vector as a control. A fluorescence decrease (negative fluorescence % variation) indicates an influx of iodide in pendrin-transfected (PDS) or control cells (empty) following treatment with 100 µM flufenamic acid or its vehicle (0.1% DMSO). n=24, one-way ANOVA with Bonferroni's post-test. ***$p<0.005$, **$p<0.01$, n.s.: not significant.

A 15% inhibition ($p<0.01$) of iodide intake in pendrin transfected cells was determined upon treatment with flufenamic acid with respect to the vehicle-treated cells (Figure 55b). As seen with the close analog of flufenamic acid, niflumic acid, an acidification of the intracellular pH was measured in some experiments (see discussion).

All the above reported results are summarize in table 6. The tested compounds are again classified according to the rationale described above. In the last section of the table, the compounds derived from the SHED profile alignment of niflumic acid and tenidap are listed.

Compound	Concentration	Vehicle	Effect
1. Chloride channels and transporters blockers			
NPPB	100 µM	DMSO 0.1%	32% inhib.
DIDS	100 µM	DMSO 0.1%	No
CFTR-inhibitor 172	1.6 µM	DMSO 0.1%	No
DNDS	100 µM	Isotonic solution	No
2. Previously identified inhibitors of SLC26A3 (DRA) or SLC26A4 (pendrin)			
Niflumic acid	100 µM	DMSO 0.1%	28% inhib. (1)
Tenidap	100 µM	DMSO 0.1%	85% inhib.
Glybenclamide	100 µM	DMSO 0.1%	No
Probenecid	100 µM	Chloroform 0.1%	No
Hydroxycinnamate	100 µM	DMSO 0.1%	No
3. Diuretics and antihypertensive agents			
Eplerenone	10 µM	DMSO 0.1%	No
Acetazolamide	100 µM	DMSO 0.1%	No
Bumetanide	100 µM	DMSO 0.1%	No
Furosemide	100 µM	DMSO 0.1%	No
Amiloride	100 µM	DMSO 0.1%	No
Hydrochlorothiazide	100 µM	DMSO 0.1%	No
Methazolamide	100 µM	Isotonic solution	No
Triamterene	100 µM	PEG400 5%	No
Torsemide	100 µM	EtOH 0.1%	No
Hydroflumethiazide	100 µM	DMSO 0.1%	No
Indapamide	100 µM	EtOH 0.1%	No
Chlorothiazide	100 µM	DMSO 0.1%	No
Spironolactone	100 µM	EtOH 0.1%	No
4a. Meta-analysis			
Cholesterol	100 µM	Chloroform 0.1%	No

Iloprost®	66 µM	--	No*
	130 nM	Isotonic solution	No*
Vasopressin	1 µM	Isotonic solution	No
Vitamin D	100 µM	DMSO 0.1%	No
Vitamin E	100 µM	Chloroform 0.3%	No
Nicotine	100 µM	Isotonic solution	No
4b. Niflumic acid and Tenidap SHED alignment			
N-(2-chlorophenyl)-2-(2,4-dibromophenoxy)acetamide	100 µM	DMSO 0.1%	14% inhib.*
2-{[(2,3-dichlorophenyl)methyl]amino}-1-phenylethanol	100 µM	DMSO 0.1%	No
Scopolamine	100 µM	Isotonic solution	No
Colchicine	100 µM	EtOH 0.1%	No
Topiramate	100 µM	DMSO 0.1%	No
Tolcapone	100 µM	DMSO 0.1%	No
Naloxone	100 µM	DMSO 0.05%	No
Levamisole	100 µM	Isotonic solution	No
6-phenylamino nicotinic acid	100 µM	DMSO 0.1%	No
Levallorphan	100 µM	Isotonic solution	No
Ticlopidine	100 µM	Isotonic solution	No
Flufenamic acid	100 µM	DMSO 0.1%	15% inhib. (1)

Table 6. Summary of the functional screening of pendrin ligands. *: effect on control cells, probably due to an effect of the treatment on endogenous transports. (1) acidification of intracellular pH was measured. Acidic pH may influence the measurement by quenching the fluorescence of EYFP.

5. Discussion

5.1 Functional and molecular characterization of pendrin variants

The genetic screening of a cohort of 58 deaf patients performed by our collaborators at the hospital of Campinas, Sao Paolo, Brazil, identified 14 patients with mutations in the pendrin coding region. The patients were all diagnosed with severe to profound deafness with or without EVA. 9 out of 14 patients display a heterozygous phenotype with one wild type and one mutated pendrin allele, two of which are double heterozygous with a monoallelic pendrin mutation and the monoallelic 35delG mutation in the *GJB6* gene. Due to the high phenotypic variability observed among individuals with pendrin mutations and the high incidence of benign polymorphisms [74], it is not possible to establish if a specific pendrin variant is the genetic determinant of deafness in a given patient without a functional characterization. Only 5 of the 14 allelic variants identified in the screening had already been characterized previously (R409H, T410M, V138F, V609G, R776C), one variant (R776C) showing discordant results in the literature [63, 72-74]. For all the other variants no functional characterization is available in the literature.

In the present study, the functional and molecular characterization of the uncharacterized pendrin variants identified in the abovementioned genetic screening have been performed, in order to define a genetic diagnosis for the observed deafness phenotype of the patients. The functional characterization, performed by means of the fluorometric assay described in the methods, delivers important information regarding the possible etiology of deafness in the patients examined (Table 7, boldface). The definition of a correct genetic diagnosis of the disease is important in order to exclude other genetic or environmental causes of deafness for which a specific treatment may exist. Furthermore, with a defined genetic diagnosis it is possible to provide the patient and the family with the more efficient counseling, both regarding an eventual progression of the disease with involvement of other organs (such as the thyroid) and the possibility of genetic transmission to the offsprings [6].

For what concerns this specific study, we can conclude that the functional impairment of pendrin is most likely the factor determining deafness in at least 5 patients out of 14 of this cohort (21AA, 06AA, 23AA, 22AA and 02AA, Table 7) as discussed in the following.

Patient 21AA has been diagnosed deaf with an enlarged vestibular aqueduct. The sequencing of pendrin coding region revealed the deletion 297T on one allele, leading to a truncated form of the protein. The variant P142L is encoded by the other allele. By means of our functional test, the variant P142L was defined as a mutation with reduction of function. It has previously been assessed that all pendrin truncations identified so far are non-functional [5], we can therefore conclude that the diagnosed deafness phenotype in patient 21AA is due to pendrin dysfunction, with no need of further investigations. The same conclusion can be drawn for patient 06AA, also diagnosed deaf with EVA. In this patient, the Q413R variant is encoded by one allele and the V138F variant by the second allele. The latter was previously characterized as a complete loss of function mutation [40], while the former has been characterized as a hypofunctional mutation in the present study. Patient 23AA bears a mutation affecting the splicing of pendrin messenger RNA on one allele, leading to a premature truncation of the protein. The second pendrin allele encodes for the L445W variant. L445W has been characterized in the present study as a complete loss of function mutation. Therefore, also in this case it is possible to identify pendrin dysfunction as the determinant factor for the development of deafness. Furthermore, this is the only patient in the cohort for which overt goiter was identified. Deafness associated to pendrin mutations and goiter are clear hallmarks of Pendred syndrome. The situation of patients 22AA and 02AA appear clear as well, as they both carry non-functional or hypofunctional pendrin variants characterized in previous studies (R409H in homozygosity and T410M and the splicing site mutation IVS15+5G>A, respectively [40,44]). Different is the case of patient C26. This patient was diagnosed deaf but with no abnormally enlarged vestibular aqueduct. From the genetic screening, a 35delG mutation on the connexin-26 coding gene, *GJB6,* was identified, in association with a mutated form of pendrin carrying the aminoacidic substitution C282Y. 35delG mutation of the connexin-26 has been assessed in a number of studies as the most common genetic cause of deafness [60]. The pendrin variant C282Y has been characterized as hypofunctional mutation in the present study. We can therefore hypothesize that a monoallelic connexin-26 mutation combined with a monoallelic pendrin mutation (*i.e.* a condition of double heterozygosity) may be the genetic determinant of deafness for this patient. Patients 16AA and 18AA both present a mutant form of the transporter in heterozygosity with the wild type. The former carries the G149R variant, characterized here as reduction of function mutation, the latter displays the T193I variant, characterized as well in this study as a complete loss of function mutation. In both cases it is possible to hypothesize that either these patients are examples of

nonsyndromic-EVA due to monoallelic pendrin mutations [53, 67] or that further genetic or environmental factors may contribute to the development of the symptoms. The first candidates to be considered for further genetic investigations are the transcription factor *FOXI1* and the potassium channel *KCNJ10* [88, 89], both known to be involved in deafness with EVA. In this study, both genes have been sequenced and were found wild type, therefore excluding their role in the observed deafness phenotype. Further genetic aspects to be considered are possible mutations in the promoter and in the 3' untranslated region of pendrin gene, possibly affecting the transcription of the gene and expression levels of mRNA. In the case of patient 15AA, the R776C variant is encoded by one pendrin allele. From the functional tests presented in this study, such aminoacidic substitution does not affect the transport activity of pendrin and the corresponding pendrin variant has to be considered as a benign polymorphism. The presence of this particular allelic variant in association with the wild type allele excludes a role of pendrin in the development of deafness in this specific case.

A particularly controversial situations is the one regarding the variant V609G in heterozygosis with the wild type allele. This aminoacidic substitution has been previously assessed as a mutation leading to a reduction of function [68]. In the present study it has been detected in heterozygosis with the wild type both in the group of patients with EVA (patient L1AA) and in the group with no EVA (patients C01, C04 and C09). In the case of patient L1AA, this pendrin mutation is associated with a monoallelic del35G mutation of the connexin-26 coding gene (*GJB6*), therefore we may hypothesize that this genetic configuration (double heterozygosis with the wild type) may be the actual determinant for the observed EVA and deafness. In this view, the V609G mutation alone would not be sufficient to determine EVA, and for patients C01, C04 and C09 other genetic or environmental causes of deafness should be taken into account. On the other hand, a similar genetic situation is present in the patient C26, where a reduction of function pendrin mutation (C282Y) is associated with the same monoallelic del35G mutation on *GJB6*. In this case no EVA could be observed. C282Y has been shown in the present study to be localized at the plasma membrane, therefore its molecular defect may be mild enough to allow for a sufficient transport activity and prevent EVA and deafness in patient C26, even in the presence of a defective connexin-26.

Patient (n=58)	Aminoacidic substitution	Patient Genotype (coding region)	Goiter	Function	Localization	Pendrin related defaness?
		Patients deaf *with EVA* (n=26)				
21AA	P142L	P142L/del 297T	No	**reduced**	**PM**	**YES**
16AA	G149R	G149R/WT	No	**reduced**	**PM/ER**	**?**
18AA	T193I	T193I/WT	No	**lost**	**ER**	**?**
22AA	R409H	R409H/R409H	No	lost/red.	Partially PM	YES
02AA	T410M	T410M/IVS15+5G>A	No	lost	ER	YES
06AA	Q413R	Q413R/V138F	No	**reduced**	**ER**	**YES**
23AA	L445W	L445W/IVS8+1G>A	Yes	**lost**	**ER**	**YES**
L1AA	V609G	V609G/WT *	No	reduced	?	?
15AA	R776C	R776C/WT	No	**unaffected**	**PM**	**NO**
		Patients deaf *without EVA* (n=32)				
C15	V138F	V138F/WT	No	lost	ER	?
C26	C282Y	C282Y/WT *	No	**reduced**	**PM**	**?**
C01	V609G	V609G/WT	No	reduced	?	?
C04	V609G	V609G/WT	No	reduced	?	?
C09	V609G	V609G/WT	No	reduced	?	?

Table 7: updated from Table 1. The results obtained in the present study are reported in boldface.
*: mono allelic mutation (35delG) in the connexin-26 gene, *GJB2*, was also found.

Further investigations were conducted in the present study, in order to determine the molecular defect leading to the measured functional impairment. The knowledge of the fate the different mutant forms undergo is the key for a possible pharmacological rescue of the transport activity. For this purpose, two molecular aspects have been investigated: the subcellular localization of the different variants and their abundance in the cell and in the plasma membrane region.

Concerning the subcellular localization of the characterized mutants, the results obtained from the co-localization experiments with the plasma membrane or with the endoplasmic reticulum show a high variability in the distribution. The observed sub-cellular distributions range from a complete retention in the ER to a trafficking to the PM comparable to the wild type.

The determined subcellular localization correlates quite well with the measured functional state of the different variants. The mutants showing the most severe functional impairment (the loss of function mutants T193I and L445W, Figure 9) are retained in the ER and completely excluded from the PM (Figure 12). Accordingly, hypofunctional forms of the transporters maintaining significant transport activity (P142L, G149R, C282Y, Figure 9) are still able to reach the plasma membrane, at least partially (Figure 12). Such an observation may be an indication that specific aminoacidic substitutions, such as P412L and C282Y do not impair the folding and/or trafficking of the protein but may instead lie in a domain important for the binding of transported ions or regulatory factors, therefore directly affecting the transport activity. The mutant G149R is the only one showing a mixed subcellular localization profile, displaying significant co-localization with the plasma membrane but also with the endoplasmic reticulum (Figure 12). In this case, the folding defect may not be as severe as for other mutants and may still allow for a partial trafficking to the plasma membrane. The residual function measured in the functional tests for this particular mutant may be due to this partial trafficking to the plasma membrane. Other mutants (T193I, Q413R and L445W, Figure 12) are clearly retained in the endoplasmic reticulum. These specific mutations may therefore reside in a domain of the protein critical for its correct processing and folding. The fully functional variant R776C results mainly localized at the plasma membrane, with a behavior indistinguishable from the wild type (Figure 12), therefore confirming its nature of benign polymorphism.

In summary, it seems that a severe loss of function correlates with a complete retention in the ER, while a residual transport activity is associated to a good trafficking to the plasma membrane. The mutant Q413R appears to represent an exception to this rule. This particular mutant showed a very strong co-localization with the endoplasmic reticulum and a complete exclusion from the plasma membrane, but in the functional tests it showed a reduction of function, with some residual transport activity. It is still possible that a small amount of this mutant, even if generally misfolded, is still capable of reaching the plasma membrane, accounting for the residual activity recorded. Considering that only an undetectable amount of protein can reach the plasma membrane, the fact that its activity was not completely abolished is surprising, and it may even be possible to hypothesize that the intrinsic transport ability of this particular mutant could be higher than the wild type itself, compensating for the impaired trafficking.

The fact that some pendrin mutants show a retention in the ER can point to the failure in the processing and folding of the protein. Misfolded proteins are targeted for degradation *via* the ER associated degradation (ERAD) system. Proteins targeted for degradation in the ER are specifically polyubiquitinated and transferred to the proteasome complex for degradation and recycling of the aminoacidic subunits. There are evidences that pendrin-GFP co-localizes with ubiquitin in the cell, suggesting therefore a role of polyubiquitination in pendrin degradation [126]. Furthermore, Lee et al. demonstrated the role of a specific ER-resident E3 ubiquitine ligase, namely Rma1, in the degradation of pendrin, both wild type and mutated. In the same article it was also shown the possibility to favor the glycosylation and subsequent trafficking of the protein to the plasma membrane by facilitating its maturation and folding. It is therefore feasible to hypothesize that also those pendrin variants investigated in the present study, displaying a folding defect, are targeted by polyubiquitination and delivered to the proteasome for degradation.

In order to support this hypothesis, the protein abundance of the different pendrin variants was investigated and quantified both by fluorescent imaging of the fusion protein pendrin-EYFP and western blotting of the untagged protein. The results of quantification experiments show significant differences in the level of expression of the different pendrin variants, correlating quite well with the observed subcellular localization. Mutants that showed and impairment in trafficking and where retained in the ER (T193I, L445W) also showed the lower expression levels both in the imaging (Figure 14-16) and in western blot experiments (Figure 18-20). On the other hand, mutant variants showing a more efficient trafficking to the plasma membrane (P142L, C282Y) showed a level of expression significantly higher with respect to the most severely impaired mutants (T193I and L445W), even though reduced if compared to the wild type.

The imaging quantification experiments have been performed both on total (Figure 13-14) and plasma membrane (Figure 15-16) pendrin. As observed in the subcellular localization experiments, the mutant Q413R shows an unexpected behavior, displaying levels of expression comparable to the two loss of function mutants, T193I and L445W, while retaining significant function. Such result is anyway consistent with the co-localization data, where the same mutant was shown being mostly retained in the ER.

It is therefore to be concluded that pendrin mutants with a reduction or loss of function invariably show expression levels reduced with respect to the wild type, with the

most severe reduction in expression correlating with a retention in the ER. The expression levels of the fully functional variant R776C, as expected, were not reduced with respect to the wild type.

These results were confirmed by the western blot experiments on total cellular extract and extracts of the total membranes fractions (Figure 19-20). Again, the functionally impaired mutants showed a very low level of expression. The pendrin variant P142L instead, showed an expression level significantly higher with respect to the most severely impaired mutants (T193I and L445W). In the western blots on total proteins (Figure 17-18), an anomalous phenomenon could be observed: the mutant P142L showed a level of expression comparable to the wild type or even higher in some individual experiments. Such unexpected result may be due to the accumulation of this particular mutant in form of inclusion bodies in the cytosol, circumventing degradation by the proteasome complex. Accordingly, this phenomenon is no more visible in the total membranes blots, where the expression level of P142L is significantly lower with respect to the wild type. Another anomaly of the western blot experiments is the total absence of signal in correspondence of the polymorphism R776C. This particular variants did not show any difference with respect to the wild type, neither in the functional tests, nor in the co-localization and imaging quantification experiments. An absence of signal is therefore only to be explained by an impaired antibody recognition due to the disruption of the epitope. The aminoacidic substitution R776C actually lies within the epitope recognized by the anti-pendrin antibody used in these experiments.

It is important to underline that the western blot experiments where performed on cells overexpressing the untagged form of the protein, whereas imaging experiments where performed on fusion proteins. The correlation of the results from the two methods reinforce not only the particular piece of data, but also the validity of the two complementary experimental approaches. Specifically, the presence of the relatively bulky EYFP protein fused to the C-terminus does not seem to affect pendrin trafficking. Therefore we can conclude that the use of fusion proteins constitutes a valid approach for determining the subcellular localization of wild type pendrin and its variants.

In Table 8, a summary of the functional and molecular characterization performed on the selected allelic variants is reported in order to underline the correlation between

determined functional impairment and molecular defect observed by co-localization and expression levels analysis experiments.

	Function	Localization	Expression levels
P142L	reduced	Plasma Membrane	⇩
G149R	reduced	Plasma Membrane/ER	⬇
C282Y	reduced	Plasma Membrane	⇩
T193I	lost	ER	⬇⬇
Q413R	reduced	ER	⬇
L445W	lost	ER	⬇⬇
R776C	unaffected	Plasma Membrane	—*

Table 8: summary of the functional and molecular characterization of the analyzed pendrin variants. Expression levels reported here correspond to the results from imaging on plasma membrane pendrin and compare each pendrin variant to the wild type. Dashed arrows in the fourth column indicate a mildly reduced level of expression. Boldface arrows indicate a more severely reduced level of expression. Double boldface arrows indicate an even more severely reduced level of expression. The dash indicates no difference in the expression level. One Way ANOVA with Bonferroni's post-test. (*) not possible to confirm the result by western blotting.

The evaluation of expression levels leads to the assumption that hypo-functional or non-functional pendrin forms are targeted to the protein degradation pathways. Identification of the specific molecular defect is a precious information for the development of a therapeutic approach aiming to a functional rescue of the mutant forms, either by facilitating their folding or potentiating their activity, possibly after inhibiting their degradation.

The efficacy of such an approach on hypofunctional and non functional forms of pendrin was also investigated in the present study.

Cells overexpressing wild type or mutated pendrin were treated with a potent proteasome inhibitor (MG132) in order to reduce the proteasomal degradation and its effect on transport activity and protein expression was analyzed. Pendrin expression levels upon treatment with MG132 or its vehicle were evaluated by fluorescence imaging of pendrin-EYFP. The analysis showed a dramatic increase in total pendrin expression (except for C282Y, Figure 22), with a massive accumulation of all pendrin variants in the ER, including the wild type and the polymorphism R776C. A similar effect was seen at the level of the plasma membrane (Figure 23), whereas in this latter case, the wild type and the polymorphism R776C were not affected. A general increase in the expression levels upon treatment with the proteasome inhibitor MG132 is confirming once more the hypothesis that pendrin mutants, as the wild type, undergo degradation *via* the ubiquitin proteasome pathway.

The functional tests performed on cells treated with the same proteasome inhibitor further confirmed the efficacy of the treatment (Figure 21). A significant increase in transport function upon treatment with MG132 was observed for 4 mutants (P142L, T193I, Q413R, L445W) out of 8 pendrin variants analyzed (including the wild type). These 4 are the mutants with the most severely impaired transport function. In particular, one of the mutants (Q413R) shows and increase in transport activity of about one third following treatment with MG132 with respect to the vehicle. Interestingly, this is the same mutant showing an almost complete exclusion from the PM but retaining a significant transport activity, as mentioned earlier. This result reinforces once more the hypothesis that this particular mutation may on one side interfere with the correct maturation of the protein but on the other side confer an intrinsic activity advantage to the transporter.

These results are highly promising for a possible development of the rescuing approach, showing that inhibition of proteasomal degradation does not only lead to a general increase in protein abundance, but, more importantly, that such a treatment leads to a protein increase at the level of PM and is also effective on restoring, at least partially, the function of the transporter.

5.2   Functional screening of pendrin ligands

As mentioned in the introduction, pendrin overexpression and/or hyperactivity is linked to pathological states such as asthma, COPD and hypertension [12, 29, 90]. The transporter constitutes therefore a novel target for possible therapeutical approaches in such pathologies. So far, no specific and potent pendrin inhibitor could be identified, not even from the screening of large compounds libraries [34]. In the present study we tested 41 compounds on pendrin chloride/iodide exchange activity in order to identify potential inhibitors/modulators of the transporter. The compounds included in the screening were selected among (i) known inhibitors of chloride channels and transporters and inhibitors of DRA, (ii) diuretics and antihypertensive agents and (iii) small compounds predicted by the bioinformatics approach called meta-analysis. The eventual identification of active compounds within these 3 groups was then exploited for a second phase selection by means of a similarity search based on the so-called SHED profiling of small compounds. The screening was performed by means of the fluorometric method developed by Dossena et al. in 2006 [69] and adapted for a semi-high-throughput approach as described in the methods.

The results of the functional screening performed on potential pendrin ligands are summarized in Table 6. From the presented outcome, a peculiar pharmacological profile of pendrin can be identified, as discussed in the following.

The first observation is that, surprisingly, the well known anion exchanger inhibitor DIDS was unable to affect pendrin iodide transport activity at the concentration of 100 µM (Figure 25), confirming the results obtained by Dossena et al. in 2006 with a different technique (radiolabelled chloride uptake) [97]. In a study from 1999, Scott et al. [99] did show an inhibitory effect of 1 mM DIDS on pendrin expressed in *Xenopus* oocytes and Soleimani et al. in 2001 showed a similar effect of 0.5 mM DIDS on pendrin transfected HEK 293 cells. Their findings are clearly in contrast with the result shown in the present study, where no inhibitory effect could be measured in HEK 293 Phoenix cells upon treatment with the same substance. Though, the contrasting results may be due to the different experimental set up and cellular system used for the evaluation of pendrin activity, but it is also to be underlined that the concentration used in the experiments of Scott et al. was 10 fold higher and in Soleimani et al. 5 fold higher than the concentration

used in the present study. In the same study, Scott et al. also showed an inhibitory effect of the diuretics probenecid and furosemide (1 mM), whereas in the present study we could not replicate the same results (Figure 31 and 35). Again, such difference may be due to the different experimental set ups and concentration tested. Another noteworthy result has been observed upon treatment with 100 µM NPPB. NPPB is a known inhibitor of chloride channels but it is not expected to inhibit anion exchangers [127]. We could show that treatment of pendrin transfected cells with NPPB was effective in reducing iodide influx with respect to vehicle treated cells (Figure 24), confirming the results shown by Dossena et al. in 2006 with a different technique [97]. In the same study, Dossena et al. could show the inhibitory effect of the DRA inhibitor niflumic acid.

Niflumic acid is known to exert its anti-inflammatory action *via* cyclooxygenase inhibition [128], but it is also involved in the modulation of chloride channels, such as CLC-Ka and ClC-Kb [129]. DRA, also known as SLC26A3, is the closest analogue of pendrin, the two proteins showing 44% of identity and a 60% of similarity. A few inhibitors of DRA have been assessed so far, none of them anyway specific, but they may represent a useful source of potential pendrin ligands. In the present study we tested known inhibitors of DRA, namely the anti-inflammatory drug niflumic acid, the anti-rheumatic drug tenidap and the anti-diabetic drug glibenclamide. The latter failed in reducing pendrin iodide transport activity at a concentration of 100 µM (Figure 30), but treatment with niflumic acid at the same concentration was successful in reducing iodide influx in pendrin transfected cells (Figure 28). As mentioned earlier, these data confirm the results previously obtained with a different technique [97], thus proving once more the validity of the fast-fluorometric method [69] exploited in the present study. Nilfumic acid was also the only compound showing an inhibitory effect on pendrin identified in a screening of a 5,000 compounds library by Pedemonte et al. in 2007 [34]. In some cases, a reduction of EYFP fluorescence following exposure to niflumic acid, independent from the iodide influx and possibly due to an intracellular acidification [130], has been observed. An excessive reduction in EYFP fluorescence may impair an exact evaluation of the effect of the drug itself on the iodide influx.

The most interesting and original result from the present study has been obtained upon treatment with the third DRA inhibitor mentioned earlier, tenidap [106]. Tenidap is an anti-rheumatic, anti-inflammatory drug effective against rheumatic arthritis [131]. Its action

is related to cyclooxygenases 1 and 2 and lipooygenase 5 inhibition, but it is known to modulate also a number of membrane transporters and channels including the rat kidney Na^+/HCO_3^- cotransporter (rkNBC) [132] and the inwardly rectifying K^+ channel Kir2.3 [133]. Treatment of pendrin transfected cells with 100 µM tenidap showed a very strong (85%) inhibitory effect on iodide transport activity in comparison to cells treated with the vehicle, which represents the most potent inhibitory effect on pendrin activity observed so far (Figure 29). This work provides therefore the first evidence of a strong inhibitory effect of tenidap on pendrin iodide transport activity. Even if tenidap cannot be considered a specific pendrin inhibitor, the finding still constitutes a precious source of information for further prediction of putative pendrin ligands.

The identification of the abovementioned active compounds has been exploited as a starting point for further refinement of the list of screening targets. Such refinement was achieved by aligning the molecule of interest against a small compounds database (www.drugbank.ca), by means of the so-called SHED profile of the molecules. A similarity analysis has been therefore performed using both tenidap and niflumic acid as templates. Both alignments delivered a new list of compounds with a high SHED profile similarity score with the respective templates of origin. Despite the great variety of chemical and pharmacological classes of the predicted compounds, according to the similarity of their SHED profiles, they are expected to have a similar pharmacological profile and therefore show a similar effect on pendrin. A number of compounds have been identified this way as potential pendrin ligands to be functionally screened. The results of this second phase of the screening are reported in Table 6, section 4b.

Two of the compounds resulting from the SHED alignment of tenidap and niflumic acid actually showed an effect on iodide influx in pendrin transfected cells during the functional tests.

N-(2-chlorophenyl)-2-(2,4-dibromophenoxy)acetamide, derived from the SHED alignment of tenidap, showed a 14% pendrin activity inhibition with respect to the vehicle (Figure 44). At the same time though, an alteration of fluorescence decrease in control (not expressing pendrin) cells was measured upon treatment with the same compound with respect to the vehicle treated cells. An effect on control cells would hint to a

117

disturbance of endogenous transports interfering therefore with an exact evaluation of the effect on pendrin.

The second active compound emerged from the SHED alignment of niflumic acid, and it is the non-steroidal anti-inflammatory drug flufenamic acid. Treatment of pendrin transfected cells with flufenamic acid resulted in a 15% pendrin activity inhibition with respect to vehicle treated cells (Figure 55). As observed upon treatment with niflumic acid though, a reduction of EYFP fluorescence following exposure to flufenamic acid, independent from the iodide influx, has been observed, possibly due to intracellular acidification [130]. As it is the case of niflumic acid therefore, a reduction in EYFP fluorescence may impair an exact evaluation of the effect of the drug itself on the iodide influx.

Despite the unspecificity of the active compounds resulting from the screening, their identification is again a precious source of information for further refinement of the search for more specific and potent pendrin ligands. From the analysis of the identified compounds it is possible to isolate molecular or chemical features that may be important for the affinity with the target protein. This peculiar feature can in turn drive the further research of active compounds. In the present study we confirmed the alignment of small compounds according to the SHED profiling as a successful bioinformatics approach for identifying potential ligands of a protein of interest.

6. Conclusions

Functional and molecular characterization and rescue of pendrin variants

In this study we performed the functional characterization of 7 uncharacterized pendrin variants identified in the genetic screening of a cohort of 58 deaf patients with or without EVA, performed at the Hospital of Campinas, Sao Paolo, Brazil. Based on the results of the functional test, 4 pendrin variants (P142L, G149R, C282Y and Q413R) were classified as mutations with reduction of function, 2 (T193I and L445W) as mutations with complete loss of function and one (R776C) as a benign polymorphism. These results contributed to define the genetic diagnosis of deafness for 4 patients out of 14 presenting pendrin mutations. For 3 of these patients deafness was assessed as linked to pendrin dysfunction, while for one patient we were able to exclude pendrin as the genetic cause of deafness. Including our findings, the genetic diagnosis was conclusive for 6 patients, while for 8 individuals, bearing monoallelic pendrin mutations, further investigations are needed, as it is possible that other genetic or environmental factors are determining the phenotype. Further investigation must include the sequencing and characterization of pendrin promoter and 3' untranslated region, which may play a role in regulating the expression of the transporter.

For what concerns the subcellular localization of the analyzed pendrin variants, we could identify forms ranging from a complete retention in the ER (T193I, Q413R and L445W), to a mixed behavior (G149R) or trafficking to the plasma membrane undistinguishable from the wild type (P142L, C282Y, R776C). The localization of the different forms correlates well with the respective functional impairment, with the loss of function mutants being retained in the ER (T193I, L445W) and the variants with residual or unaffected function being localized to the PM (P142L, G149R, C282Y, R776C). The only exception is the mutant Q413R, showing a near to complete retention in the ER but also a residual transport activity, for which an intrinsic gain of function could be hypothesized.

Expression levels of the different pendrin variants, analyzed both *via* imaging and western blot, are reduced for all functionally impaired variants. The lower expression levels were observed for those mutants retained in the ER, while for variants capable of reaching the PM the reduction of expression levels was milder. The picture obtained in this study

confirms that functionally impaired pendrin forms are largely, but not exclusively, retained in the ER and degraded, possibly *via* ER associated degradation (ERAD).

The definition of the specific molecular defect allows for the investigation of a possible rescuing approach. In this sense we could show that by inhibiting the proteasomal degradation it was possible not only to increase the global expression levels of the mutants, but also their expression at the PM. Importantly, also the transport activity was significantly recovered in 4 out of 6 characterized mutants, upon treatment with MG132.

The evidence of a recovery of the transport activity of pendrin hypo-functional forms opens the way to a number of possible therapeutical approaches. It is therefore possible to hypothesize that a targeted approach aimed to the modulation of the degradation and/or folding assistance of defective pendrin forms may be the key for a future treatment of pendrin related deafness and Pendred syndrome.

Ligands screening

Screening of large compound libraries failed in delivering any specific ligand for pendrin. By means of a more targeted approach, we were able to identify a number of putative pendrin ligands to be confirmed by functional testing. The functional screening could be performed in a semi-high-throughput fashion thanks to the same fluorometric test used for the functional characterization of pendrin variants.

The screening of the candidate ligands led to the confirmation of the effect of previously identified inhibitors (NPPB and niflumic acid, showing 32 and 28% inhibition, respectively), therefore reinforcing once more the validity of the technical approach. Furthermore, we were able to identify previously unknown pendrin modulators. In particular, the first of the newly identified pendrin inhibitors was the anti-inflammatory drug tenidap. Short term treatment with 100 µM tenidap showed a strong inhibition (85%) of the iodide influx in pendrin transfected cells with respect to the vehicle treated cells. Even if this particular compound cannot be regarded to as specific for pendrin inhibition, its structure is a precious piece of information for further refinement of the ligand search.

From the active compounds identified (niflumic acid and tenidap), structure alignments according to the SHED profile principle have been performed, in order to identify further candidate compounds to be screened. N-(2-chlorophenyl)-2-(2,4-dibromophenoxy)acetamide, predicted by tenidap alignment, did show a slight (14% inhibition) effect on iodide influx in pendrin transfected cells. A further active compound identified, flufenamic acid, was predicted by the SHED alignment of niflumic acid, and did show a 15% inhibition of pendrin-dependent iodide transport.

To conclude, we were able to identify active compounds capable of inhibiting pendrin transport activity and exploit this information to further refine the selection of putative ligands by means of the bioinformatic approach defined as SHED alignment. The identification of pendrin inhibitors may represent an important step in the treatment of pathological conditions associated to an increased pendrin function or expression, such as bronchial asthma, COPD and hypertension.

7. Acknowledgements

I would like to expresses my deepest thank to all those who made this doctoral work possible, starting from my main supervisor and head of the Institute of Pharmacology and Toxicology of the Paracelsus Medical University, Prof. Paulmichl, together with all the lab members, the post docs Dr. Charity Nofziger, PD Selma Soyal Patsch, Prof. Wolfgang Patsch, Dr. Davide Civello and the present and former students, Giada Scantamburlo, Greta Zara, Roberta Costa, Simone Vanoni, among others, for their advice, support and friendship.

A special thank goes to my first co-supervisor Prof Brandstetter, who provided precious feedbacks during our meetings, Prof. Konrat from the institute of Biochemistry & Biophysics, Structural & Computational Biology, University of Vienna (Austria) who provided the essential bioinfromatic support and last but definitely not least my second co-supervisor, PD Silvia Dossena, who generously guided me the whole way through my work, and whose expertise and professionalism will always accompany me anywhere the future may take me.

Of course nothing would have been possible without the love and support of my dearest, Laura, sunshine always at my side, my mum, strong and lovely as only a mother can be and my father, always believing in me and now looking down at me from up there.

8. Bibliography

1.   Dossena, S., et al., *The expression of wild-type pendrin (SLC26A4) in human embryonic kidney (HEK 293 Phoenix) cells leads to the activation of cationic currents.* European Journal of Endocrinology, 2005: p. 693-699.

2.   Royaux, I.E., et al., *Localization and functional studies of pendrin in the mouse inner ear provide insight about the etiology of deafness in pendred syndrome.* Journal of the Association for Research in Otolaryngology, 2003. **4**: p. 394-404.

3.   Royaux, I.E., et al., *Pendrin, the protein encoded by the Pendred syndrome gene (PDS), is an apical porter of iodide in the thyroid and is regulated by thyroglobulin in FRTL-5 cells.* Endocrinology, 2000. **141**: p. 839-45.

4.   Royaux, I.E., et al., *Pendrin, encoded by the Pendred syndrome gene, resides in the apical region of renal intercalated cells and mediates bicarbonate secretion.* Proceedings of the National Academy of Sciences of the United States of America, 2001. **98**: p. 4221-6.

5.   Kuperman, D.A., et al., *Dissecting asthma using focused transgenic modeling and functional genomics.* The Journal of allergy and clinical immunology, 2005. **116**: p. 305-11.

6.   Dossena, S., et al., *Molecular and Functional Characterization of Human Pendrin and its Allelic Variants.* Cellular Physiology and Biochemistry, 2011. **28**: p. 451-466.

7.   Dossena, S., et al., *Synopsis of the 48 Annual Meeting of the Lake Cumberland Biological Transport Group and the Second Biannual Meeting of the Pendrin Consortium.* Cellular physiology and biochemistry, 2013. **32**: p. 1-13.

8.   Everett, L.A., et al., *Pendred Syndrome is caused by mutations on a putative sulphate transporter gene (PDS).* Nature genetics, 1997. **17**: p. 411-422.

9.   Pendred, V., *DEAF-MUTISM AND GOITRE.* The Lancet, 1896. **148**: p. 532.

10.   Morgans, M.E. and W.R. Trotter, *Association of congenital deafness with goitre; the nature of the thyroid defect.* Lancet, 1958. **1**: p. 607-9.

11.   Verlander, J.W., et al., *Deoxycorticosterone Upregulates PDS (Slc26a4) in Mouse Kidney: Role of Pendrin in Mineralocorticoid-Induced Hypertension.* Hypertension, 2003. **42**: p. 356-362.

12.   Nofziger, C., et al., *Pendrin Function in Airway Epithelia.* Cellular Physiology and Biochemistry, 2011: p. 571-578.

13.   Everett, L.A., *New insights into the role of pendrin (SLC26A4) in inner ear fluid homeostasis.* Novartis Foundation symposium, 2006. **273**: p. 213-25; discussion 225-30, 261-4.

14.   Wangemann, P., et al., *Loss of cochlear HCO3- secretion causes deafness via endolymphatic acidification and inhibition of Ca2+ reabsorption in a Pendred syndrome mouse model.* American journal of physiology. Renal physiology, 2008. **292**: p. F1345-F1353.

15.   Cremers, F.P., *Genetic causes of hearing loss.* Current opinion in neurology, 1998. **11**: p. 11-6.

16.   Wangemann, P., et al., *Loss of KCNJ10 protein expression abolishes endocochlear potential and causes deafness in Pendred syndrome mouse model.* BMC medicine, 2004. **2**: p. 30.

17.   Dror, A.a., et al., *Calcium oxalate stone formation in the inner ear as a result of an Slc26a4 mutation.* The Journal of biological chemistry, 2010. **285**: p. 21724-35.

18.   Choi, B.Y., et al., *Mouse model of enlarged vestibular aqueducts defines temporal requirement of Slc26a4 expression for hearing acquisition.* The Journal of clinical investigation, 2011. **121**: p. 4516-25.

19. Porra, V., et al., *Characterization and semiquantitative analyses of pendrin expressed in normal and tumoral human thyroid tissues.* The Journal of clinical endocrinology and metabolism, 2002. **87**: p. 1700-7.

20. Bidart, J.-m.M., et al., *Expression of pendrin and the Pendred syndrome (PDS) gene in human thyroid tissues.* The Journal of clinical endocrinology and metabolism, 2000. **85**: p. 2028-2033.

21. Twyffels, L., et al., *Pendrin: The thyrocyte apical membrane iodide transporter?* Cellular Physiology and Biochemistry, 2011. **28**: p. 491-496.

22. Fugazzola, L., et al., *High phenotypic intrafamilial variability in patients with Pendred syndrome and a novel duplication in the SLC26A4 gene: clinical characterization and functional studies of the mutated SLC26A4 protein.* European journal of endocrinology / European Federation of Endocrine Societies, 2007. **157**: p. 331-8.

23. Kopp, P., L. Pesce, and J.C. Solis-S, *Pendred syndrome and iodide transport in the thyroid.* Trends in endocrinology and metabolism: TEM, 2008. **19**: p. 260-8.

24. Reardon, W., et al., *Pendred syndrome — 100 years of underascertainment ?* QJM : monthly journal of the Association of Physicians, 1997. **90**: p. 443-447.

25. Ladsous, M., et al., *Analysis of the thyroid phenotype in 42 patients with Pendred syndrome and nonsyndromic enlargement of the vestibular aqueduct.* Thyroid : official journal of the American Thyroid Association, 2014. **24**: p. 639-48.

26. Kim, Y.-H., et al., *Immunocytochemical localization of pendrin in intercalated cell subtypes in rat and mouse kidney.* American journal of physiology. Renal physiology, 2002. **283**: p. F744-54.

27. Wall, S.M., et al., *Localization of pendrin in mouse kidney.* American journal of physiology. Renal physiology, 2003. **284**: p. F229-41.

28. Wall, S.M. and V. Pech, *The interaction of pendrin and the epithelial sodium channel in blood pressure regulation.* Current opinion in nephrology and hypertension, 2008. **17**: p. 18-24.

29. Eladari, D., et al., *Pendrin as a regulator of ECF and blood pressure.* Current opinion in nephrology and hypertension, 2009. **18**: p. 356-62.

30. Pela, I., M. Bigozzi, and B. Bianchi, *Profound hypokalemia and hypochloremic metabolic alkalosis during thiazide therapy in a child with Pendred syndrome.* Clinical nephrology, 2008. **69**: p. 450-3.

31. Kandasamy, N., et al., *Life-threatening metabolic alkalosis in Pendred syndrome.* European journal of endocrinology / European Federation of Endocrine Societies, 2011. **165**: p. 167-70.

32. Amlal, H., et al., *Deletion of the anion exchanger Slc26a4 (pendrin) decreases apical Cl-/HCO-exchanger activity and impairs bicarbonate secretion in kidney collecting duct.* 2010. **4**: p. 33-41.

33. Wall, S.M., et al., *NaCl restriction upregulates renal Slc26a4 through subcellular redistribution: role in Cl- conservation.* Hypertension, 2004. **44**: p. 982-7.

34. Pedemonte, N., et al., *Thiocyanate transport in resting and IL-4-stimulated human bronchial epithelial cells: role of pendrin and anion channels.* Journal of immunology (Baltimore, Md. : 1950), 2007. **178**: p. 5144-53.

35. Rillema, J.A., M.A. Hill, and M.E.A.H. III, *Pendrin Transporter Carries Out Iodide Uptake into MCF-7 Human Mammary Cancer Cells.* Experimental Biology and Medicine, 2003: p. 1078-1082.

36. Bidart, J.M., et al., *Expression of Na+/I- symporter and Pendred syndrome genes in trophoblast cells.* The Journal of clinical endocrinology and metabolism, 2000. **85**: p. 4367-72.

37.   Lacroix, L., et al., *Na(+)/I(-) symporter and Pendred syndrome gene and protein expressions in human extra-thyroidal tissues.* European Journal of Endocrinology, 2001. **144**: p. 297-302.

38.   Suzuki, K., et al., *Expression of PDS/Pds, the Pendred Syndrome Gene, in Endometrium.* The Journal of Clinical Endocrinology & Metabolism, 2002. **87**: p. 938.

39.   Alesutan, I., et al., *Impact of Bicarbonate, Ammonium Chloride, and Acetazolamide on Hepatic and Renal SLC26A4 Expression.* Cellular Physiology and Biochemistry, 2011. **28**: p. 553-558.

40.   Nofziger, C., et al., *STAT6 links IL-4/IL-13 stimulation with pendrin expression in asthma and chronic obstructive pulmonary disease.* Clinical pharmacology and therapeutics, 2011. **90**: p. 399-405.

41.   Carpenter, E.P., et al., *Overcoming the challenges of membrane protein crystallography.* Curr Opin Struct Biol, 2008. **18**(5): p. 581-6.

42.   Gillam, M.P., et al., *Functional characterization of pendrin in a polarized cell system. Evidence for pendrin-mediated apical iodide efflux.* J Biol Chem, 2004. **279**(13): p. 13004-10.

43.   Aravind, L. and E.V. Koonin, *The STAS domain - a link between anion transporters and antisigma-factor antagonists.* Curr Biol, 2000. **10**(2): p. R53-5.

44.   Dossena, S., et al., *Functional characterization of wild-type and mutated pendrin (SLC26A4), the anion transporter involved in Pendred syndrome.* Journal of molecular endocrinology, 2009. **43**: p. 93-103.

45.   Shafrir, Y. and H.R. Guy, *STAM: simple transmembrane alignment method.* Bioinformatics, 2004. **20**(5): p. 758-69.

46.   Lee, K., T.-J. Hong, and J.-S. Hahn, *Roles of 17-AAG-induced molecular chaperones and Rma1 E3 ubiquitin ligase in folding and degradation of Pendrin.* FEBS letters, 2012. **586**: p. 2535-41.

47.   Azroyan, A., et al., *Regulation of pendrin by pH: depence on glycosylation.* Biochemical Journal, 2011.

48.   Fraser, G.R., *Association of congenital deafness with goitre (Pendred's syndrome): A study of 207 families.* Annals of Human Genetics, 1964. **28**: p. 201-250.

49.   Blons, H., et al., *Screening of SLC26A4 (PDS) gene in Pendred's syndrome: a large spectrum of mutations in France and phenotypic heterogeneity.* Clinical Genetics, 2004. **66**: p. 333-340.

50.   Yoshinaga-itano, C., et al., *Language of early- and later-identified children with hearing loss.* Pediatrics, 1998. **102**: p. 1161-1171.

51.   White, K.R., et al., *The evolution of early hearing detection and intervention programs in the United States.* Seminars in perinatology, 2010. **34**: p. 170-9.

52.   Force, U.P.S.T., *Universal screening for hearing loss in newborns: US Preventive Services Task Force recommendation statement.* Pediatrics, 2008. **122**: p. 143-8.

53.   Pryor, S.P., et al., *SLC26A4/PDS genotype-phenotype correlation in hearing loss with enlargement of the vestibular aqueduct (EVA): evidence that Pendred syndrome and non-syndromic EVA are distinct clinical and genetic entities.* Journal of medical genetics, 2005. **42**: p. 159-65.

54.   Nivoloni, K.D.a.B., et al., *Newborn hearing screening and genetic testing in 8974 Brazilian neonates.* International journal of pediatric otorhinolaryngology, 2010. **74**: p. 926-9.

55.   Ramos, P.Z., et al., *Etiologic and diagnostic evaluation: Algorithm for severe to profound sensorineural hearing loss in Brazil.* International journal of audiology, 2013. **52**: p. 746-52.

56. Kopp, P., et al., *Phenocopies for Deafness and Goiter Development in a Large Inbred Brazilian Kindred with Pendred ' s Syndrome Associated with a Novel Mutation in the PDS gene.* Journal of Clinical Endocrinology and Metabolism, 1999. **84**: p. 336-341.

57. Camargo, R., et al., *Aggressive Metastatic Follicular Thyroid Carcinoma with Anaplastic Transformation Arising from a Long-Standing Goiter in a Patient with Pendred's Syndrome.* Thyroid, 2001. **11**: p. 981-988.

58. Hilgert, N., R.J.H. Smith, and G. Van Camp, *Forty-six genes causing nonsyndromic hearing impairment: which ones should be analyzed in DNA diagnostics?* Mutation research, 2009. **681**: p. 189-96.

59. Lang, F., et al., *Functional significance of channels and transporters expressed in the inner ear and kidney.* American journal of physiology. Cell physiology, 2007. **293**: p. C1187-208.

60. Kelsell, D.P., et al., *Connexin 26 mutations in hereditary nono-syndromic sensorineural deafness.* Nature, 1997. **387**: p. 80-83.

61. Gasparini, P., et al., *High carrier frequency of the 35delG deafness mutation in European populations.* 2000. **8**: p. 19-23.

62. Kikuchi, T., et al., *Gap Junction Systems in the Rat Vestibular Labyrinth: Immunohistochemical and Ultrastructural Analysis.* 2009.

63. Dai, P., et al., *Molecular etiology of hearing impairment in Inner Mongolia: mutations in SLC26A4 gene and relevant phenotype analysis.* Journal of translational medicine, 2008. **6**: p. 74.

64. Del Castillo, I., et al., *Prevalence and evolutionary origins of the del(GJB6-D13S1830) mutation in the DFNB1 locus in hearing-impaired subjects: a multicenter study.* American journal of human genetics, 2003. **73**: p. 1452-8.

65. Torroni, a., et al., *The A1555G mutation in the 12S rRNA gene of human mtDNA: recurrent origins and founder events in families affected by sensorineural deafness.* American journal of human genetics, 1999. **65**: p. 1349-58.

66. de Moraes, V.C.S., et al., *Molecular analysis of SLC26A4 gene in patients with nonsyndromic hearing loss and EVA: identification of two novel mutations in Brazilian patients.* International journal of pediatric otorhinolaryngology, 2013. **77**: p. 410-3.

67. Choi, B.Y., et al., *Hypo-functional SLC26A4 variants associated with nonsyndromic hearing loss and enlargement of the vestibular aqueduct: genotype-phenotype correlation or coincidental polymorphisms?* Human mutation, 2009. **30**: p. 599-608.

68. Pfarr, N., et al., *Goitrous congenital hypothyroidism and hearing impairment associated with mutations in the TPO and SLC26A4/PDS genes.* The Journal of clinical endocrinology and metabolism, 2006. **91**: p. 2678-81.

69. Dossena, S., et al., *Fast Fluorometric method for measuring pendrin (SLC26A4) Cl-/I- transport activity.* Cellular Physiology and Biochemistry, 2006: p. 67-74.

70. Adato, a., et al., *Deafness heterogeneity in a Druze isolate from the Middle East: novel OTOF and PDS mutations, low prevalence of GJB2 35delG mutation and indication for a new DFNB locus.* European journal of human genetics : EJHG, 2000. **8**: p. 437-42.

71. Dossena, S., et al., *Identification of allelic variants of pendrin (SLC26A4) with loss and gain of function.* Cellular physiology and biochemistry 2011. **28**: p. 467-76.

72. Gillam, M.P., et al., *Molecular analysis of the PDS gene in a nonconsanguineous Sicilian family with Pendred's syndrome.* Thyroid : official journal of the American Thyroid Association, 2005. **15**: p. 734-741.

73.   Taylor, J.P., et al., *Mutations of the PDS gene, encoding pendrin, are associated with protein mislocalization and loss of iodide efflux: implications for thyroid dysfunction in Pendred syndrome.* The Journal of clinical endocrinology and metabolism, 2002. **87**: p. 1778-84.

74.   Pera, A., et al., *Functional assessment of allelic variants in the SLC26A4 gene involved in Pendred syndrome and nonsyndromic EVA.* Proceedings of the National Academy of Sciences of the United States of America, 2008. **105**: p. 18608-13.

75.   Rotman-pikielny, P., et al., *Retention of pendrin in the endoplasmic reticulum is a major mechanism for Pendred syndrome.* Human molecular genetics, 2002. **11**: p. 2625-33.

76.   Schröder, M. and R.J. Kaufman, *The mammalian unfolded protein response.* Annual review of biochemistry, 2005. **74**: p. 739-89.

77.   Qin, H., et al., *Lysosomal and proteasomal degradation play distinct roles in the life cycle of Cx43 in gap junctional intercellular communication-deficient and -competent breast tumor cells.* The Journal of biological chemistry, 2003. **278**: p. 30005-14.

78.   Travers, K.J., et al., *Functional and Genomic Analyses Reveal an Essential Coordination between the Unfolded Protein Response and ER-Associated Degradation.* Cell, 2000. **101**: p. 249-258.

79.   Kim, Y.E., et al., *Molecular Chaperone Functions in Protein Folding and Proteostasis.* Annual Review of Biochemistry, 2013. **82**: p. 323-355.

80.   Masuda, A., M. Kuwano, and T. Shimada, *Ultrastructural Changes during the Enhancement of Cellular 3-Hydroxy-3-Methyl-Glutaryl-Coenzyme A Reductase in a Chinese Hamster Cell Mutant Resistant to Compactin (ML 236B).* Cell Structure and Function, 1983. **8**: p. 309-312.

81.   Lecker, S.H., A.L. Goldberg, and W.E. Mitch, *Protein degradation by the ubiquitin-proteasome pathway in normal and disease states.* Journal of the American Society of Nephrology : JASN, 2006. **17**: p. 1807-19.

82.   Schulman, B.A. and J.W. Harper, *Ubiquitin-like protein activation by E1 enzymes: the apex for downstream signalling pathways.* Nature reviews. Molecular cell biology, 2009. **10**: p. 319-331.

83.   Semple, C.A.M., R.G.E.R. Group, and G.S.L. Members, *The Comparative Proteomics of Ubiquitination in Mouse.* Genome research, 2003(13): p. 1389-1394.

84.   Walter, P. and D. Ron, *The unfolded protein response: from stress pathway to homeostatic regulation.* Science (New York, N.Y.), 2011. **334**: p. 1081-6.

85.   Ishihara, K., et al., *Salicylate restores transport function and anion exchanger activity of missense pendrin mutations.* Hearing research, 2010. **270**: p. 110-8.

86.   Yoon, J.S.S., et al., *Heterogeneity in the processing defect of SLC26A4 mutants.* Journal of medical genetics, 2008. **45**: p. 411-9.

87.   Mount, D.B. and M.F. Romero, *The SLC26 gene family of multifunctional anion exchangers.* Pflügers Archiv : European journal of physiology, 2004. **447**: p. 710-21.

88.   Yang, T., et al., *Mutations of KCNJ10 together with mutations of SLC26A4 cause digenic nonsyndromic hearing loss associated with enlarged vestibular aqueduct syndrome.* American journal of human genetics, 2009. **84**: p. 651-7.

89.   Yang, T., et al., *Transcriptional control of SLC26A4 is involved in Pendred syndrome and nonsyndromic enlargement of vestibular aqueduct (DFNB4).* American journal of human genetics, 2007. **80**: p. 1055-63.

90.   Nakao, I., et al., *Identification of pendrin as a common mediator for mucus production in bronchial asthma and chronic obstructive pulmonary disease.* Journal of immunology, 2008. **180**: p. 6262-9.

91. Xu, J., et al., *Double Knockout of Carbonic Anhydrase II (CAII) and Na-Cl(-) Cotransporter (NCC) Causes Salt Wasting and Volume Depletion.* Cellular physiology and biochemistry, 2013. **32**: p. 173-83.

92. Kim, Y.H., et al., *Role of pendrin in iodide balance: going with the flow.* Am J Physiol Renal Physiol, 2009. **297**(4): p. F1069-79.

93. Leviel, F., et al., *The Na+-dependent chloride-bicarbonate exchanger SLC4A8 mediates an electroneutral Na+ reabsorption process in the renal cortical collecting ducts of mice.* Journal of Clinical Investigation, 2010. **120**: p. 1627-1635.

94. Kim, Y.H., et al., *Reduced ENaC protein abundance contributes to the lower blood pressure observed in pendrin-null mice.* American journal of physiology. Renal physiology, 2007. **293**: p. F1314-24.

95. Pech, V., et al., *Angiotensin II increases chloride absorption in the cortical collecting duct in mice through a pendrin-dependent mechanism.* American journal of physiology. Renal physiology, 2007. **292**: p. F914-20.

96. Nakagami, Y., et al., *The epithelial anion transporter pendrin is induced by allergy and rhinovirus infection, regulates airway surface liquid, and increases airway reactivity and inflammation in an asthma model.* Journal of immunology (Baltimore, Md. : 1950), 2008. **181**: p. 2203-10.

97. Dossena, S., et al., *Functional Characterization of Wild-Type and a Mutated Form of SLC26A4 Identified in a Patient with Pendred Syndrome.* Cellular Physiology and Biochemistry, 2006: p. 245-256.

98. Quentin, F., et al., *The Cl-/HCO3- exchanger pendrin in the rat kidney is regulated in response to chronic alterations in chloride balance.* American journal of physiology. Renal physiology, 2004. **287**: p. F1179-88.

99. Scott, D.A., et al., *The Pendred syndrome gene encodes a chloride-iodide transport protein.* Nature genetics, 1999. **21**: p. 440-3.

100. Soleimani, M., et al., *Pendrin: an apical Cl-/OH-/HCO3- exchanger in the kidney cortex.* American journal of physiology. Renal physiology, 2001. **280**: p. F356-64.

101. Dossena, S., et al., *Functional Characterization of Pendrin Mutations Found in the Israeli and Palestinian Populations.* Cellular Physiology and Biochemistry, 2011: p. 477-484.

102. Byeon, M.K., et al., *The down-regulated in adenoma (DRA) gene encodes an intestine-specific membrane glycoprotein.* Oncogene, 1996. **12**: p. 387-396.

103. Jacob, P., et al., *Down-regulated in adenoma mediates apical Cl−/HCO3− exchange in rabbit, rat, and human duodenum.* Gastroenterology, 2002. **122**: p. 709-724.

104. Melvin, J.E., et al., *Mouse Down-regulated in Adenoma (DRA) Is an Intestinal 3 Exchanger and Is Up-regulated in Colon of Mice Lacking the NHE3 Na ⁄ H ⁄ Exchanger *.* 1999. **274**: p. 22855-22861.

105. Xiao, F., et al., *Slc26a3 deficiency is associated with loss of colonic HCO3 (-) secretion, absence of a firm mucus layer and barrier impairment in mice.* Acta physiologica (Oxford, England), 2014. **211**: p. 161-75.

106. Chernova, M.N., et al., *Acute regulation of the SLC26A3 congenital chloride diarrhoea anion exchanger (DRA) expressed in Xenopus oocytes.* The Journal of physiology, 2003. **549**: p. 3-19.

107. Lamprecht, G., et al., *Transport properties of the human intestinal anion exchanger DRA (down-regulated in adenoma) in transfected HEK293 cells.* Pflügers Archiv : European journal of physiology, 2005. **449**: p. 479-90.

108. Brater, D.C., *Diuretic Therapy.* New England Journal of Medicine, 1998. **339**: p. 387-395.

109. Ernst, M.E. and M. Moser, *Use of Diuretics in Patients with Hypertension.* New England Journal of Medicine, 2009. **361**: p. 2153-2164.

110. Denton, J.S., A.C. Pao, and M. Maduke, *Novel diuretic targets.* American journal of physiology. Renal physiology, 2013. **305**: p. F931-42.

111. Frye, S.V., *Structure-activity relationship homology (SARAH): a conceptual framework for drug discovery in the genomic era.* Chemistry & biology, 1999. **6**: p. R3-7.

112. Konrat, R., *The protein meta-structure: a novel concept for chemical and molecular biology.* Cellular and molecular life sciences : CMLS, 2009. **66**: p. 3625-39.

113. Gregori-Puigjané, E. and J. Mestres, *SHED: Shannon entropy descriptors from topological feature distributions.* Journal of chemical information and modeling, 2006. **46**: p. 1615-22.

114. Galietta, L.J., P.M. Haggie, and A.S. Verkman, *Green fluorescent protein-based halide indicators with improved chloride and iodide affinities.* FEBS letters, 2001. **499**: p. 220-4.

115. DiCiommo, D.P., et al., *Retinoblastoma protein purification and transduction of retina and retinoblastoma cells using improved alphavirus vectors.* Invest Ophthalmol Vis Sci, 2004. **45**(9): p. 3320-9.

116. Azroyan, A., et al., *Regulation of pendrin by pH: dependece on gycosilation.* Biochemical Journal, 2011. **434**(1): p. 61-72.

117. Cirello, V., et al., *Molecular and functional studies of 4 candidate loci in Pendred syndrome and nonsyndromic hearing loss.* Molecular and cellular endocrinology, 2012: p. 1-9.

118. Knauf, F., et al., *Identification of a chloride-formate exchanger expressed on the brush border membrane of renal proximal tubule cells.* Proc Natl Acad Sci U S A, 2001. **98**(16): p. 9425-30.

119. Hoffmann, E.K., *Anion Exchange and Anion-Cation Co-Transport Systems in Mammalian Cells.* Vol. 299. 1982. 519-535.

120. Sonawane, N.D., et al., *In vivo pharmacology and antidiarrheal efficacy of a thiazolidinone CFTR inhibitor in rodents.* J Pharm Sci, 2005. **94**(1): p. 134-43.

121. Taddei, A., et al., *Altered channel gating mechanism for CFTR inhibition by a high-affinity thiazolidinone blocker.* FEBS letters, 2004. **558**: p. 52-6.

122. Barzilay, M. and Z.I. Cabantchik, *Anion transport in red blood cells. II. Kinetics of reversible inhibition by nitroaromatic sulfonic acids.* Membr Biochem, 1979. **2**(2): p. 255-81.

123. Stewart, A.K., et al., *Molecular characterization of Slc26a3 and Slc26a6 anion transporters in guinea pig pancreatic duct.* The journal of medical investigation : JMI, 2009. **56 Suppl**: p. 329-31.

124. Mcniff, P., R.P. Robinsont, and C.A. Gabel, *Reduction of intracellular pH by Tenidap - Involvement of cellular anion transporters in the pH change.* Biochemical Pharmacology, 1995. **50**: p. 1421-1432.

125. Friedman, P.A., *Bumetanide inhibition of [CO2 + HCO3]-dependent and -independent equivalent electrical flux in renal cortical thick ascending limbs.* The Journal of pharmacology and experimental therapeutics, 1986. **238**: p. 407-14.

126. Shepshelovich, J., et al., *Protein synthesis inhibitors and the chemical chaperone TMAO reverse endoplasmic reticulum perturbation induced by overexpression of the iodide transporter pendrin.* J Cell Sci, 2005. **118**(Pt 8): p. 1577-86.

127. Myssina, S., et al., *Cl- channel blockers NPPB and niflumic acid blunt Ca(2+)-induced erythrocyte 'apoptosis'.* Cell Physiol Biochem, 2004. **14**(4-6): p. 241-8.

128. Kim, B.M., et al., *Combined treatment with the Cox-2 inhibitor niflumic acid and PPARγ ligand ciglitazone induces ER stress/caspase-8-mediated apoptosis in human lung cancer cells.* Cancer Letters, 2011. **300**(2): p. 134-144.

129. Picollo, A., et al., *Mechanism of interaction of niflumic acid with heterologously expressed kidney CLC-K chloride channels.* J Membr Biol, 2007. **216**(2-3): p. 73-82.

130. Brown, C.D. and A.J. Dudley, *Chloride channel blockers decrease intracellular pH in cultured renal epithelial LLC-PK1 cells.* British Journal of Pharmacology, 1996. **118**(3): p. 443-444.

131. Breedveld, F., *Tenidap: a novel cytokine-modulating antirheumatic drug for the treatment of rheumatoid arthritis.* Scand J Rheumatol Suppl, 1994. **100**: p. 31-44.

132. Ducoudret, O., et al., *The renal Na-HCO3-cotransporter expressed in Xenopus laevis oocytes: inhibition by tenidap and benzamil and effect of temperature on transport rate and stoichiometry.* Pflugers Arch, 2001. **442**(5): p. 709-17.

133. Liu, Y., et al., *Tenidap, a novel anti-inflammatory agent, is an opener of the inwardly rectifying K+ channel hKir2.3.* European Journal of Pharmacology, 2002. **435**(2–3): p. 153-160.